2008

Evaluation of exhaust after-treatment device effectiveness in reducing regulated and unregulated emissions from natural gas fueled heavy duty transit bus

Arvind Padmavathy Thiruvengadam
West Virginia University

Evaluation of Exhaust After-Treatment Device Effectiveness in Reducing Regulated and Unregulated Emissions from Natural Gas Fueled Heavy Duty Transit Bus

Arvind Thiruvengadam Padmavathy

Thesis Submitted to the
College of Engineering and Mineral Resources
at West Virginia University
in partial fulfillment of the requirements
for the degree of

Master of Science
in
Mechanical Engineering

Mridul Gautam, Ph.D., Chair

Mohan Krishnamurthy, Ph.D.

Benjamin C. Shade, Ph.D.

Daniel. K. Carder

Department of Mechanical and Aerospace Engineering
Morgantown, West Virginia
2008

ABSTRACT

Evaluation of Exhaust After-Treatment Device Effectiveness in Reducing Regulated and Unregulated Emissions from Natural Gas Fueled Heavy Duty Transit Bus

Arvind Thiruvengadam Padmavathy

The promulgation of the public transit fleet rule by the California Air Resources Board (CARB) in 2000, has given transit fleet operators the option of choosing the alternative fuel path in order to reduce their fleet average NOx and PM emissions. Natural gas being an abundant domestic fuel, has found its way as an economically and technologically feasible alternative fuel option. Many studies have shown the clean burning nature of natural gas with lower NOx and near zero Particulate Matter (PM) emissions from heavy duty natural gas vehicles. Though natural gas fueled vehicles emit lower NOx and PM than their diesel counterparts, the emissions of carbon monoxide (CO) and total hydrocarbons (THC) are higher. This necessitates the use of a suitable exhaust after-treatment device to attain complete emission benefits.

The objective of the study was to measure regulated and unregulated emissions from CNG fueled heavy-duty transit bus with and without the after-treatment device present. The study conducted in Riverside, California utilized two CNG fueled transit buses one from Riverside Transit Authority (RTA) and the other from Los Angeles County Metro Transit Authority (LACMTA). The study required the complete chemical speciation of exhaust from the RTA bus with and without the after-treatment device so as to evaluate the effectiveness of the after-treatment device in reducing both regulated and unregulated emissions. The buses were retrofitted with an oxidation catalytic converter manufactured by Engine Control Systems (ECS). The buses were tested on a heavy duty chassis dynamometer part of the West Virginia University Transportable Heavy Duty Vehicle Emissions Testing Laboratory (WVTHDVETL). The transit buses were exercised over a double length Orange County Transit Authority (OCTA) cycle to characterize its emission levels. The analysis of the unregulated sample, which included Poly Aromatic Hydrocarbons (PAH), aldehydes, Volatile Organic Compounds (VOC), metals and elemental/organic carbon was done by Desert Research Institute (DRI).

The results of the regulated emissions showed a 99% reduction in CO and 62% reduction in THC with the after-treatment device present. The unregulated speciation results showed 96% reduction in carbonyl compounds with formaldehyde being the major contributor, 46% reduction in PAH compounds, 60% reduction in nitro-PAH compounds and 93% reduction in VOC. There was an overall 27% increase in metal content in exhaust with the after-treatment device present. There was no effect on the organic carbon concentration with the after-treatment device present.

in this field, I am so passionate about. Sukanya congrats for your job and I know you would excel in all your endeavors.

I thank Karthik for helping me out, when I was new to the lab. I thank Hema for all the help and taking good care of me. I thank Avinash for being a great roommate. I thank Abishek for being a very good friend for the past 7 years. We had very memorable happy college days which I would never forget. I thank Hari Menon for the great friendship and the humorous graduate student life. I thank Siva and his family for their friendship and support.

I thank Tom Fortuna for supporting me initially at WVU, and molding me into a true AUTOCAD professional.

Table of Contents

List of Tables

List of Figures

CHAPTER 1 - INTRODUCTION

1.1 Introduction

Amidst stringent emission regulations in the US, diesel engines have gained popularity as the preferred power plant for heavy duty on and off road applications. This is due to the fact that diesel engines which operate on the diesel thermodynamic cycle, have high torque output and operate with greater fuel economy compared to its gasoline powered counterparts. Diesel engines are built robust in order to withstand the high in cylinder temperature and pressure, this aspect makes them long-lasting with minimal maintenance. Diesel engines serve as a boon to the truck industry and public transportation segment because of its reliability and economy involved in operating these engines.

Some of the hurdles the diesel engine industry would face are the constant rise in crude oil price per barrel, and the upcoming 2010 emission regulations which would necessitate the use of after-treatment devices, to meet the emission norms. These factors would definitely increase the costs associated with operating diesel engines. Though these setbacks would not prove detrimental to the burgeoning growth of the diesel engine industry as whole, it necessitates certain segments of the transportation industry to look into alternative fuel technologies to get that cost advantage.

Of the current alternative fuel options available natural gas seems to be the most feasible and easily obtained resources. Natural gas engines have proven to be excellent replacement for diesel engines in meeting 2010 emissions, with the added cost advantage the transportation industry is looking for. The TIAX report aimed at assessing the comparative cost involved in 2010 heavy duty diesel and natural gas engine, shows that certain segments of the transportation industry which include transit agencies, refuse truck agencies and short haul fleet owners find natural gas engines to be equally economical in their operating cost. And moreover future predictions in this report shift the cost advantage balance towards natural gas engines [1]. A study conducted by research group INFORM Inc. have found that between 2002 and 2005 the number of natural gas powered trucks operating in the refuse truck industry has doubled [2]. The study also points that majority of the natural gas initiative exists in the state of California.

From an emissions stand point on-road diesel engine exhaust has been identified as the greatest contributor towards Particulate Matter (PM) and oxides of nitrogen (NOx) concentration

in the atmosphere. With the existence of a trade-off curve between NOx and PM formation, diesel engine manufacturers today face the biggest challenge of reducing both these constituents regulated by the Environmental Protection Agency (EPA). Modern diesel engines have been designed to control Carbon Monoxide (CO) and Total Hydrocarbon (THC) emissions very effectively. CNG fueled vehicles on the other hand tend to emit lesser amount of NOx and PM than diesel engines. A study conducted by California Air Resources Board (CARB) shows that PM emissions from CNG fueled vehicles are equivalent to those from diesel engines equipped with diesel particulate filters (DPF) [3]. However the study also shows that CNG vehicles emissions of THC and CO are an order of magnitude greater than emissions from diesel engine with oxidation catalyst present. Studies have also shown that though CNG vehicles PM emissions on a mass basis might be very low, the higher number concentrations of ultrafine nanoparticles found in the exhaust would definitely pose a health hazard, as nanoparticles have the greatest penetration into the human lung. Studies from various agencies have shown clearly that use of CNG fueled vehicles without some form of after-treatment device is not a cleaner alternative from diesel engines.

The EPA has identified list of Toxic Air Contaminants (TAC) which are carcinogenic and mutagenic in nature. Though these emissions form the unregulated emissions category, the hazardous nature of these constituents to humans makes it necessary to quantify TAC levels in vehicle exhaust. The TAC list includes various Poly Aromatic Hydrocarbon chains (PAH), Volatile Organic Compounds (VOC) and various aldehydes compounds. These contaminants are basically the result of organic fuel combustion, and these quantities are present in significant quantities in CNG vehicles emissions too. This necessitates the use of after-treatment devices with CNG fueled vehicles.

1.2 Objective

The global objective of the study this thesis is based upon was measuring the regulated and unregulated emissions from CNG fueled heavy-duty transit buses with and without the after-treatment device present. The study, conducted in Riverside, California, utilized two CNG fueled transit buses with one from Riverside Transit Authority (RTA) and the other from Los Angeles County Metro Transit Authority (LACMTA). The study required the complete chemical speciation of exhaust from the RTA bus with and without the after-treatment device so as to

evaluate the effectiveness of the after-treatment device in reducing both regulated and unregulated emissions. The buses were retrofitted with an oxidation catalytic converter manufactured by Engine Control Systems (ECS). The buses were tested on a heavy duty chassis dynamometer part of the West Virginia University Transportable Laboratory. The transit buses were driven over a double length Orange County Transit Authority (OCTA) cycle to evaluate its emission levels. Table 1.1 lists the exhaust species measured.

Table 1.1 Regulated and Unregulated Emissions Sampled

Regulated Emissions	Unregulated Emissions
Carbon monoxide (CO)	Polyaromatic hydrocarbon (PAH)
Oxides of nitrogen (NOx)	Volatile organic compounds (VOC)
Total hydrocarbons (THC)	Carbonyl compounds
Non-methane hydrocarbons (NMHC)	Metals
Total particulate matter (TPM)	Elemental/Organic carbon (EC/OC)
	Carbon dioxide(CO_2)

CHAPTER 2 - LITERATURE REVIEW

2.1 Introduction

Rising fuel costs and upcoming stringent emission norms are forcing operators of heavy duty diesel engines to look into the alternative fuel strategy. Public transit agencies find the need to adopt this strategy as a cost cutting measures for meeting emission norms. The state of California constituted the public transit bus fleet rule in February 2000. The ordinance, which was directed towards the California transit fleet operators, required the operators to choose between diesel fueled vehicles and alternate fuel vehicles for their fleet expansion [4]. The rule required the operators to procure or lease 85% of buses through model year 2015 to be fueled with alternate fuels [4]. Alternate fuels include CNG, Propane (LPG), ethanol, and even hybrid electric buses.

Natural gas is one of the most feasible alternate fuel options available to us. Natural gas is a clean burning fuel producing no soot from its combustion. This fact makes it an excellent choice to meet the Particulate Matter (PM) emission norms. Existing diesel engines could be fueled using natural gas with minimal modifications, although durability and performance would be of primary concern. Though natural gas seems to be a greener alternative to diesel, emissions from natural gas vehicles are also of concern, especially without the presence of suitable after-treatment devices. This chapter would discuss the various studies that have been carried out with Natural Gas Vehicle (NGV) emissions in comparison to current diesel engines with after-treatment device. The chapter will also discuss the engine technology that power current NGVs.

The EPA and the CARB have identified several organic carbon compounds and metals that are part of diesel engine exhaust and that are harmful to humans. These compounds are basically carcinogenic and mutagenic in nature. This chapter will also discuss the effects and levels of emissions of these compounds from CNG fueled vehicles. Finally this chapter deals with levels of ultrafine nano particles emitted from the NGVs.

2.2 Natural Gas Fuel

Natural gas was formed due to the decay of organic matter buried deep in the soil for thousands of years. Natural gas is the most abundantly available fossil fuel after coal. The annual report prepared by the Energy Information Administration, shows that the current natural gas

reserves worldwide total to 6000 trillion cubic feet and this number has been steadily increasing since 1980 [5]. The report shows that the US share of the world natural gas reserve stands at 3.3%.

The major constituent of natural gas is methane. It also contains varying quantities of non-methane hydrocarbons, water vapor, hydrogen sulphide and other gases. Natural gas would typically contain 80 to 99% methane with trace quantities of higher hydrocarbons [5]. The composition of natural gas varies in accordance to the geography of the gas well. Natural gas that are transported to delivery stations are governed by fuel specifications which limit the quantity of higher hydrocarbons in it. Natural gas properties are also specified through the Wobbe index [5]. Wobbe index is the ratio of higher heating value to the square root of specific gravity of the fuel.

$$W = \text{Higher heating Value} / \sqrt{\text{Sp. Gravity of fuel}} \quad \text{``MJ''} \qquad \textbf{Equation 2.1}$$

The current natural gas specifications that are to be adhered in the state of California are shown below in Table 2.1 [6].

Table 2.1 California CNG fuel specification

Specification	Value	Test Method
Hydrocarbons (Expressed as mole percentage)		
Methane	88.0 % (min.)	ASTM D 1945-81
Ethane	6.0% (max.)	ASTM D 1945-81
C3 and Higher HC	3.0% (max.)	ASTM D 1945-81
C6 and Higher HC	0.2% (max.)	ASTM D 1945-81
Other Species (Expressed as mole percent unless otherwise indicated)		
Hydrogen	0.1% (max.)	ASTM D 2650-88
Carbon Monoxide	0.1% (max.)	ASTM D 2650-88
Oxygen	1.0% (max.)	ASTM D 1945-81
Inert Gases		
Sum of CO_2 and N_2	1.5-4.5% (range)	ASTM D 1945-81
Water	-	
Particulate matter	-	
Odorant	-	
Sulfur	16ppm by vol. (max)	Title 17 CCR Section 94112

Natural gas has excellent anti-knock properties. This is due to the fact that its major component is methane which in turn is highly knock resistant. The scale of anti-knock property of natural gas far exceeds that of any liquid fuel, and for this reason the anti-knock property of natural gas is specified in terms of Methane Number (MN) rather than the Motor Octane Number (MON). Highly knock resistant methane has MN of 100 and hydrogen which has very high

5

capability to auto ignite, is assigned MN of 0. A study by Callahan et al. has derived a linear relationship between MON and MN [7,8].

$$MON = 84.9 + 0.37 \ (MN) \hspace{3cm} \textbf{Equation 2.1}$$

2.3 Natural Gas Engine Technology

Natural gas can be used as a fuel in compressed ignition engines provided there is some kind of ignition source. The high antiknock property of natural gas due to the presence of high quantity of methane makes it an unsuitable fuel for compressed ignition technology. The auto ignition temperature of diesel fuel is around 250-300°C and that of natural gas is around 600°C, hence an additional ignition source is required to initiate combustion while using natural gas with compressed ignition engines.

The current technological options available for natural gas fueled engines are:

1. Spark Ignited Natural Gas Engines (SING)
2. Direct Injection Natural Gas Engines (DING)
3. Dual Fuel Natural Gas Engines (DFNG)

Of these current technologies SING engines are based on the Otto cycle and DING and DFNG are based on the diesel cycle [9].

2.3.1 Spark Ignited Natural Gas Engines (SING)

These engines basically follow the Otto cycle and the source of ignition is the spark plug. The engines generally operate under stoichiometric air fuel ratios. Since natural gas has high octane number spark ignited engines with high compression ratios can be used. This increases the thermal efficiency of an Otto cycle engine. One of the main advantages of these types of engine is that the combustion is clean without any soot. Modern heavy duty natural gas engines operate under lean burn conditions with excess of air present in the combustion chamber; this increases performance and reduces hydrocarbon emissions. Cummins-Westport successfully developed a heavy duty 8.9L lean burn spark ignited engine, which satisfied the 0.2g/bhp-hr NOx emission limits [10]. John Deere developed a 8.1L, 280hp spark ignited engine and successfully installed it on a Washington Metropolitan Area Transit Authority (WMATA) bus and tested the engine deterioration factor. The engine acquired 14500 miles during a 6 month

period and operated with an average fuel economy of 2.35 miles/gallon. The vehicles was tested using WVU's THDVETL and yielded higher fuel economy [11].

2.3.2   Direct/Dual Fuel Injection Natural Gas Engine (DING/DFNG)

Both the DING and the DFNG engines are based on the diesel cycle. DING engine uses direct injection of natural gas into the cylinder and using a source of ignition such as diesel pilot injection or the glow plug. The DFNG engines induct a premixed charge of air and natural gas with diesel fuel injected late into the compression cycle [9]. Most direct injection natural gas engines use glow plugs as source of ignition. Glow plugs in a diesel engine serve only during cold start and the circuitry is disconnected once the engine warms up. Incase of direct injection natural gas engines, the glow plug circuitry is enabled throughout the engine operation duration. This requires a more durable glow plug design to serve this process. Westport undertook a project to develop a glow plug for this purpose. Westport successfully designed and implemented a catalyst coated glow plug which would reduce the ignition delay and also satisfy durability standards of the automotive industry [12]. The combustion in these types of engines is usually not complete, hence higher PM, hydrocarbons and CO emissions would be seen.

2.4   Exhaust Constituents – Formation and Effects

Combustion of fossil fuels is one of the main causes of air pollution. Automobile exhaust is one of the main concerns of urban air pollution today. Theoretically a stoichiometric combustion of a hydrocarbon fuel would yield only carbon dioxide, water vapor and some oxides of nitrogen. But in reality internal engines combustion process, under high temperature and pressure is a complex mechanism. The products of internal combustion include Carbon Monoxide (CO), unburned Total Hydrocarbons (THC), Oxides of Nitrogen (NOx) which include NO_2, NO and other oxides of nitrogen, Particulate Matter (PM), Carbon Dioxide, water vapor. All these byproducts of combustion are detrimental to the environment. The adverse effects of these constituents have forced environmental agencies to regulate the levels of emissions from internal engine combustion source. The fact that the combustion itself is a complex mechanism, necessitates us to understand the kinetics involved in the formation of these exhaust constituents, so as to better regulate their emissions from internal combustion engines. The EPA has

formulated regulations to regulate the emissions from internal combustion engines. The EPA regulated constituents are CO, NOx, PM, and THC. Although these are the only regulated exhaust constituents, internal combustion of hydrocarbons yield many hazardous air pollutants, for which regulations have not come into effect. These pollutants include aldehyde compounds, Poly Aromatic Hydrocarbons (PAH), Volatile Organic Compounds (VOC), metals, and ultrafine nanoparticles.

2.4.1 Carbon Monoxide (CO)

2.4.1.1 *Carbon Monoxide Formation*

Carbon Monoxide is usually formed as result of incomplete combustion of a fuel rich mixtures. The presence of lesser amount of air with reference to the amount of fuel present inhibits the formation of CO_2 from CO [9]. CO emissions are low from diesel engines as they predominantly operate at lean air to fuel ratios. On the other hand CO emissions from spark ignited engines are significant as they operate close to stoichiometric air fuel ratios [13]. However in diesel engine technology with the absence of sufficient in cylinder charge motion or turbo charging, fuel rich zones may be created within the cylinder resulting in localized incomplete combustion resulting in increased CO concentrations. Natural gas fueled engines would emit higher concentrations of CO due to the fact it is more prone to incomplete combustion. However lean-burn natural gas engines would counter the CO emissions with their controlled lean air-fuel ratios.

2.4.1.2 *Environmental Effects Of Carbon Monoxide*

Carbon monoxide, a colorless, tasteless and odorless gas, is an extremely poisonous gas to animal life. CO has the ability to diffuse quickly into the blood from the lungs and bind with the hemoglobin present in the blood to form Carboxy-Hemoglobin (COHb). This reversible compound is an oxygen inhibitor and prevents the blood from carrying oxygen to the tissues [14]. Although only direct and continuous exposure of CO to humans would prove fatal, it is important to note the effect of ambient levels of CO exposure to animal life. Studies have shown that ambient levels of CO could also interfere with tissue respiration and cause hypoxia

(inadequacy of oxygen to tissues). Studies have also proved that CO affects the functioning of the heart and various actions performed by the brain [14].

2.4.2 Total Hydrocarbons (THC)

2.4.2.1 Total Hydrocarbons (THC) Formation

Hydrocarbon emissions from internal combustion engines are basically the result of incomplete combustion. Hydrocarbon emissions consist of many different hydrocarbon compounds usually the result of pyrolitic reactions undergone by the unburned fuel at high temperature and pressure. All the different hydrocarbon species together are quantified as Total Hydrocarbon emissions (THC). The entry of lubrication oil into the combustion chamber is also a significant source of hydrocarbon emissions, especially in diesel engines. The hydrocarbon emission depends on various factors, such as injection pressure, injection timing, engine load, air-fuel ratio, engine design and fuel type.

One of the primary factors that govern THC emission is the fuel-air ratio of the combustion cycle. Rich fuel mixture yields high levels of THC emission due to the lack of oxygen to burn the excess fuel. In spark ignited engines, which normally operate close to stoichiometric ratios, the main mechanism of THC formation is the deposition of fuel spray on the walls of the combustion chamber and subsequently being exhausted out into the atmosphere during the exhaust cycle of the engine [13]. In the case of diesel engines, the air fuel ratio varies within the cylinder hence regions of rich mixture might be created within the cylinder and these regions might act as the source of THC emission. In both diesel and spark ignited engines THC emission is dominant during cold start of the engine. It is estimated that about 70% of tailpipe hydrocarbon emissions is during the cold start phase of engine operation [15].

The air motion within the cylinder plays a very important role in the mixing process of fuel and air and thereby affects THC emissions. Better fuel air mixing provides better control over the combustion process and lesser THC emissions. Turbocharging of diesel engines has proved to be an excellent solution for controlling hydrocarbon emissions. Turbocharging not only increases the amount of air inducted into the engine per suction stroke but it also creates better in cylinder mixing of fuel and air. The injector design is another important factor governing THC emissions from direct injection spark ignited and diesel engines. Higher injection pressure causes better fuel atomization hence better combustion. Higher fuel

atomization also decreases the ignition delay of the fuel and decreases THC emissions during light engine loads. Better control of fuel accumulation in the sac volume of the injector also reduces THC emissions [16].

2.4.2.2 *Environmental Effect Of THC*

Hydrocarbon emissions into the atmosphere aid in the formation of smog. Smog is a result of reaction between hydrocarbon compounds and oxides of nitrogen in the presence of sunlight. Smog is an adverse environmental effect, which affects both plant and animal life. Smog consists of ozone, and this ground level ozone affects the functionality of the lungs. The ability of smog to block sunlight affects plant life. A study carried out by Geiger [17] elucidates the adverse effect of diesel exhaust in the photo oxidation smog formation process. The study points to the fact that diesel exhaust consists of both oxides of nitrogen, and unburned hydrocarbons (in particular formaldehyde) react immediately in the presence of sunlight to form ozone.

2.4.3 Particulate Matter (PM)

2.4.3.1 *Particulate Matter (PM) Formation*

Particulate matter emissions from internal combustion engines are solid phase emission constituents. PM along with NOx is the most strictly regulated emission constituents from diesel engines. The fact that PM formation is inversely proportional to NOx formation makes the regulations even more stringent. PM basically consists of solid carbon with some amounts of semi volatile hydrocarbons and sulfates adsorbed on to its surface. The actual mechanism of formation of particulate matter is not clear. The nature of PM and quantity of PM measured would greatly vary with sampling method. For uniformity of measurement, regulations have prescribed the method of sampling PM so as to try and quantify every form of PM. Formation and nature of PM would vary with engine load, fuel injection, type of fuel, sampling method. Considering the engine factors that affect PM formation, fuel injection, engine load and fuel type are major factors affecting PM formation. Soot, which is the carbonaceous part of PM is formed in the fuel rich region of the fuel spray. It is believed that combustion in the fuel rich region of the fuel spray freezes and the carbon atoms fuse together to form soot. These soot particles

increases in size as unburned hydrocarbons get adsorbed onto the carbon [18]. Soot formation is a characteristic of liquid fuel jets. Use of very high fuel injection pressure reduces the size of fuel droplets which in turn reduces the amount of soot produced. This is due to the better combustion of highly atomized fuel spray and subsequent reduction in size of carbonaceous soot particles. Studies have shown the use of ultra high pressure injectors in reducing soot content [19]. Lubrication oil consumption has proved to be an important source of PM formation. As diesel engines operate over a long lifespan the gap between piston and cylinder widens, and causes the entry of lube oil into the combustion chamber. Lube oil predominantly made of heavier hydrocarbons, undergoes incomplete combustion and forms the non volatile part of PM. Studies have shown the effect of lube oil viscosity and engine load on the consumption of lube oil and the subsequent effect on PM. Lower viscosity oil and light loads contribute most towards PM emissions from lube oil [20]. Study by Bruce, et al. [21] aimed at calculating the contribution of lube oil to the total PM emissions from a 1993 Cummins diesel engine. Their results showed a 4% average contribution of lube oil to the total PM emissions.

2.4.3.1.1 Ultrafine Nanoparticles

In an effort to reduce the mass of PM emitted, modern diesel engine manufacturers have adapted engine control strategies and after-treatment devices that has resulted in formation of ultrafine nanoparticles [22]. Ultrafine nanoparticles are classified as those which are below 100nm in their aerodynamic diameter. Existing regulations quantify PM gravimetrically in the size range of PM_{10} (PM less than 10 microns in size), which are coarse mode particles and $PM_{2.5}$ (PM less 2.5 microns in size), which are fine mode particles. Ultrafine nanoparticles are further classified as nucleation mode and accumulation mode particles. Nucleation mode particles are those which are less than 30nm in size, and accumulation mode particles are those between 50 and 300nm in size [24]. Particulate matter size distribution usually follows a log normal bimodal distribution, with the first peak in the nucleation mode and the second peak at the accumulation mode. Though the formation of nanoparticles is not clear, the general view point is that accumulation mode particles are made of carbonaceous material, and nucleation mode particles are volatile in nature. Studies involving Scanning Electron Microscope (SEM) analysis have substantiated these claims [25]. The fact that accumulation mode particles are made entirely of carbon, could be used to concluded that their formation is usually in the fuel rich region of the

injector spray jet. However the formation of nucleation mode particles is an unpredictable event. The formation is strongly dependent on atmospheric dilution conditions. Volatile nanoparticles are formed as result of rapid cooling of engine exhaust on mixing with atmospheric air. The hydrocarbons present in the exhaust, undergo nucleation and form nanoparticles [26]. These nanoparticles coalesce with each other and form longer chains of agglomerates. The figure 2.1 [23] shows the mass and particle size distribution of diesel exhaust with the respiratory deposition regions.
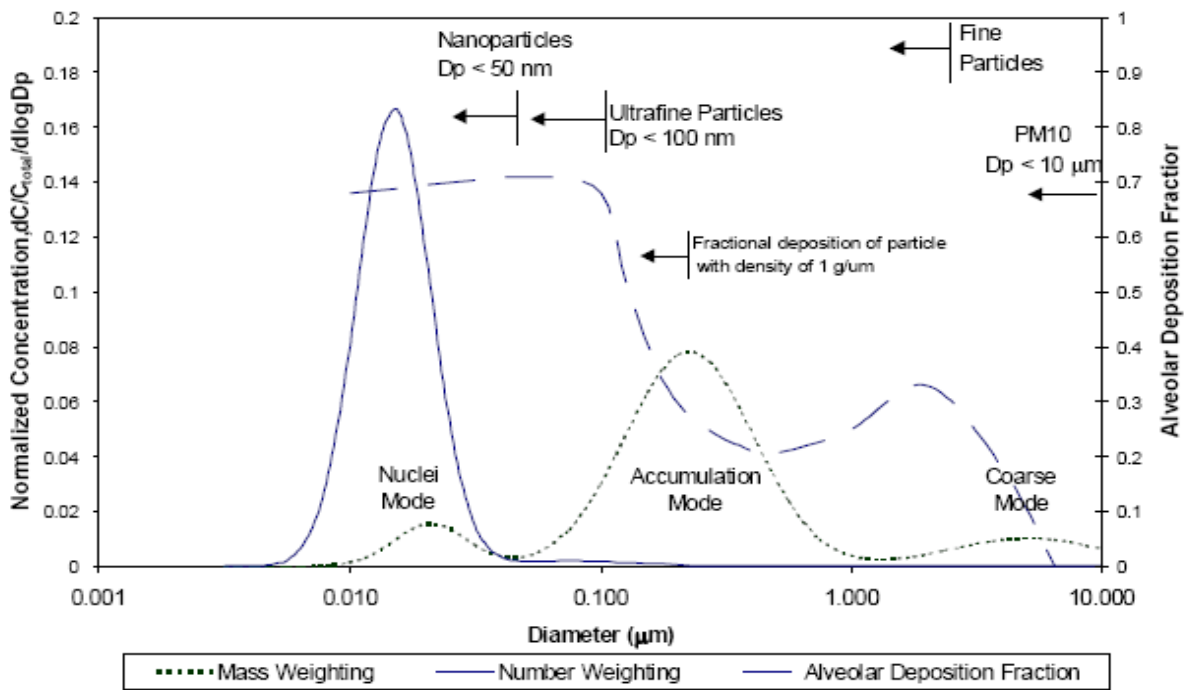
Figure 2.1 Diesel particle size and mass distribution, with respiratory deposition curve [23]

The above figure shows the high number concentrations and minimal mass contribution of nanoparticles. The presence of after-treatment device such as a Diesel Particulate Filter (DPF) increases the concentration of nanoparticles from tailpipe emissions of vehicles. This is due to the fact that unburned hydrocarbons nucleate more in the absence of carbonaceous particles [26]. In the presence of carbon particles, unburned hydrocarbons are adsorbed by it and the process of nucleation is inhibited by the lack of gaseous hydrocarbons in the exhaust. However with the presence of a DPF, the carbon particles are trapped leaving behind only the gaseous hydrocarbons in the exhaust. And when this exhaust cools upon atmospheric dilution, favorable

saturation ratios are attained and volatile nanoparticles are formed [26]. The use of gaseous fuels such as natural gas would not produce any soot, however due to the increased hydrocarbon emissions; there would be increased nucleation mode nanoparticles. A similar phenomenon is seen with spark ignited engines, which operate at stoichiometric air-fuel ratios. The particle size distribution tends to peak, in the nucleation region, and shifting towards accumulation with higher engine loads [27].

2.4.3.2 Environmental Effect Of PM

Particulate matter poses a huge health hazard because of its ability to penetrate into the human airway. And concerns are growing over particles of smaller in size which have the greatest penetration ability into the lungs. The branches of the human airway act as natural impactors filtering out particles inhaled according to their size. Of these the smallest nanoparticles could penetrate all the way into the gas diffusion region of the lungs. This aspect has found to create many lung associated disorders. Diesel engine PM emissions are broadly classified under $PM_{2.5}$ category. A study conducted by the Helsinki metropolitan area, Finland on the health effects of transit bus $PM_{2.5}$ emissions reveals that; in a year there are around 3 to 18 cases of cardiopulmonary and lung associated mortalities [28]. The nature and property of PM is an important factor that has to be considered in order to better understand the health effects. Volatility of PM is an issue which is being widely addressed in the medical field. This is because of the fact that these volatile PM (nano size range) could travel into the alveolar region of the lungs, and the volatile property of these particle take part in the gas exchange process in the lungs. Volatile and semi volatile PM can cause lung inflammation, cancer and gene mutations [29]. Exhaust particle inhalation has found to cause respiratory diseases [30]. PM from vehicle exhaust also contain fine metals, whose source could be traced to fuel additives, lube oil additives and engine wear parts. Most of these metals are very toxic to humans. Exhaust of diesel and gasoline engines contain metals such as lead, zinc, copper, nickel and cadmium [31]. These metals can trigger DNA damage, and affects cell permeability by creating hydroxyl compounds [29]. These metals could also be as a result of degradation of the catalytic after-treatment devices which often contain heavy metals as reducers.

2.4.4   Oxides Of Nitrogen (NOx)

2.4.4.1   NOx Formation

Air contains 78% nitrogen, and combustion of fossil fuels in air would result in the formation of oxides of nitrogen (NOx). Although theoretically a stoichiometric combustion of air and fuel in an internal combustion engine should result only in the emission of un-oxidized nitrogen, practically that it is not the case. The high pressure and temperatures in the combustion chamber, results in the oxidation of nitrogen with the oxygen present inside the combustion chamber. This chemical reaction is further aggravated in diesel engines which operate at very lean conditions, and the excess air present, initiates further NOx formation. The emission of nitric oxide (NO) and nitrogen dioxide (NO_2) are collectively known as NOx. The ratio of NO_2/NO is very small. On an average NO_2 is 10 to 20% of the total NOx [13]. The reactions involving the formation of NOx are known as the Zeldovic mechanism.

$$O + N_2 \longleftrightarrow NO + N \qquad \qquad \textbf{Equation 2.2}$$

$$N + O_2 \longleftrightarrow NO + O \qquad \qquad \textbf{Equation 2.3}$$
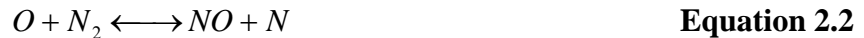
The reactions given by the Zeldovic mechanism is the main source of NOx formation and it is highly dependent on temperature, flame speed and residence time of exhaust gas in the combustion chamber. The NOx forming reactions have very high rate constants; hence NOx production is increased with greater residence time of gases within the combustion chamber. During the exhaust stroke, temperatures drop and the NOx formation freezes. The bulk of the NOx is formed during the diffusion burn phase of the combustion process. This phase is characterized by very lean local air-fuel ratio and high in cylinder temperatures [32]. NOx production rate follows a trade-off curve between itself and PM formation rate. Any steps taken to reduce NOx from the combustion point of view would result in the increase in PM production and vice versa. Turbo charging of diesel engines increases the amount of air intake into the engine and subsequently increases the nitrogen content as well as peak combustion temperatures, and paving the way for increased NOx production. Figure 2.2 [32] explains the rate of NOx formation with respect to heat release, injection pressure and in cylinder temperature. The figure shows the decrease in equivalence ratio with the progress of combustion and subsequent increase

in NOx formation. The higher the injection pressure lower the ignition delay, hence faster the combustion, and subsequently lower NOx emissions [32].
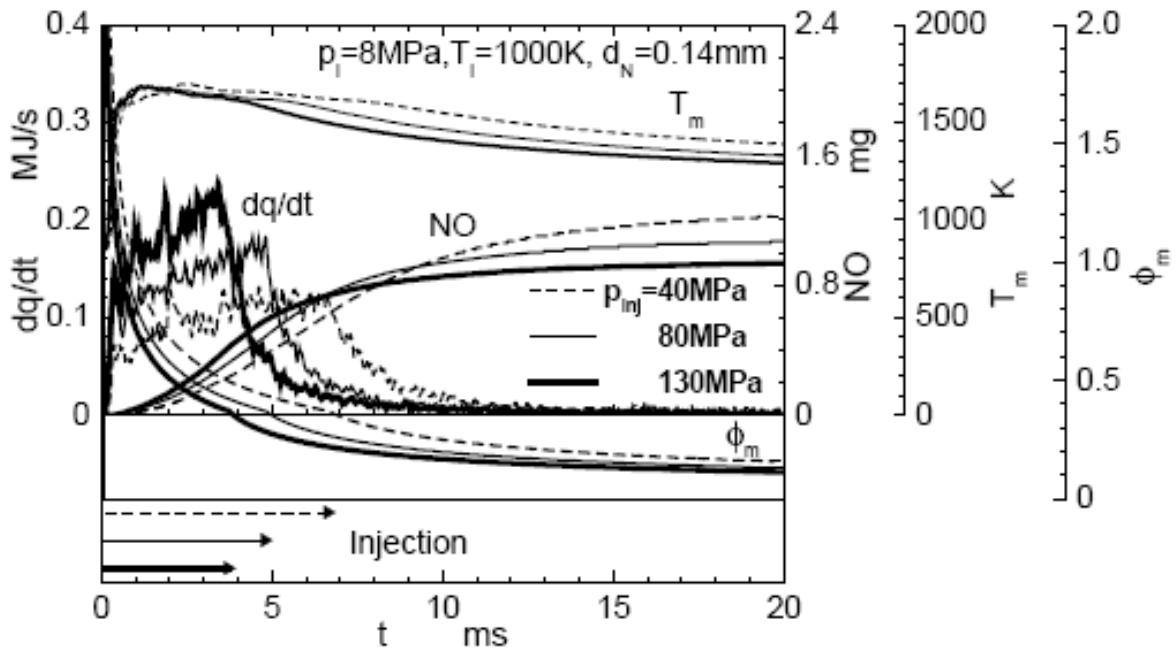
Figure 2.2 Factors affecting NOx formation [32]

One of the upcoming strategies to combat NOx formation is Exhaust Gas Recirculation (EGR) which lowers combustion temperature and thereby decreases NOx formation. Advancing the injection increases the residence time of gases within the cylinder and results in increased NOx production. NO_2 formation is usually a result of oxidation of NO. However NO_2 quickly converts back to NO in the absence of flame quenching. If flame quenching occurs the formation NO_2 freezes. The period of the combustion cycle in which nitrogen dioxide is formed can be traced to a period towards end of the combustion process to the beginning of the expansion stroke when cooling of exhaust begins. This mechanism would agree with NO/NO_2 ratios in the exhaust. NOx production from natural gas engines operating at stoichiometric ratios would be very less than diesel engines, however operating natural gas vehicles, in the diesel cycle with lean burn configurations would result in equal or even higher levels of NOx than diesel vehicles.

15

2.4.4.2 Environmental Effects of NOx

NOx is responsible for the formation of ground level ozone. NOx reacts with hydrocarbon compounds in the presence of sunlight to form ozone. NOx is involved in the formation of smog, which has many adverse environmental effects on plants and animals. NOx reacts with atmospheric water to form acid rain. The increase acidity of water is detrimental to plant life. Acid rain is very corrosive in nature and destroys the aesthetic appearance of many buildings.

2.4.5 Unregulated Emissions

CARB and EPA have identified a list of 244 Hazardous Air Pollutants (HAPs) or Toxic Air Contaminants (TACs). All these pollutants are extremely harmful for humans. Many of these HAP compounds are byproducts of internal combustion of hydrocarbons. They are direct result of pyrolitic reactions within the combustion chamber of an internal combustion engine. These pollutants can be classified as Polyaromatic Hydrocarbons (PAHs), Nitro-Polyaromatic Hydrocarbons (nPAH), Volatile Organic Compounds (VOCs), carbonyls, metals and ions. Regulations to control emissions of these compounds from internal combustion engines have not been put in place. This might be due to the fact that the chemistry of formation of these compounds is unknown. However catalytic after-treatment deices have found to reduce the concentrations of these harmful pollutants from vehicle exhaust. Carbon dioxide is another unregulated emission. Carbon dioxide is an inevitable product of hydrocarbon combustion. In fact the level of carbon dioxide would indirectly represent the efficiency of combustion. Although carbon dioxide is major green house gas and participates in global warming, regulations are not in place to regulate CO_2. Methane is another hydrocarbon which is not regulated. This is due to the fact that methane is non-reactive and not harmful. However methane is a major greenhouse gas and natural gas engines are major emitters of unburned methane.

2.4.5.1 Polyaromatic Hydrocarbons/NitroPolyaromatic Hydrocarbons (PAH/nPAH)

Polyaromatic hydrocarbons are those which contain aromatic or benzene ring in them. Aromatics are present in diesel fuels and hence combustion of diesel fuel would yield unburned aromatic hydrocarbons. PAH compounds also arise as a result of lubrication oil combustion.

PAH compounds are Semi Volatile Organic Compounds (SVOC), they can be either quantified as gas phase or particle bound SVOC. Sampling of PAH compounds would include both particle phase and gas phase compounds. Benzene is one of the basic PAH compounds emitted from diesel engines. There are 93 different PAH compounds and 29 different nPAH compounds that are to be analyzed from vehicle exhaust. PAH generally occur in different phases. PAH compounds could be particle bound, semi volatile phase PAH and gas phase PAH. PAH compounds are found to be extremely carcinogenic in nature [33], and hence it is necessary to quantify the emission levels of these compounds from heavy duty vehicle exhaust. nPAH compounds are extremely toxic compounds whose formation in the engine is not clear. The general viewpoint is that nPAH compounds form with exhaust reacting with atmospheric nitrogen [9].

2.4.5.2 Carbonyls

Carbonyls are compounds in which a carbon-oxygen double bond is present. Aldehydes are formed due to partial oxidation of alcohols or heavier hydrocarbons. Emissions of aldehyde would correlate with the extent of incomplete combustion of engine. Aldehyde emissions increase in low NOx and low PM mode. This could be due to the fact that in the presence of PM aldehydes tend to adhere to them and subsequently concentration decreases while sampling into media [34]. This could be the reason for higher aldehyde emissions in natural gas vehicles. Formaldehyde, acetone, acetaldehyde and acrolein are the major aldehyde compounds seen in diesel and natural gas vehicle exhaust [35].

Aldehydes have found to induce cancer and tumor in exposure studies with rats [29]. They have also identified aldehyde compounds to produce allergic reactions in human exposure studies. Though the carcinogenic effects of aldehyde compounds have not been clearly established, the fact that aldehydes are also responsible for ozone formation reactions in atmosphere makes them a TAC.

2.4.5.3 Volatile Organic Compounds (VOCs)

Volatile Organic Compounds are those categories of hydrocarbons that remain in gas phase in atmospheric conditions. They are basically a more detailed classification of THC

compounds. They can be classified as alkanes, olefins, alkynes and aromatics. They can further be subdivided into their respective groups based upon the number of carbon atoms. There are about 73 different VOC compounds identified in diesel exhaust, which are TACs.

VOCs are extremely harmful to plants and animals. They are carcinogenic and mutagenic in nature [29]. Compounds such as benzene are extremely carcinogenic and it is the widely found aromatic compound in diesel exhaust. VOCs react with NOx in the presence of sunlight to form ground level ozone.

2.4.5.4 *Carbon-dioxide (CO₂)*

CO_2 is an inevitable product of hydrocarbon fuel combustion. The cleaner the combustion more the CO_2 produced. Current regulations do not regulate the quantity of CO_2 produced by internal combustion engines. The only method of reducing CO_2 would be the use of fuel containing lesser number of carbon atoms, such as methane (CH_4) or no carbon atoms such as hydrogen (H_2). Carbon dioxide is major green house gas responsible for the global warming phenomenon. Though CO_2 emission control devices such as CO_2 scrubbers have come into effect in large scale thermal power plants, it's yet to gain importance in the automobile industry. CO_2 measurements in emission testing are merely used as data quality indicator and to compare actual and theoretical fuel consumption values.

2.4.5.5 *Organic/Elemental Carbon(EC/OC) and Metal emissions*

Elemental carbon is primarily the soot residue of combustion and organic carbon is that which has hydrocarbons attached to it. The emission of elemental carbon is usually greatest from diesel engines. And gaseous fuels like natural gas would emit more of organic carbon. However after-treatment device also play an important role in EC/OC emissions as DPF's reduce EC and subsequently the levels of OC appears to be high. Emissions of metals are predominantly a source of engine wear and lubrication oil. Metals emissions also are increased due to wear of after-treatment device which contain metals as catalyst. Metals such as iron, copper and zinc are widely seen in exhaust of internal combustion engines. Elements like phosphorous are used as anti-wear agents in lube oil, and they are also quite often found in vehicle exhaust. Sulfur is a

common element found in vehicle exhaust, which is often detrimental to the functioning of after-treatment devices

2.5   Urban Bus Emission Regulations

The heavy duty truck and bus emissions have undergone continuous periodic changes, so as to keep up with engine technology and increasing vehicle population. Table 2.2 and Table 2.3 summarize the changes in the emission regulations from 1988 to 1998 [9]. It can be seen that California regulations are more stringent than federal emission regulations. Looking at the regulations we see that the bus emissions regulations for NOx and PM is more stringent than other on road heavy duty engines. This is due to the fact that buses operate in populated regions and within city limits were the impact on human population is more.

Table 2.2 EPA Heavy Duty Diesel Engines Emission Standard in g/bhp-hr

Heavy-Duty Truck Engines				
Year	HC	CO	NOx	PM
1988	1.3	15.5	10.7	0.6
1990	1.3	15.5	6.0	0.6
1991	1.3	15.5	5.0	0.25
1994	1.3	15.5	5.0	0.1
1998	1.3	15.5	4.0	0.1
Heavy Duty Urban Bus Engines				
Year	HC	CO	NOx	PM
1991	1.3	15.5	5.0	0.25
1993	1.3	15.5	5.0	0.1
1994	1.3	15.5	5.0	0.07
1996	1.3	15.5	5.0	0.05
1998	1.3	15.5	4.0	0.05

Table 2.3California Heavy Duty Diesel Engines Emission Standard in g/bhp-hr

Heavy-Duty Truck Engines					
Year	NMHC	HC	CO	NOx	PM
1987	-	1.3	15.5	6.0	0.6
1991	1.2	1.3	15.5	5.0	0.25
1994	1.2	1.3	15.5	5.0	0.1
Heavy-Duty Urban Bus Engines					
Year	NMHC	HC	CO	NOx	PM
1991	1.2	1.3	15.5	5.0	0.1
1994	1.2	1.3	15.5	5.0	0.07
1996	1.2	1.3	15.5	4.0	0.05

The US EPA gain reviewed the regulations in 1997 and formulated new regulations for 2004 later model year heavy-duty engines. The regulations required a NOx plus Non-Methane Hydrocarbon (NMHC) limit of 2.4 g/bhp-hr or 2.5g/bhp-hr NOx and a 0.5 g/bhp-hr NMHC. All other standards remained the same. The EPA further tightened regulations for 2007 model year engines with 0.01g/bhp-hr PM, 0.2g/bhp-hr NOx and 0.14g/bhp-hr NMHC.

Air Resource Board (ARB) in 2000 adopted the public transit bus fleet which aimed at regulating emissions of transit fleet agencies. The regulations targeted the transit fleet operators and the engine manufacturers for reducing emissions from urban buses. Pertaining to the transit agencies, transit agencies were required to acquire buses which ply on alternative fuels and hybrid technology to reduce their fleet average emissions and engine manufacturers were regulated to manufacture engines complying with stringent emissions norms. Transit agencies were given the choice of choosing between an alternate fuel path and diesel path [4]. The alternate fuel path requires 85% of buses purchased through model year 2015 to be fueled by alternative methods. Alternative fuels include, propane, LPG, Natural Gas, and hybrid vehicles. The diesel path would require advance engine technology to reduce emissions to very low value. Some key aspects of the transit bus fleet regulations are:

1. To maintain a minimum fleet average NOx value of 4.8g/bhp-hr in both alternative fuel path and diesel path.

2. Regulations require the reduction of PM values by 85% from all urban buses by retrofitting them with ARB-certified particulate traps.

3. 15ppm diesel fuel sulfur content requirement is enforced.

4. Large transit agencies are required to participate in zero-emissions bus demonstration project.

5. Transit agencies in both alternate fuel and diesel path are required to make 15% of all new purchases as zero emission buses.

2.6   Emission Comparison Studies- Diesel and Natural Gas Vehicles

This section would review various studies that have illustrated the emission comparisons between diesel fueled and natural gas fueled heavy duty vehicles. The studies reviewed in this

section would also deal with the effect of after-treatment device on regulated and unregulated emissions from both diesel and natural gas fueled vehicles.

2.6.1 CARB Transit Bus Study

CARB conducted a study in 2001, which aimed at collecting emissions from two late model heavy-duty transit buses in three different configurations. The study aimed at assessing the effects of various driving cycle on regulated emissions, assessing the TAC levels from diesel and CNG buses, and to quantify the levels of ultrafine nanoparticle emissions from the two buses. The CNG buses were powered by a 2000 DDC Series 50G engine, and the diesel buses were powered by a 1998 DDC Series 50 engine. The diesel bus was tested with an Oxidation Catalyst (OC) and with a Johnson Matthey manufactured Continuously Regenerating Technology (CRT) diesel particulate filter. The CNG bus was certified to operate without an oxidation catalyst (OC) [3]. The buses were driven over 5 different driving cycles, which were:

1) Idle operation

2) 55 mph steady state (SS)

3) Urban Dynamometer Driving Schedule (UDDS)

4) Central Business District (CBD)

5) New York City Bus Cycle (NYBC)

Regulated emissions were collected through all the driving cycles to evaluate the differences in emission levels over the different driving cycles. Some cycles were driven over multiple lengths to get sufficient PM mass loading [3]. The first phase of the study examined the effect of 5 different driving cycles on regulated emissions from CNG without after-treatment device and Diesel bus in 3 different after-treatment configurations. The second phase involved unregulated emissions sampling on 55mph steady state and CBD cycle from CNG bus with and without OC and diesel bus with OC and with DPF. Particle sizing was performed in this phase with the help of Scanning Mobility Particle Sizer (SMPS).

The results of the study showed consistent lower NOx emissions from CNG vehicles in comparison to the diesel fuel vehicles of different configurations. Figure 2.3 shows the distance specific NOx emissions over the different driving cycles and different vehicle configurations. The figure reveals a CNG re-test data which has consistent increase in NOx emissions from the original CNG test results. The author's clarification regarding this behavior is that, prior to the retest of the CNG vehicle the vehicles engine control unit (ECU) software was upgraded and

new oxygen sensor was fitted to the vehicle as a maintenance procedure. This might have operated the engine at leaner fuel-air mixture than before [3].
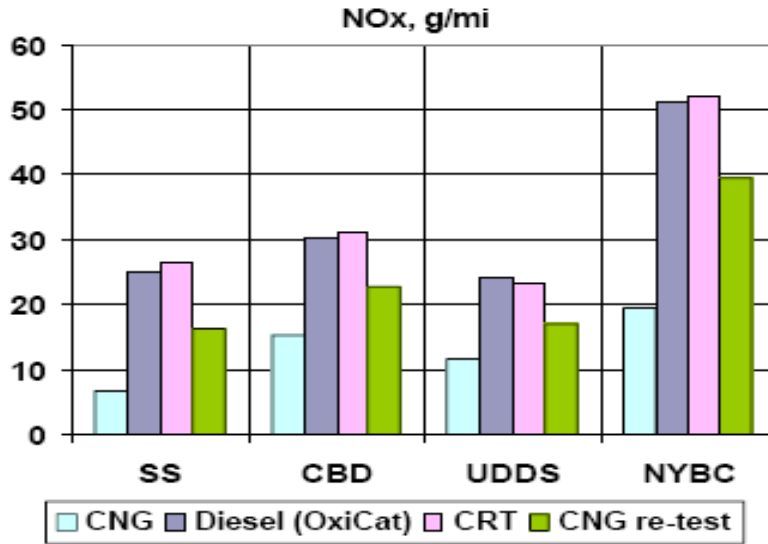
Figure 2.3 NOx emissions results from CARB 2001 study [3].

CARB PM results from the study shown in Figure 2.4 cleary illustrate the effect of CRT on reducing soot. The levels of PM from the CRT in most cases were less than PM emissions from CNG vehicle operating without an after-treatment device. The only exception in this trend was seen in the NYBC, which emitted the highest PM loading from all test configurations with CNG emissions being the least. A similar trend was seen in hydrocarbon emissions results shown in Figure 2.5, with CRT THC levels were below detectable limits in most cases. Methane was found to be the major hydrocarbon constituent from CNG vehicles hence hydrocarbon emission values for CNG vehicles are presented as Non-Methane Hydrocarbon (NMHC) [36].
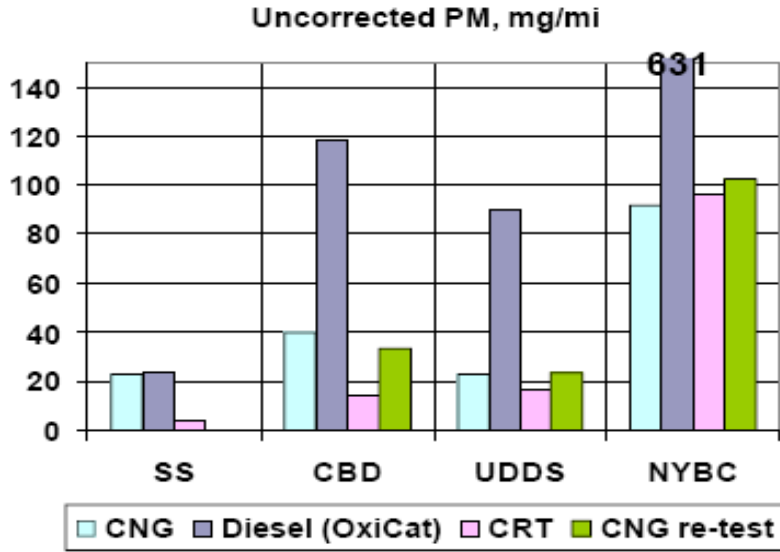
Figure 2.4 Uncorrected PM emissions results from CARB 2001 study [3].
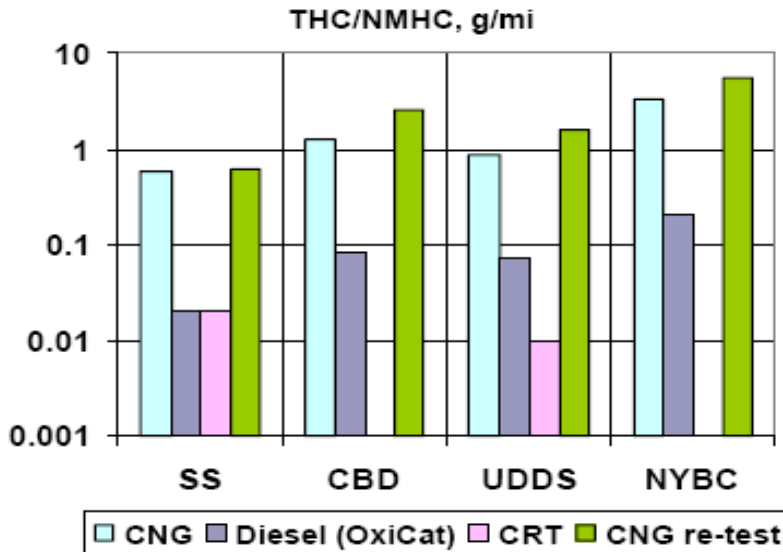
Figure 2.5 THC/NMHC emissions results from CARB 2001 study [3].

The CO emissions from CRT and OC equipped diesel vehicles were lesser than the CNG vehicles. CO from CRT equipped vehicles was close to detection limits. Figure 2.6 shows the CO emissions from the CARB study.
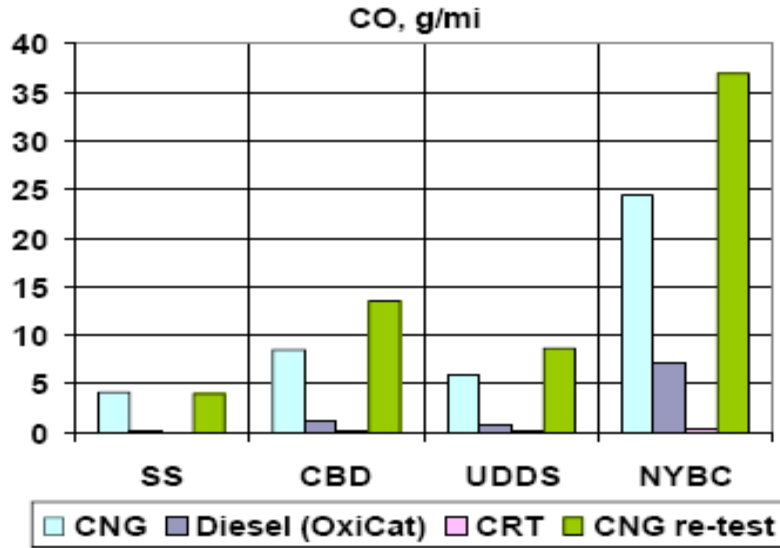
Figure 2.6 CO emissions results from CARB 2001 study [3].

Figure 2.7 shows CARB's data of elemental/organic carbon (EC/OC) and metals emissions form the diesel and CNG vehicles. Elemental carbon was found to be the highest from the Organic Carbon equipped diesel vehicles, in the absence of particulate trap. The concentration of both elemental carbon and organic carbon decreased with the presence of DPF. The oxidation catalyst did not affect the organic carbon fraction. The results also indicated the higher concentration of organic carbon from CNG vehicles. The results also indicated the decrease in organic carbon concentration from OC equipped CNG vehicles. The results have revealed a consistent increase in metal content with the presence of OC in both diesel and CNG fueled vehicles [36]. The study has not interpreted this result; however it could be due to the shedding of metallic elements from wear of the oxidation catalyst.
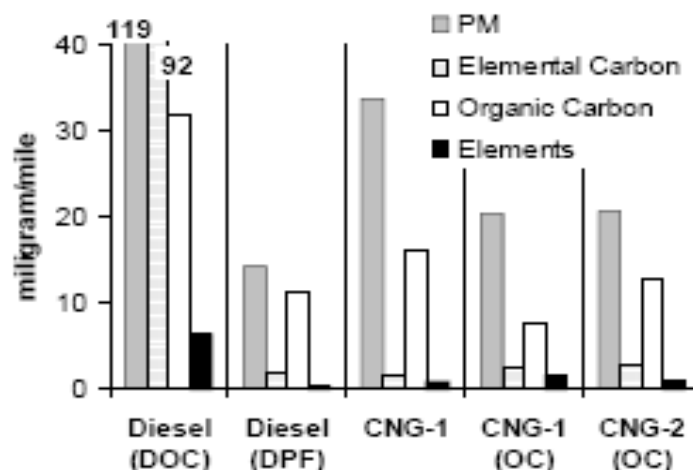
Figure 2.7 EC/OC and Metals emissions results from CARB 2001 study [36].

From CARB's results, the highest total aldehyde concentration was seen in CNG vehicle without OC configuration. Formaldehyde and acetaldehyde were seen as the major constituent in the aldehydes emissions of CNG vehicle. There was about 90% reduction in aldehyde concentrations with OC. The least aldehyde concentrations were seen from diesel vehicle with DPF present. Figure 2.8 shows carbonyl emissions from CARB study. The VOC speciation results showed benzene as the major constituent, and its concentration from diesel vehicle with OC and CNG vehicle without the catalyst were of the same order of magnitude. The PAH speciation showed volatile and semi-volatile PAH dominant in CNG vehicles and diesel vehicle with DPF. The OC reduced PAH concentration by half [36].
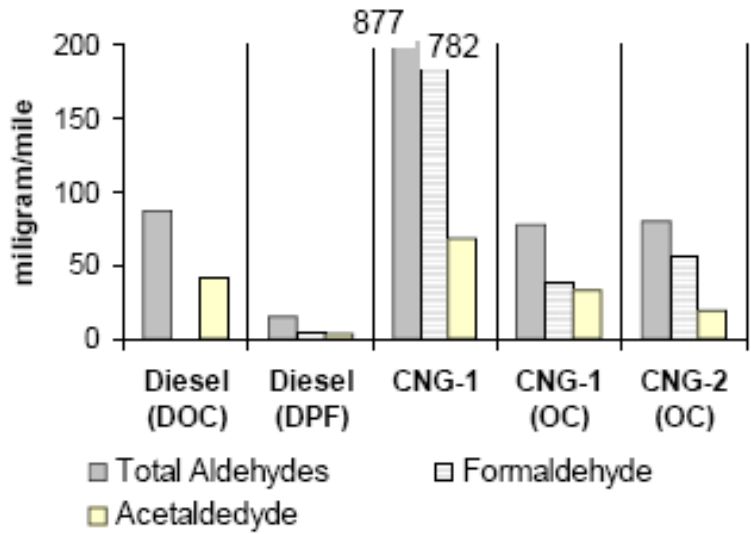
Figure 2.8 Carbonyl emissions results from CARB 2001 study [36].

CARB results on particle sizing showed that emissions of ultrafine nanoparticles from CNG vehicle were lower by an order of magnitude than diesel vehicles. However the nature of ultrafine nanoparticles from CNG vehicles was generally nucleation mode particles. The results also showed concentrations of nanoparticles from diesel vehicles equipped with CRT trap was of the same order of magnitude from that emitted by CNG vehicles [37].

2.6.2 Southwest Research Institute (SWRI) School Bus Study

This research was conducted by SWRI in collaboration with International Truck and Engine Corporation. The study was conducted on school buses meeting the 1998 diesel engine emission norms. This study focused extensively on sampling and quantifying unregulated emissions from diesel and CNG fueled school buses. Two buses (Diesel fuel bus and CNG fueled bus) were tested in three different configurations. The diesel bus was operated on a conventional diesel (CD) mode, and low emitting diesel (LED) mode with a Catalyzed Diesel Particulate Filter (CDPF) fitted to it, and the CNG fueled vehicle was certified to operate without and after-treatment device. The diesel engine tested was a model year 2001 enigne manufactured by International and CNG engine was a model year 2000 engine manufactured by John Deere. Both the engines were similar in their power rating and engine capacity. The buses were tested on chassis dynamometer and driven over a City Suburban Heavy Vehicle Cycle (CSHVC).

Figure 2.9 shows the regulated emissions results obtained by SWRI. The results also include sulfates and soluble organic fraction (SOF) emissions. The results of the study showed the greatest emission benefit in terms of CO, THC, PM and NOx was obtained from diesel vehicle equipped with CDPF [38].
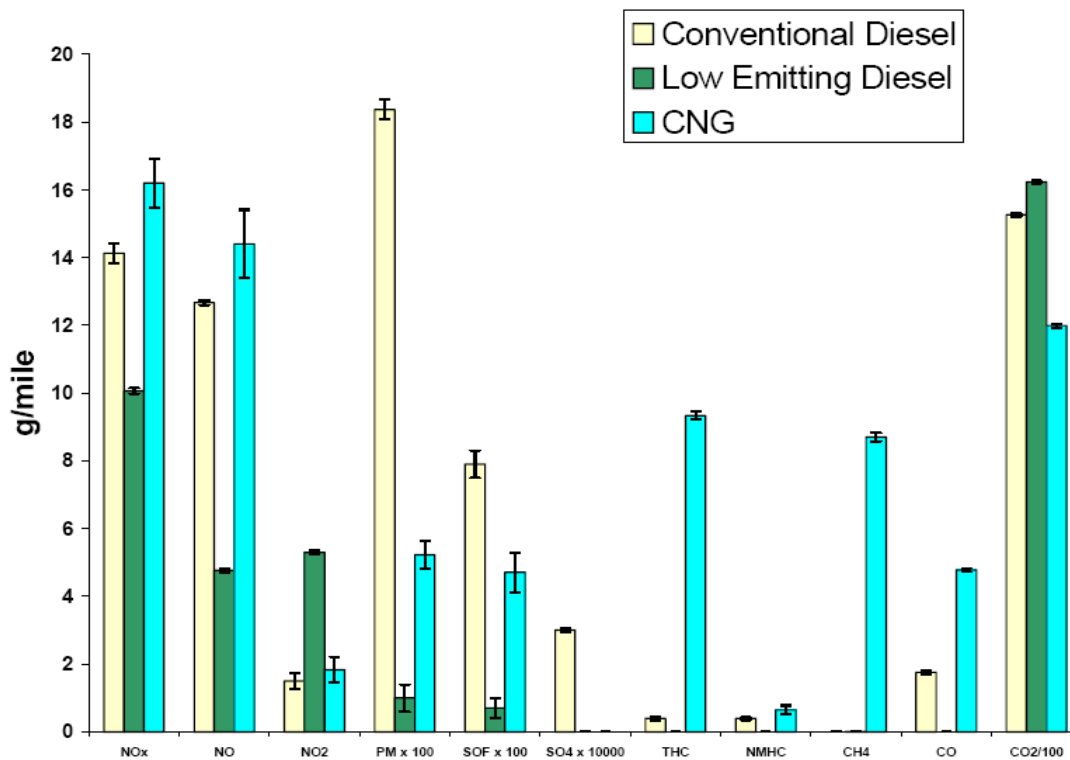
Figure 2.9 Regulated emissions results from SWRI school bus study [38].

The unregulated emissions results of this study showed no traces of 21 of the 41 TACs listed by CARB as sources from diesel exhaust [38]. SWRI had setup their sampling and analysis system to sample and detect even extremely low concentrations of TACs. Figure 2.10 shows the emissions of the remaining 20 of the 41 TACs. Statistical analysis of the TAC data by SWRI showed that for many compounds the levels of emissions between CNG vehicle and CDPF equipped diesel vehicles were statistically the same. CNG vehicles emissions were extremely high for formaldehyde, acetaldehyde, acrolein, methyl ethyl ketone, Phosphorous and propionaldehyde when compared to LED configuration diesel vehicle. The total PAH emissions from LED and CNG vehicles were lesser than CD vehicle by over 2 orders of magnitude.
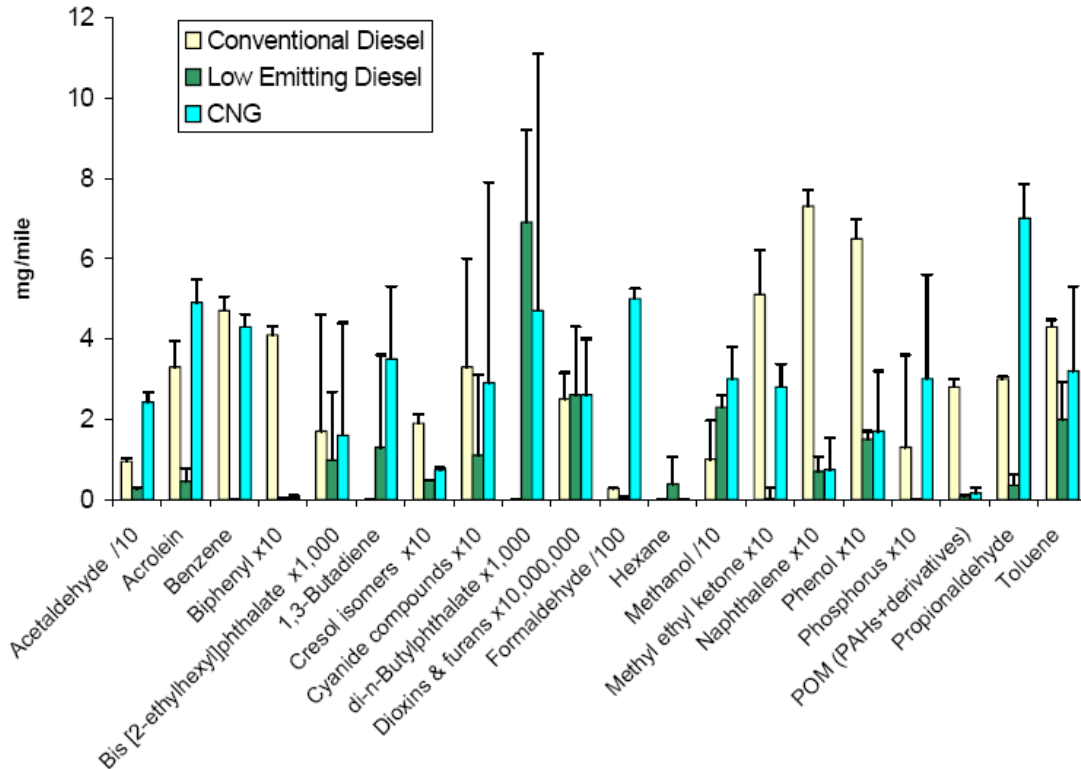
Figure 2.10 TAC emissions results from SWRI school bus study [38].

Finally a caner potency test was also carried out by SWRI and international. The test identifies TACs responsible for cancer a gives weightage according to the threat level associated with it. Formaldehyde and 1, 3 Butadiene were given the highest weightage of more than 95% and subsequently CNG vehicles without any after-treatment device came out to be the most cancer potent vehicle. However it is to be noted that an oxidation catalyst efficiently reduces formaldehyde and 1,3 butadiene to ambient concentrations.

2.6.3 VTT Processes Transit Bus Study

VTT processes a research organization based in Finland carried out emission performance testing of both diesel and CNG vehicles. The study utilized three diesel buses and four natural gas buses. The vehicles tested were fitted with engines of model year 2002 through 2004. The diesel buses were Euro 3 complaint models. The vehicles tested included vehicles configurations with no after-treatment device, with an oxidation catalyst, and with CRT. The

study was conducted on a chassis dynamometer over a European Braunschweig cycle and the OCTA cycle [39].

The main objectives of this study were to evaluate the performance of clean diesel fuel, diesel after-treatment devices, and the performance of CNG vehicles. The study also wanted to substantiate or refute certain claims made in previous studies about natural gas engines emission performance with respect to aldehyde emissions and particulate number concentrations. For this purpose VTT tested buses which were of the latest engine model and excellent conditions [39].

VTT results showed Lean Burn (LB) CNG vehicles CO emissions were of the same order of magnitude of that of diesel with after-treatment device. However the CO emissions from Lean Mixture (LM) CNG vehicle with three way catalyst was twice that of diesel and CNG vehicle with OC. Further CO emissions from Stoichiometric Mixture (SM) CNG vehicles was twice the CO emissions from diesel vehicle with no after-treatment device. The results also showed that OC reduced CO emissions by about 85% [39]. Figure 2.11 shows VTT results of CO emissions from various configuration vehicles.
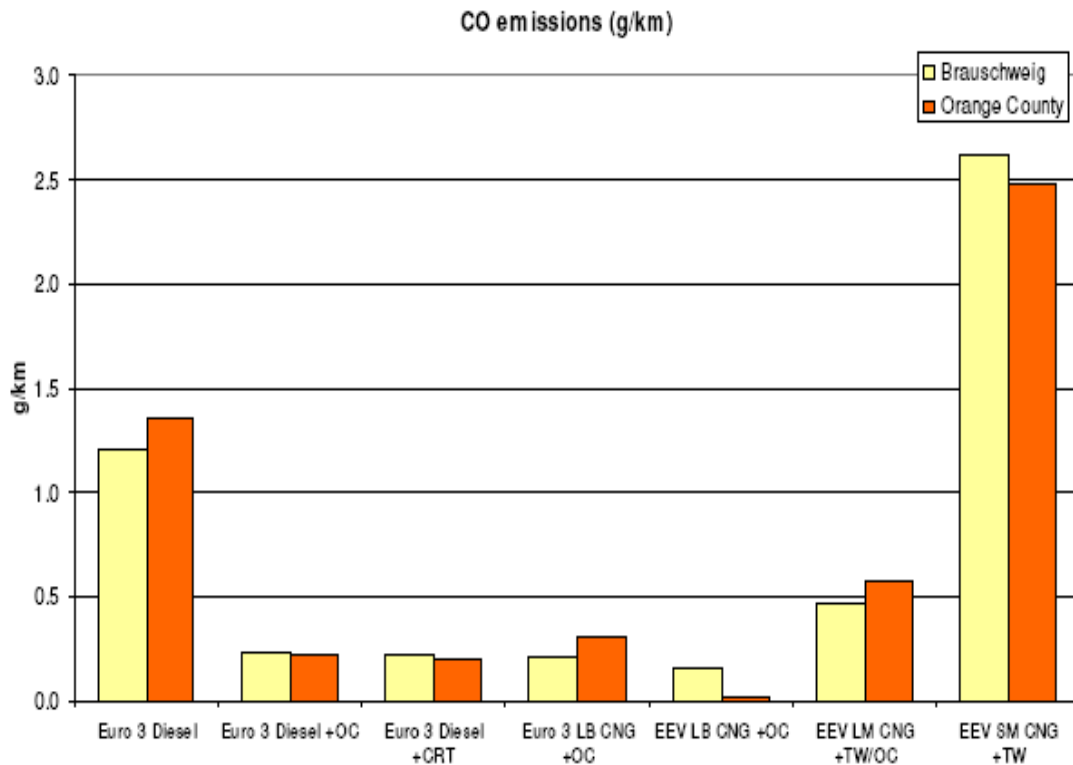
Figure 2.11 CO emission results from VTT study [39].

The results for THC obtained VTT showed the usual trend of CNG vehicles producing higher THC emissions than diesel vehicles. The results showed OC reduced THC emissions by 75% and CRT reduced THC emissions by 90%. The THC emission results showed that CNG vehicles produced more than 98% methane as HC emissions and the catalyst was not very effective in reducing methane. Figure 2.12 shows the Methane/NMHC split results from Braunschweig cycle [39].
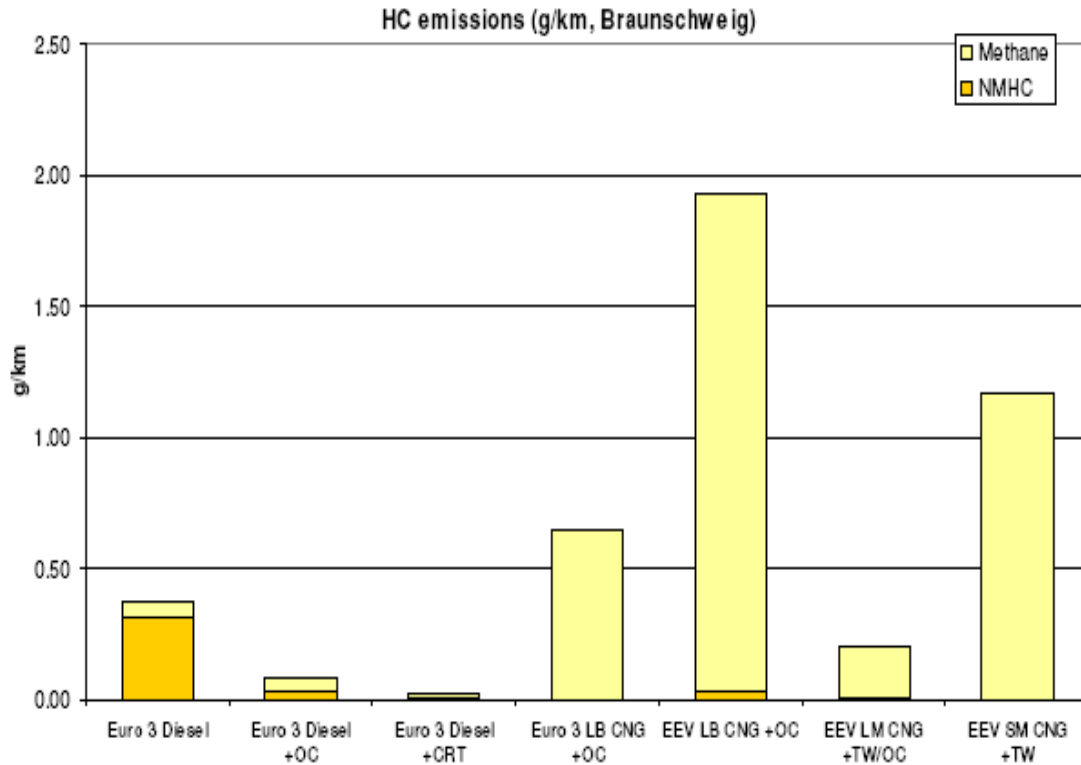
Figure 2.12 CH$_4$/NMHC emissions results from VTT study [39].

The NOx emissions from VTT study showed the usual results of CNG vehicles producing lesser NOx than diesel vehicles, with the exception of LB CNG vehicle whose NOx emissions where equivalent to diesel vehicles NOx output. VTT presented results of NO$_2$ fraction of NOx from one of the driving cycles, and the NO$_2$ fraction of NOx from CRT equipped vehicles was about 6 times that of baseline diesel vehicle [39]. This is due to the fact that NO is oxidized to NO$_2$ by catalytic oxidation reactions to enable oxidation of carbon in the trap. Increased NO$_2$ was also seen from OC equipped vehicles due to similar reason. Figure 2.13 shows NOx results over two different driving cycles.
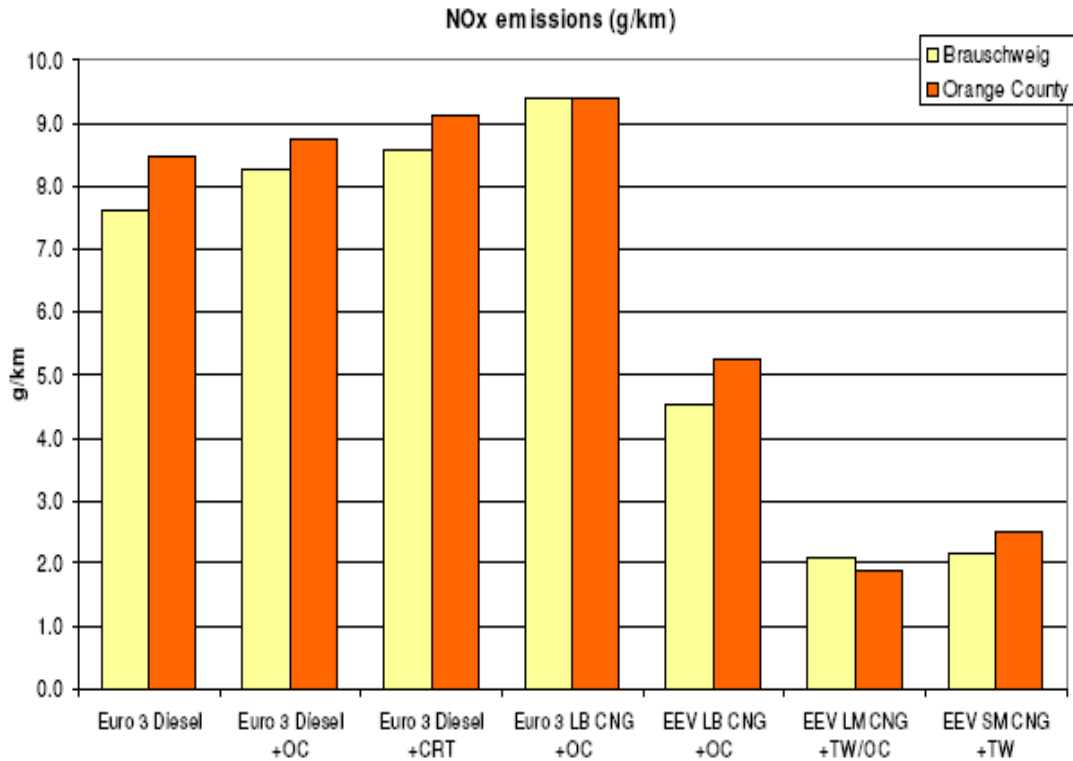
Figure 2.13 NOx emissions result from VTT study [39].
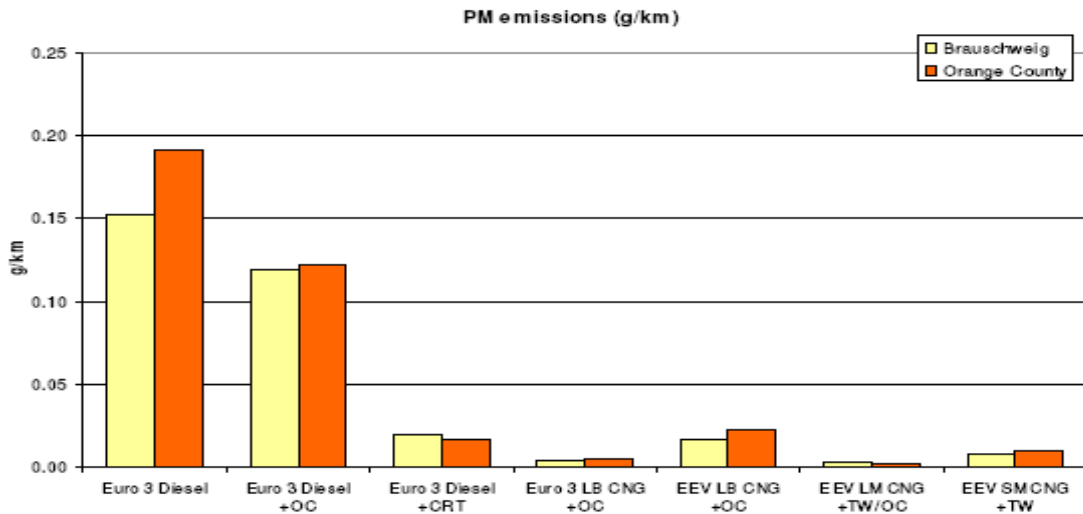
Figure 2.14 PM emissions results from VTT study [39].

VTT PM emissions results shown in Figure 2.14 reveals the usual trend of very low PM emissions from CNG vehicles. Diesel vehicle with CRT produced PM emissions close to CNG vehicles [39].

VTT also conducted particle sizing study using Electrostatic Low Pressure Impactor (ELPI). However their results do not establish a clear particle size distribution even for baseline diesel vehicle. The results show that an accumulation mode is seen from baseline diesel vehicle around 100nm. But the results also show the occurrence of the same peak with the CRT present and very marginal difference in size distribution. Study conducted by Ayala. et al. [37] clearly show the formation of nucleation mode peak downstream of DPF due to condensation of hydrocarbon in the absence of soot. One possible interpretation to this data could be that smaller particles were lost due to diffusion in the upper stages of the electrostatic impactor. However VTT results show a decrease in total particle concentration by one order of magnitude between baseline diesel and diesel with OC. Further it also shows that total particle concentration between diesel vehicle with OC and LB CNG vehicle with OC of the same order of magnitude [39].

VTT performed exhaust gas hydrocarbon speciation of 12 compounds. The results revealed presence of 1,3 Butadiene only from baseline diesel vehicle. OC reduced VOC concentration by 50% [39]. Formaldehyde results of VTT contradict SWRI school bus study results by showing the highest formaldehyde emissions were from baseline diesel rather than CNG vehicle. Figure 2.15 shows the aldehyde emissions over Braunschweig cycle. FA represents formaldehyde and AA represents acetaldehyde.
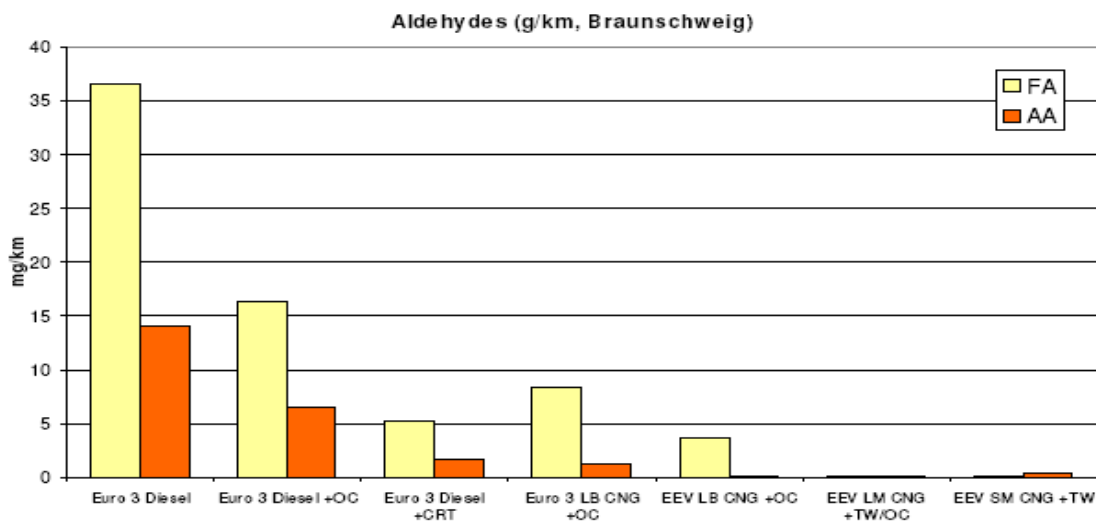
Figure 2.15 Aldehyde emissions from VTT study [37].

Results showed highest PAH levels from diesel with and without OC and lowest from CNG with OC. Most of the PAH emissions from CNG vehicles were found to be engine oil derived. CRT was very effective in reducing PAH emissions [39].

2.6.4   WVU-BP Truck and Bus Study

This study was conducted in the spring of 2001 and focused extensively on the characterization of organic compounds from the exhaust of trucks and buses. This study was industry-government collaborative testing of vehicle fleets from southern California. The study was aimed at assessing the levels of toxic organic compound emissions from vehicles running on different fuels and retro fitted with different after-treatment devices. Though the entire project consisted of testing about 150 vehicles from six different fleets only a subset of the vehicles were used to characterize the unregulated emissions. This study proves as an excellent basis to understand the comparative emission profiles from different technology vehicles. The analysis of the unregulated species was carried out by Desert Research Institute, Reno, Nevada. The chosen vehicles were part of a school bus fleet, transit bus and a grocery truck fleet. The unregulated speciation included unregulated gravimetric PM, VOC, carbonyl compound and PAH [40].

As the work in this thesis is based only on CNG transit bus, the review of this literature will be limited only to the results of the transit buses. The diesel vehicles were equipped with CRT and tested in two configurations with and without the CRT on two different fuels. The two CNG vehicles were not equipped with any after-treatment device [40]. The results of VOC speciation show that the CNG fueled transit bus emissions are greater than diesel vehicle of all fuels and configurations by one order of magnitude. This is due to the stoichiometric operation of the CNG transit buses.
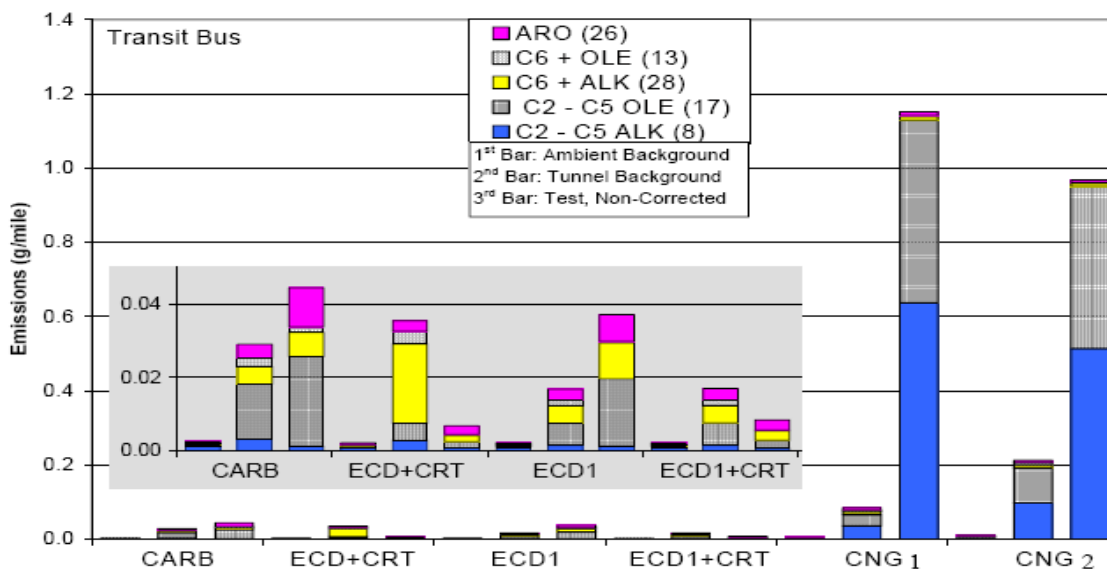
Figure 2.16 Transit Bus VOC Speciation Results from WVU-BP Study [40].

The results also show the higher concentrations of lower carbon number hydrocarbons in the exhaust of CNG vehicles than the diesel fueled vehicles [40]. WVU's presentation of the data in the form of tunnel back ground, ambient background and test uncorrected helps us better understand the interference of the background levels of species to the test value.

The results of the carbonyl compounds speciation show that emissions from CNG vehicles are one order of magnitude higher than diesel vehicles and moreover the presence of CRT in diesel vehicles has reduced carbonyl compounds below ambient levels [40]. This could be due to the trapping of carbonaceous compounds onto which aldehydes were adsorbed. Formaldehyde and acetaldehyde was the major contributor to emissions from all vehicles.
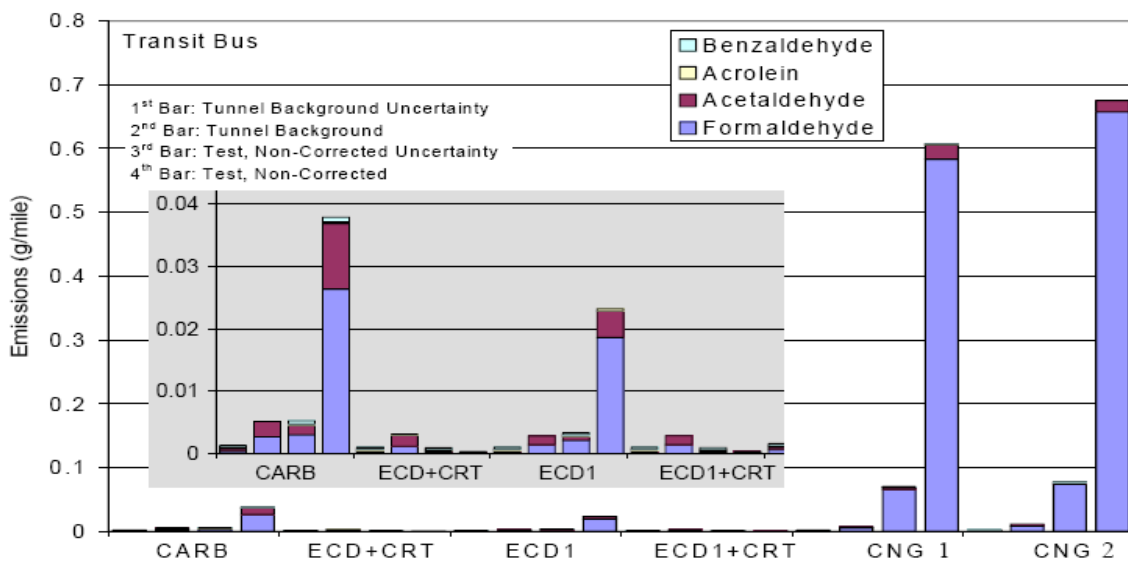
Figure 2.17 Transit Bus Carbonyl Compounds Speciation Results from WVU-BP Study [40].

The results of the semi volatile PAH analysis shown in figure, figure, figure reveals that emissions from baseline configuration diesel buses were an order of magnitude greater than baseline CNG vehicles [40]. This is due to the fact that unlike diesel fuel CNG does not contain aromatic fractions in it. Most of the aromatic compounds emissions from CNG vehicle are due to lubrication oil combustion. The results of the PAH emissions show that the CRT DPF reduces PAH emissions by over 90% and levels found with the DPF were lesser than levels from CNG vehicles [40]. A similar trend is also seen in emissions of nitro-PAH compounds [40]. These compounds are believed to be formed in ambient air as a result of reaction between ambient nitrogen oxides and PAH compounds from automobile exhaust [40].
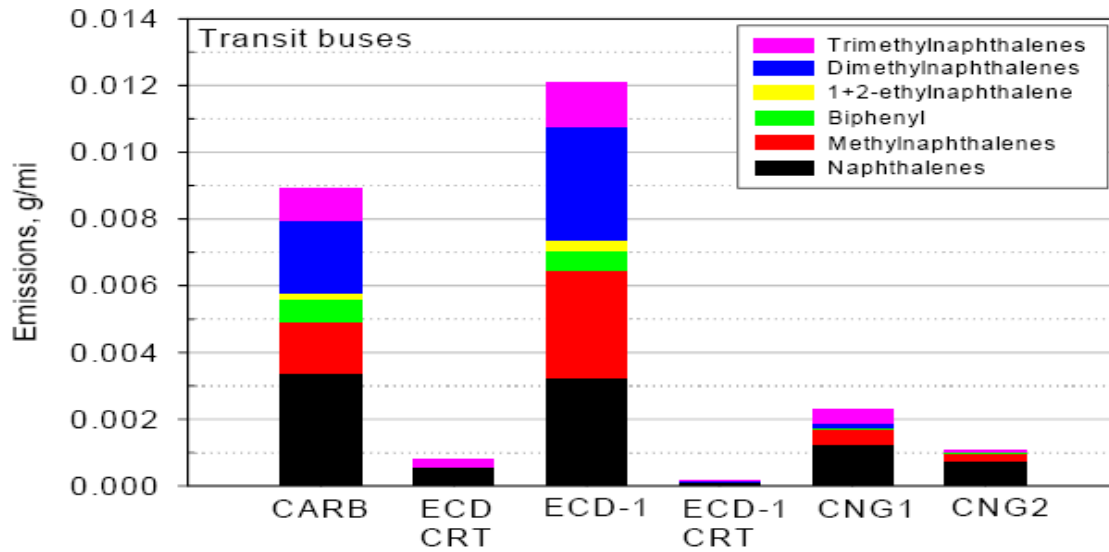
Figure 2.18 Transit Bus Semi Volatile 2 Ring PAH Compounds Speciation Results from WVU-BP Study [40].
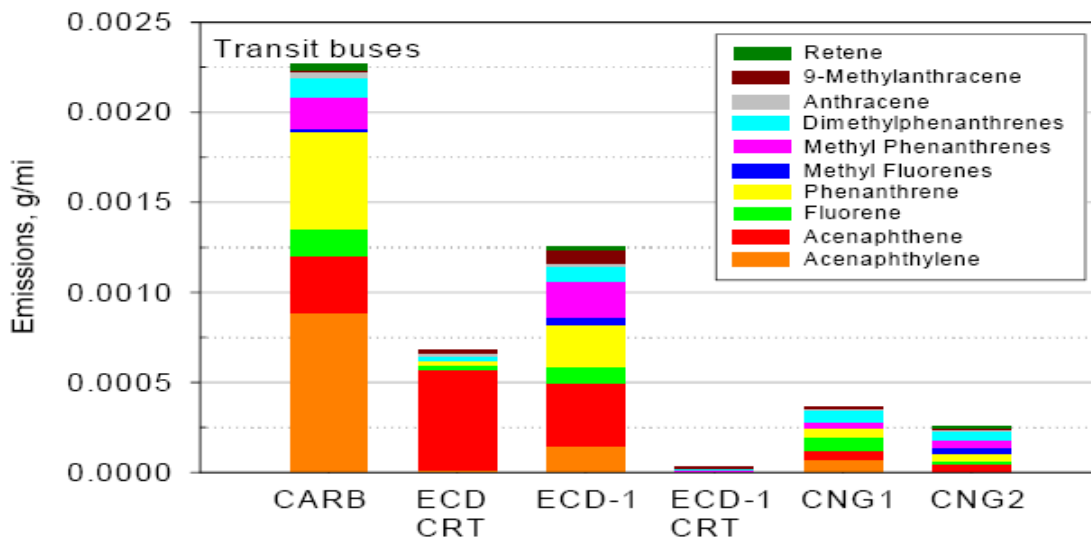
Figure 2.19 Transit Bus Semi Volatile 3 Ring PAH Compounds Speciation Results from WVU-BP Study [40].
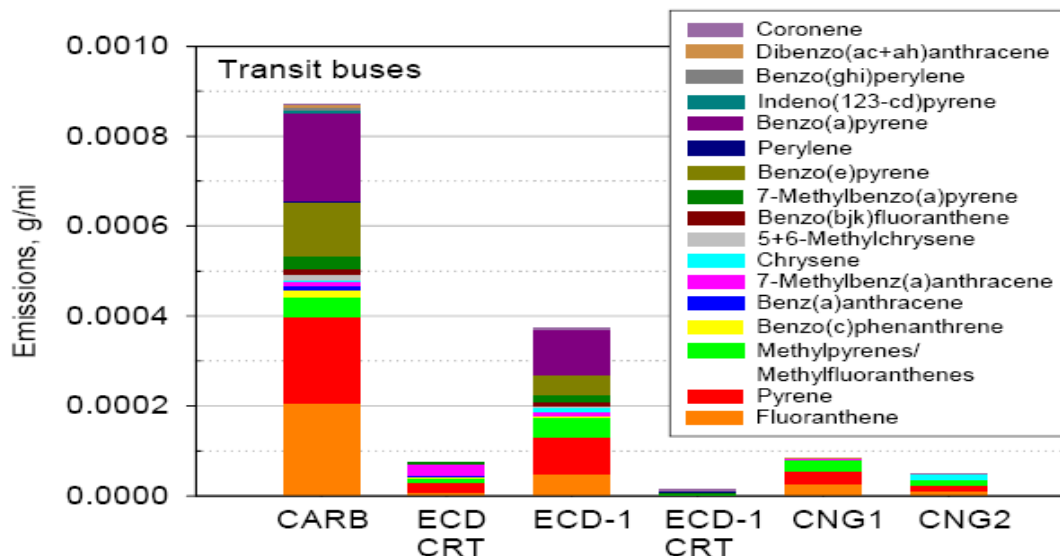
Figure 2.20 Transit Bus Semi Volatile 4 Ring PAH Compounds Speciation Results from WVU-BP Study [40].

2.6.5   WVU-WMATA Study

This study was conducted by National Renewable Energy Laboratory (NREL) in conjunction with WVU for evaluating emissions from transit bus operating in the Washington Metropolitan Area Transit Authority (WMATA). The study was aimed at assessing the emissions from natural gas transit buses and improving emissions from comparable diesel engine buses by suitable after-treatment device. 12 WMATA buses were tested using WVU's heavy duty vehicle emission testing transportable laboratory. The test buses were of lean burn CNG buses with oxidation catalyst and diesel buses fueled by ultra low sulfur diesel and equipped with catalyzed particulate trap. Some buses also operated with EGR. CNG buses were powered by either a 2004 mode year John Deere engine or a 2001 model year Cummins Westport, Inc (CWI) C Gas Plus engines. Diesel buses were powered by Detroit Diesel Corporation (DDC) Series 50 engines. The buses were tested on a WMATA custom driving cycle, which represents the driving pattern of the WMATA buses [41].

WMATA results showed NOx emissions from CWI CNG vehicles operating under lean burn conditions equivalent to diesel vehicles. However NOx emissions from John Deere CNG vehicles were about 50% lower than emissions from vehicles of other configuration. This could have been due to the John Deere vehicles operating at a richer mixture than CWI CNG vehicles.

PM emissions from CNG and Catalyzed Particulate Trap quipped diesel vehicles were close to detection limit. Since all vehicles were equipped with some sort of catalytic after-treatment system, the CO and THC emissions were very low and close to detection limits [41]. Methane emissions for the WMATA study were characterized separately by WVU and NREL. WVU method involved calculating the methane fraction using a Gas Chromatograph (GC) and the standard THC FID analyzer. Methane concentration is obtained by subtraction of NMHC (obtained as ratio from GC analysis) from FID THC value. NREL method involved the complete speciation of exhaust for all hydrocarbon species and quantifying methane concentration. The results showed a very good correlation between both methods [41]. Figure 2.16 shows the methane values obtained by the two different methods.
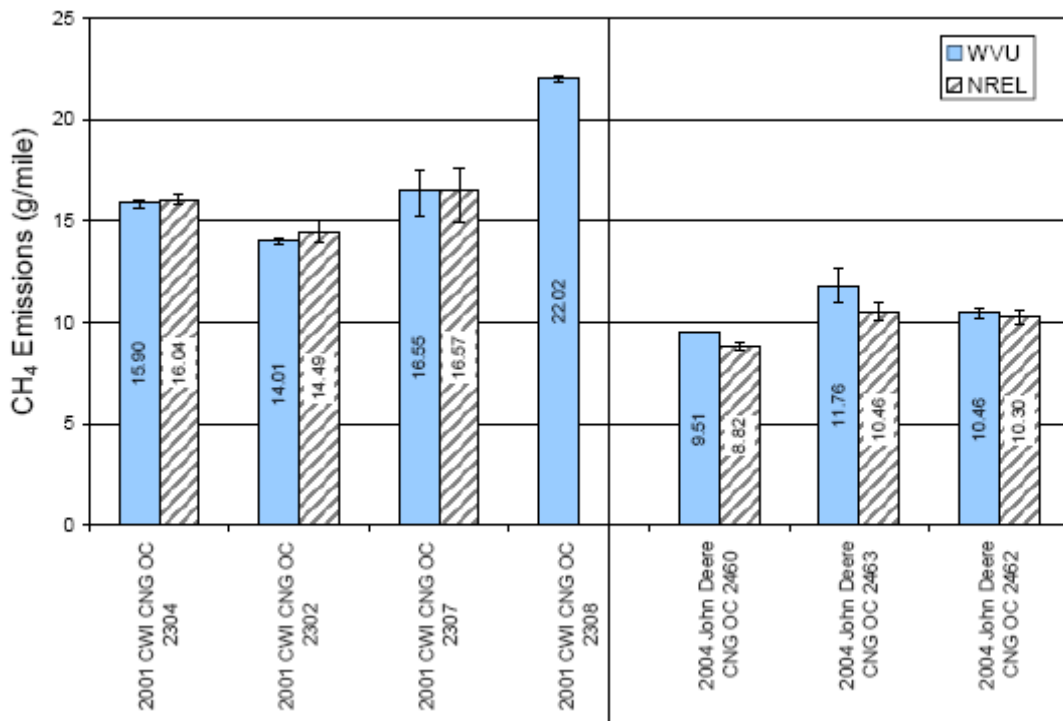
Figure 2.21 CH$_4$ emissions comparison between WVU and NREL method from WMATA study [41].

The WMATA study conducted very limited unregulated speciation work. The project had involved only the speciation of carbonyl compounds. However the report states the attempt made

to quantify BTEX compounds and 1,3 Butadiene. Due to sensitivity issues with the GC the numbers were not reported. The results of formaldehyde emissions show that the levels of emission for John Deere engines quipped CNG vehicles and diesel buses as nearly same. However the CWI CNG vehicles showed increased levels of formaldehyde emissions. Oxidation catalyst had seemed to reduce formaldehyde concentrations to ambient levels in most vehicles. Figure 2.17 shows formaldehyde emission results from the WMATA study. The CWI CNG vehicles were the highest emitters of acetaldehyde. Acetaldehyde concentrations for all other vehicle configurations were close or below detection limit [41]. Figure 2.18 shows the acetaldehyde emissions from WMATA study. Figure 2.19 shows acetone levels in the exhaust. The oxidation catalyst had reduced acetone levels to background levels.
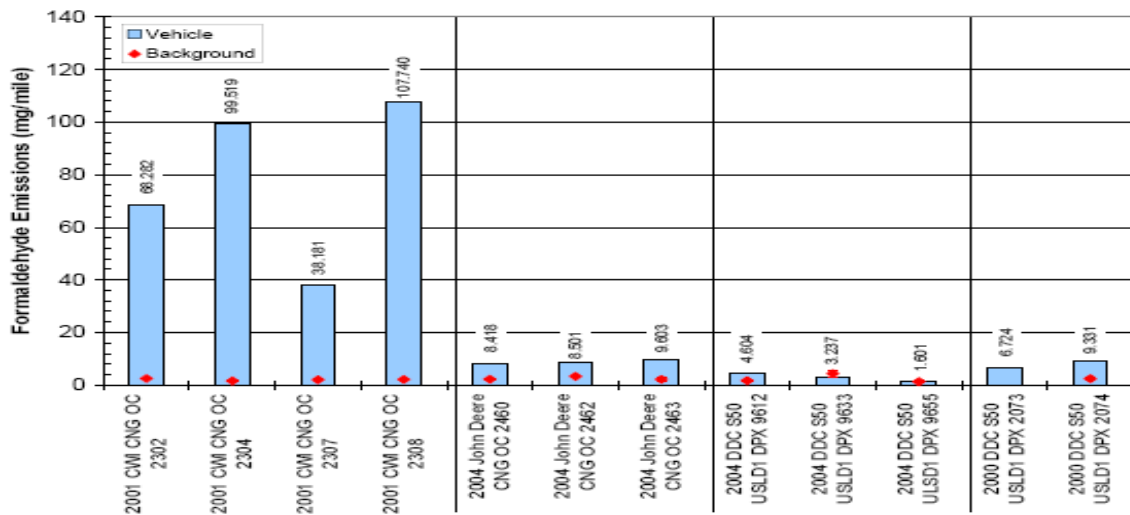
Figure 2.22 Formaldehyde emissions results from WMATA study [41].
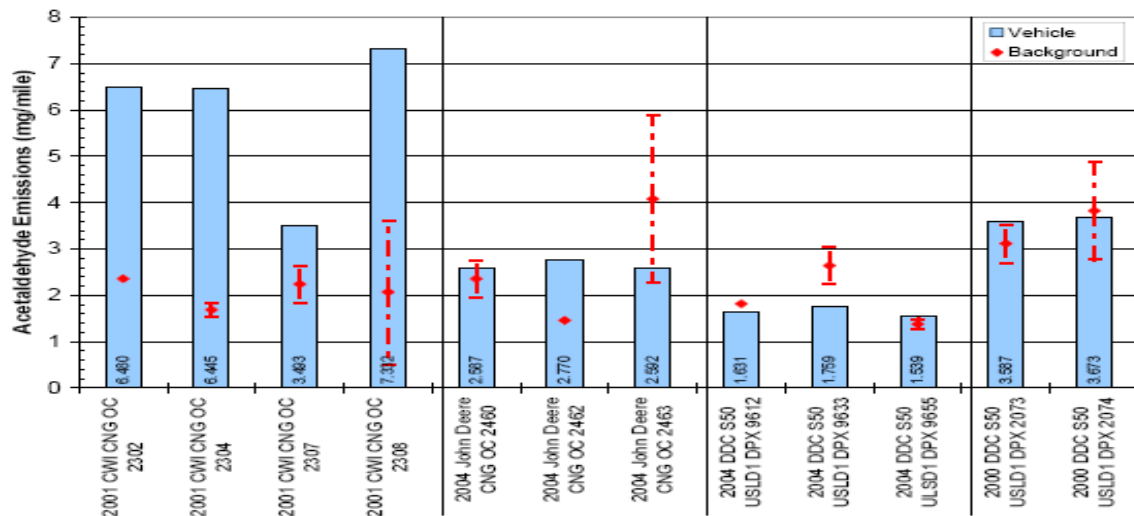
Figure 2.23 Acetaldehyde emissions results from WMATA study [41].

38
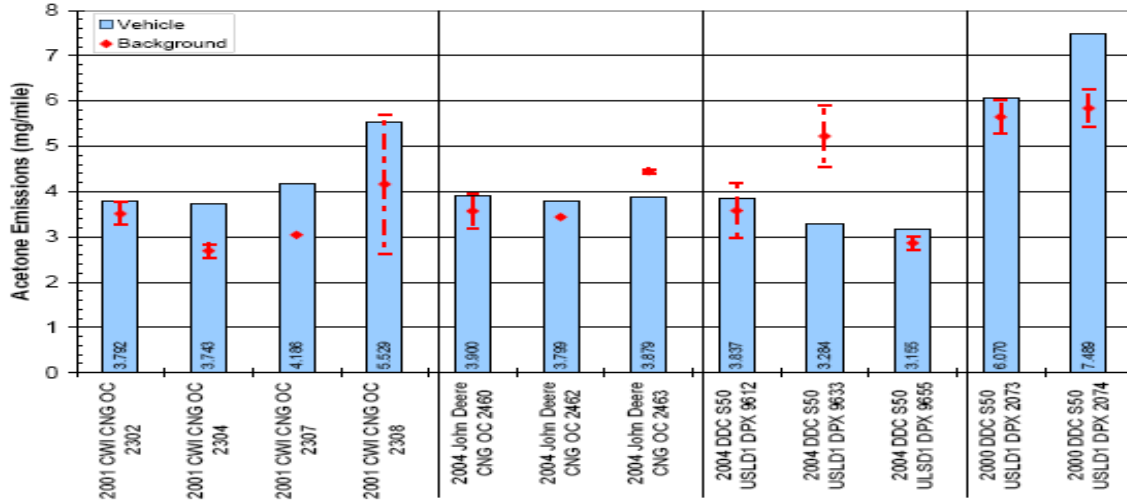
Figure 2.24 Acetone emission results from WMATA study [41].

2.7 Exhaust After-Treatment

2.7.1 Summary of Exhaust After-Treatment Systems

Heavy duty diesel engine manufacturers have reached new levels in fine tuning and controlling in cylinder combustion in an effort to reduce engine out emissions. Advent of intelligent Engine Control Units (ECU) has greatly transformed the performances of heavy duty diesel engines. With emission regulations becoming extremely stringent engine manufacturers realize the need for exhaust gas after-treatment systems to meet the norms. One of the predominant concern of diesel engines emission is PM and NOx, and with the trade off curve between them it becomes an even bigger challenge to simultaneously reduce both of them. Current heavy duty diesel engines make use of Diesel Particulate Filter (DPF) or catalyzed version of DPF known as the Continuously Regenerative Trap (CRT) to counter PM emissions. While NOx is being either controlled through Exhaust Gas Recirculation (EGR) or through Selective Catalytic Reduction (SCR) systems.

With the advent of heavy duty natural gas engines increased CO and hydrocarbon emissions are seen. To counter this engine manufacturers use Oxidation Catalyst (OC) to treat the exhaust gas. As CNG vehicles use only OC as their after-treatment device, this section will deal with OC technologies, efficiencies and limitations.

2.7.2 Oxidation Catalyst (OC)

The main purpose of oxidation catalyst is to oxidize CO and HC to carbon-dioxide and water in the presence of certain noble metal catalyst. OC after-treatment device consists of a monolithic substrate which supports a wash coat, which in turn supports the catalytic material. The conversion efficiency of a catalytic after-treatment system depends on four factors:

- Light-Off temperatures
- Catalyst window
- Space velocity
- Noble metal loading

In general the conversion efficiency of catalytic after-treatment system increases with increasing temperatures and starts to decrease after further increase in temperature. Light-off temperature is defined as the temperature at which 50% conversion efficiency is reached. And catalyst window is the temperature range within which the conversion efficiency is at least 50%. Catalyst specifications are usually specified in terms of space velocity and noble metal loading. Space velocity is defined as the ratio between volumetric exhaust flow rate to the total volume of the catalyst.

$$SV = V / Vr \ \ (\text{hr}^{-1})$$

Where

V= Volumetric flow rate of exhaust at STP (m^3/hr)

Vr = Volume of catalyst (m^3)

Space velocity is an important parameter of catalyst specification. Catalyst used in automobile applications use noble metals as the catalyst. And these noble metals belong to the platinum group metals. Widely used platinum group metals are Platinum (Pt), Palladium (Pd) and Rhodium (Rh). Normally metal loading are specified in units of grams per volume of catalyst substrate. This is an important parameter which governs the conversion efficiency and cost of the OC system [9]. Based upon the species OC oxidizes they are classified as:

- Two way catalyst: Those which oxidize CO and HC only.
- Three way catalyst: Those which oxidize CO, HC and NOx.

Three way catalysts (TWC) usually require strict control over the air-fuel ratio. For this purpose an exhaust gas oxygen sensor is used in closed loop with the fuel metering device to maintain stoichiometric air fuel ratio for good conversion efficiencies. These types of after-treatment devices are usually found in gasoline engine vehicles. Diesel engines usually contain two way catalysts due to their very lean fuel-air mixture. Oxidation catalysts do not oxidize PM but they do oxides the soluble organic fraction (SOF) of the PM. The percentage conversion of particulate bound SOF is usually 50 to 60% [42]. Study by Johnson and kittelson showed that gas diffusion reaction of hydrocarbon with catalyst usually dominates more than PM bound hydrocarbon reaction with the catalyst. The results also showed increased conversion efficiency for heavier hydrocarbon than lighter ones especially with carbon number between 20 and 24 [43]. Platinum is the preferred choice of noble metal for diesel engines as they are able to operate under low light-off temperatures and more resistant to fuel sulfur and lube oil additives. On the other hand Palladium and other non-precious metal catalyst which have higher light-off temperatures and prefer a hotter exhaust would be suitable for CNG applications. Moreover Pd is less resistant to sulfur and lube oil additives in exhaust [44].

The performance of catalytic after-treatment system usually degenerates with aging. This can be due to various factors which hinder the catalytic action by either decreasing the surface area of the reaction or deactivating the noble metal catalyst. Reduction in surface area could be due to clogging of catalyst pores with soot or structural degradation of the substrate. Although this type of deactivation mainly arises through long use of the catalyst another factor which is detrimental to the functioning of the catalyst are substances which poison the catalyst coating. Sulfur is known to be a substance which poisons catalyst coating. Source of sulfur in exhaust is from the fuel and lubricating oil which in turn forms sulfur dioxide (SO_2). Sulfur dioxide is catalytically oxidized to SO_3 which combines with water to form sulfuric acid. This phenomenon not only increases undesirable sulfate content in the exhaust it also increases the light-off temperature of the catalyst thereby decreasing conversion efficiencies [45]. In addition to sulfur phosphorous and zinc can deactivate catalytic after-treatment device. Phosphorous along with zinc is added as an anti-wear and anti-oxidant in the lube oil. At low loads when oil consumption is high, phosphorous and zinc are present in exhaust. These compounds would deposit on catalyst wall hindering with gas diffusion processes [45].

One of the main challenges in designing oxidation catalyst for CNG vehicles would be to regulate methane and formaldehyde. Although methane is found to be not phototoxic it is found to be a greenhouse gas. Hence it is desirable to regulate the high quantities of methane in exhaust of CNG vehicles. The reason that methane conversion efficiency is less in an oxidation catalyst is that the light of temperatures of methane is greater than 500^oC as shown in Figure 2.25. If an engine exhaust must reach this temperature the engines thermal efficiency must be very low, which again is not a favorable engine design factor.
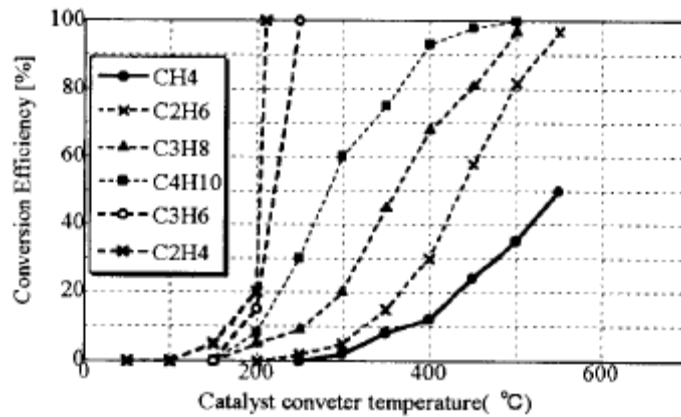
Figure 2.25 Methane Conversion Efficiency Vs Catalyst Temperature [45].

Gluck et al. formulated a Pd/Rh based catalyst specifically for stoichiometric natural gas engines. This catalyst formulation was able to bring down light-off temperatures to 375^oC at an equivalence ratio of 0.98 and methane conversion efficiency of up to 90% was reached. The study also showed that Pd based catalyst maintained a good conversion efficiency over a wider equivalence ratio window [46].

CHAPTER 3 - EXPERIMENTAL SETUP

This section details the construction and working of the heavy duty chassis dynamometer lab. It also provides descriptions of the various instruments and sampling devices part of the lab.

3.1   Equipment and Procedures

The study of the chemical speciation of Riverside urban transit bus was carried out using WVU's Heavy Duty transportable chassis dynamometer lab. The lab was stationed at Riverside, California where the testing was conducted. THDVETL was built by WVU and is operational since 1993. This laboratory has the unique capability of traveling on road to any place in the country to perform chassis dynamometer emissions testing. The lab is credited with many successful emission testing projects carried throughout the country.

The essential components of the HDVETTL are the chassis dynamometer, the instrument trailer integrated with a full fledged primary dilution tunnel, a separate clean primary dilution tunnel for ultra low emission vehicles, control systems, analyzers and special sampling train housed within the instrument trailer. The design specifications and working of all components of the chassis lab conforms to the procedures stated in CFR 40 Part 86 Subpart N. A more detailed description of the laboratory functioning will follow.

3.2   Chassis Dynamometer

The chassis dynamometer consists of free spinning rollers, vehicle loading devices, frame, and jacks integrated into a semi-trailer. The dynamometer components were designed for a maximum rotational speed of 560rpm, which translates to a vehicle speed of 55miles/hour with an added safety margin [47]. The various parts of the dynamometer are:

- Rollers: The dynamometer consists of 4 free spinning rollers. The vehicle's wheels once mounted on the dynamometer would rest on these rollers. The rollers are 12.6 inches in diameter. Four rollers support single or forward rear axle assembly. The rear pair of rollers can be adjusted to three different positions to accommodate tandem spacing of 4 to 5 feet. Each roller pair houses a 2.4 inch diameter shaft connected by flexible coupling to maintain same speed on each tire [47].

- Wheel Adapters: The power from the wheels is transferred using wheel adapters. This form of power absorption was preferred over power absorption from rollers because of the fact that in the absence of large size rollers, the increased slippage and heat generation between rollers and tires would bring about in accuracies in test data. The adapter consisted of wheel rims of 1.8feet diameter and 0.5 inches thick aluminum faceplates attached to a Spicer 1810 series coupled assembly. The wheel rim is bolted to the aluminum faceplate for power transfer to the power transfer shafts [47].

- Power Transfer Shafts: The coupled assemblies drive a short shaft of 24 inches in length through a pillow block on either side of the dynamometer. The splined shaft with a companion flange drives a 16,665 lb-ft Lebow torque and speed sensor, which provides instantaneous torque and speed measurement of the wheel to the computer. The transducer is connected to another shaft through a companion flange. This shaft passes into a right angle speed increasing drive to the flywheel assembly. The speed increasing drive consists of a differential to maintain the same speed of a second output shaft which emerges from the far side of the drive. This shaft drives another short shaft through a universal joint to transfer power to the eddy current dyno power absorbers [47].

- Flywheel Assembly: The flywheel system is to simulate the inertia of the vehicle. Hence the flywheel system is designed to simulate different inertias for different vehicle weights. This is achieved by provisions to engage and disengage various flywheel combinations based on the required test weights. There are eight flywheels on either side of the dynamometer. The flywheels rest on bearings on the shaft and are designed to simulate a maximum load of 66,000 lb [47].

- Power Absorbers: The power absorbers are a pair of eddy current dynamometers used to simulate the road and wind resistance. The dynamometers are air cooled Mustang model CC300 capable of absorbing 1000hp peak power. The dynamometer case is fitted with a torque arm to which a force transducer is fitted to measure the absorbing torque. The test procedures require an accurate control of speed and torque. Speed is controlled by the driver and torque is controlled transiently by the control computer. The vehicle inertia is controlled through the flywheel assemblies rotational speed, and the torque load equivalent to the actual wind and road resistance experienced by the

vehicle is applied through the power absorbers via a Dyne-Systems Dyn-Loc IV controller. These controllers work on a closed loop Proportional Integral Differential (PID) principle. The control computer transiently transmits the calculated set points to the controller, and the controller calculates the error involved in the signal through the PID principle and continuously updates and sends the required direct current to the eddy dyno to apply the necessary load torque. The set point is calculated by the control computer using the following road-load equation:

$$P_r = (C_r * M * g + \frac{1}{2}\rho_a * C_d * A * V^2) * V$$

Where

P_r = Road-Load power
C_r = Coefficient of rolling resistance
M = Vehicle gravitational mass
ρ_a = Air density
A = Frontal area of vehicle
C_d = Coeffecient of drag
V = Vehicle speed
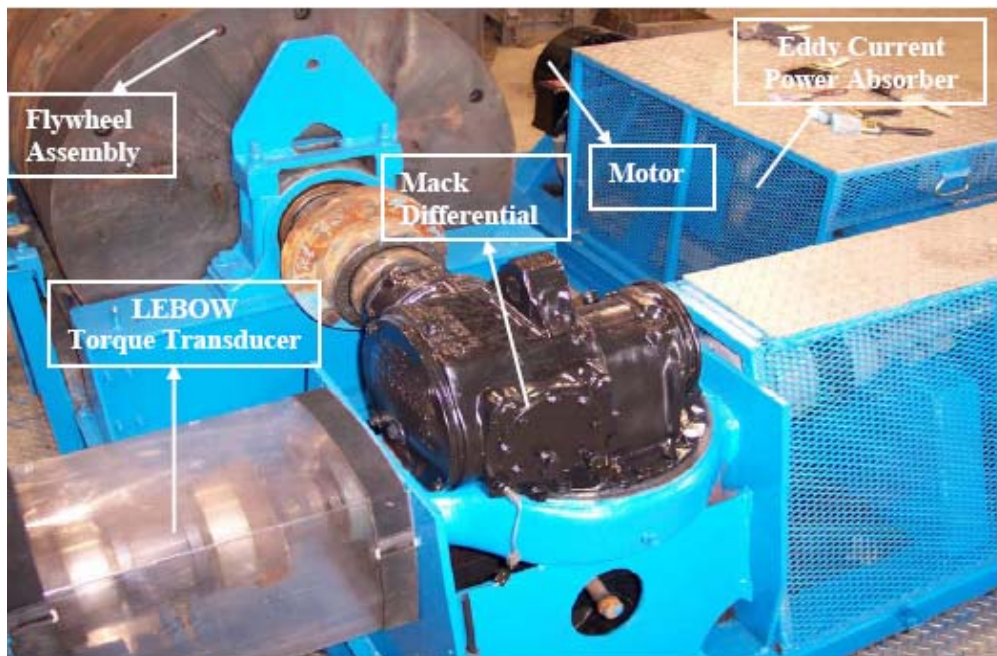
Figure 3.1 Load simulation components of chassis dynamometer [35].
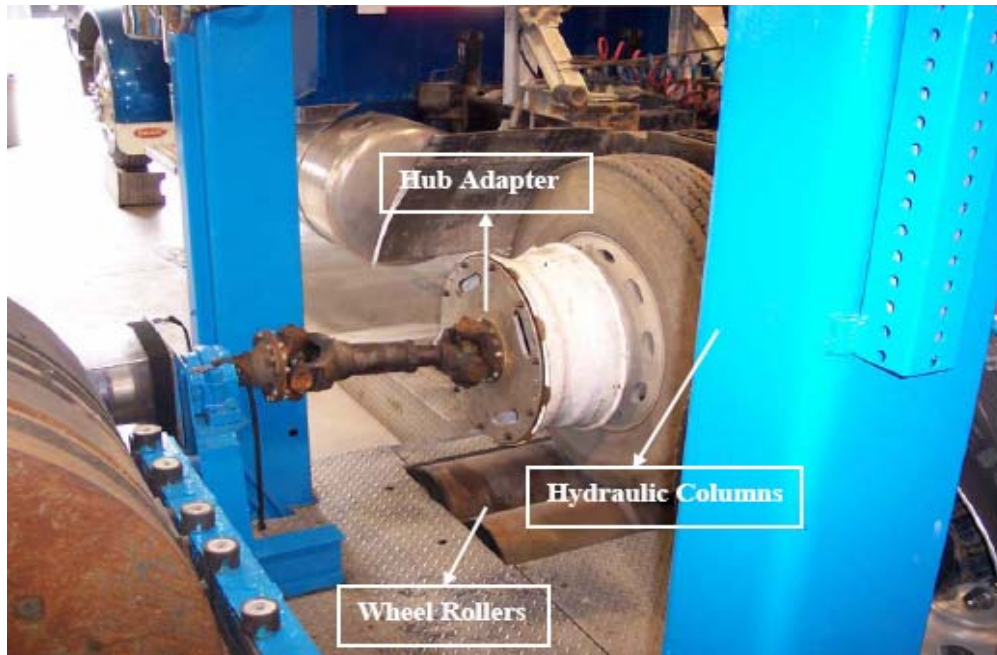
Figure 3.2 Dynamometer support structures and power transfer shafts [35].

- Motor: The motor was added to the chassis lab dynamometer to overcome frictional losses in various rotating elements. The coast down test performed would calculate the frictional losses incurred in the system and might use the motors as an aid to overcome frictions in dynamometer parts. The motor is a 20hp motor with a maximum torque of 59 lb-ft. The motor is directly coupled to the eddy current dyno and is controlled by a speed encoder connected to it.

3.3 Full Flow Clean Primary Dilution Tunnel

An addition to the transportable laboratory is the clean primary dilution tunnel. This is a stand alone tunnel built exclusively to test CNG vehicles and ultra low emission vehicles. The need for a separate tunnel arose due to the fact that testing of CNG and ultra low emission vehicles in the same tunnel used for testing diesel vehicles would bring about an error in the final background corrected emission values because of increased tunnel background concentration. Higher tunnel background emission concentrations are seen in the conventional primary dilution tunnel because of high concentration of soot deposited on the tunnel walls while testing diesel vehicles. These deposited soot particles absorb chemical species from exhaust and also shed them when sufficient high temperatures are reached during testing. Since emission levels from

CNG and ultra low emission vehicles are very close to atmospheric background concentrations, an error in emission measurements may occur while using the conventional primary dilution tunnel to test these vehicles.

The clean tunnel was designed as per regulations stated in CFR 40 Part 86 Subpart N. The dilution air was High Efficiency Particulate (HEPA) filtered air at ambient conditions inducted through a HEPA filter manifold connected to the inlet section of the tunnel. The outlet section of the tunnel was connected to a blower through a Critical Flow Venturi Constant Volume Sampler (CFV-CVS). The tunnel is 18 inches in inner diameter and the size was chosen as per CFR 40 regulations with reference to tunnel diameter in relation to particulate sampling from single dilution method. Since the tunnel was designed to be used with any of the transportable labs, it was built as five small sections [48].

- Section 1: This is the inlet section of the tunnel which is connected to the HEPA filter manifold. This section was designed as necking section which changes from 20 inches inner diameter on the inlet side to 24 inches inner diameter on the outlet side of this section. A flange on the outlet side would connect to section 2 [48].

- Section 2: This is the inlet section for the raw exhaust and the dilution air from section 1. Raw exhaust enters into section 2 through a stainless steel tube through the top. The section is built such that a 24 in flanged section connects to an 18 in section via ribs. This change in diameter creates an opening for overflow of the dilution air. This provision is made so that changes in dilution air flow do not affect tunnel flows [48].
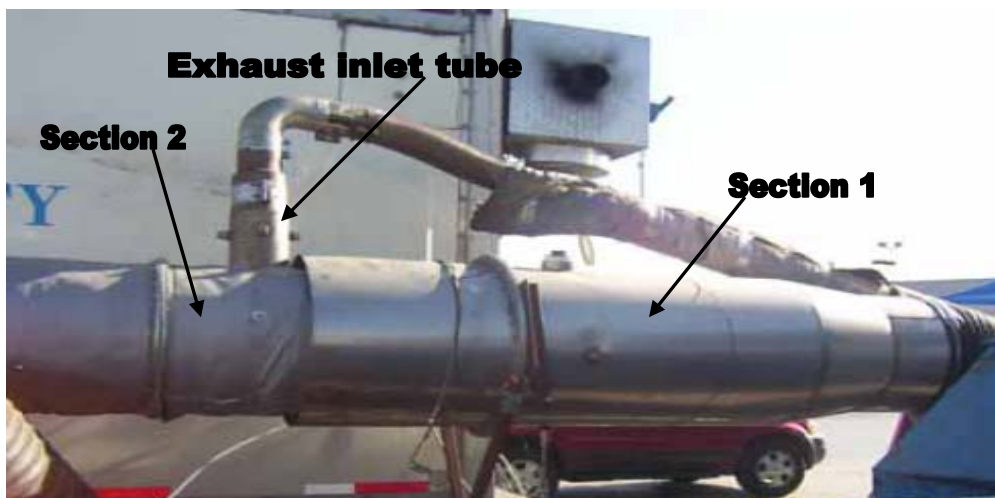
Figure 3.3 Section 1 and section 2 of the clean tunnel [48].

- Section 3: This is the mixing section for raw exhaust and the dilution air. This section is connected to section 2 via flange with a mixing orifice in-between the flanges. The orifice would create the necessary turbulence required for mixing. The raw exhaust inlet is positioned such that it is very close to the mixing orifice. The mixing section is wrapped around with insulating material to avoid steep temperature gradients radially and thereby reducing thermophoretic losses Mixing section consists of two 7ft long sections connected by flanges to satisfy the 10-diameter rule of CFR 40 [48].

- Section 4: The sampling zone is 15 ft 6 in downstream of the mixing orifice so that it is at a minimum distance of 10 times the inner diameter of the mixing zone from the orifice (10-diameter rule). The unregulated sampling plane was located 3ft further downstream of the regulated sampling plane. There are 8 sampling ports each for regulated and unregulated with radially positioned flanges to attach the different sampling probes. The probe flanges were bolted and fitted with gaskets to prevent any leak [48].

Figure 3.4 Sampling section of clean tunnel [48].

- Section 5: The outlet section of the tunnel is connected to the CFV-CVS blower via flexible tubing.

3.4   Critical Flow Venturi-Constant Volume Sampler (CFV-CVS)

The volumetric flow rate through the dilution tunnel is maintained constant by using a critical flow venturi at the outlet of the tunnel. The blower unit draws the tunnel flow through the CFV at choked flow conditions which creates a constant flow rate through it. The flow rate of the CFV is dependent on its throat diameter and governed by the following equation:

$$A^* = \frac{\dot{m}}{C_d} * \frac{\sqrt{T_t}}{P_t} * \sqrt{\left[\frac{R}{\gamma} * \left(\frac{\gamma+1}{2}\right)^{\frac{\gamma+1}{\gamma-1}}\right]} \qquad \text{Equation 3.1}$$

Where temperature and pressure are at standard conditions.

The transportable lab's CFV system has flow rate capabilities of 1000, 1500, 2000, 2500 and 3000 scfm. The variations in flow rate are achieved by changing the throat diameter of the CFV by inserting various venturis which achieve this purpose. The decision on the tunnel flow rate is based upon the test vehicle configuration, expected emission levels and analyzer ranges and also temperature of exhaust. For a given exhaust flow rate a higher the tunnel flow rate means more the dilution air, consequently lesser concentrations of emission constituents in the tunnel and cooler tunnel flows.

Theoretically the flow through the CFV should be constant, but a variation in the temperature of the dilute mixture creates fluctuations in the flow rate. In order to measure the actual flow rate through the venturi a pressure transducer and a resistance temperature device measure the pressure and temperature at venturi inlet. With this flow rate is calculated using the following equation:

$$Q(scfm) = \frac{K_v * P(Kpa)}{\sqrt{T(^oK)}} \qquad \text{Equation 3.2}$$

Where the calibration coefficient K_v is obtained by calibrating the CFV against a sub-sonic venturi that was traceable to National Bureau of Standards.

3.5 Secondary Dilution Tunnel for Particulate Matter Sampling

The secondary dilution tunnel is used to sample PM from the main tunnel for collecting them on filters for gravimetric measurement of PM. The tunnel has the capability of double diluting the sample to maintain the filter face temperature below 125°F as prescribed in CFR40. A filter housing containing a pair of 70mm Teflon coated glass fiber filters is connected downstream of the secondary dilution tunnel for collection of TPM. The secondary dilution tunnel can operate without double dilution incase of a cooler exhaust and extremely less PM content as from DPF equipped diesel fuel vehicles.

The secondary dilution tunnel is 3.0 in diameter and 30 in long to provide sufficient residence time for sampled exhaust and dilution air to mix. The dilute sample from the main tunnel is sampled through a 0.5in diameter probe located at the sampling plane. The sample and dilution air are drawn into the secondary dilution tunnel with the help of Gast rotary vane pumps. The total flow and the flow of dilution air are controlled through electronic mass flow controllers. The total secondary tunnel flow mass flow controller operates in a proportional sampling mode, whereby it varies its flow rate proportional to primary tunnel flow variations. The mass flow controllers are calibrated using a laminar flow element. The total flow ranges from 0-6 scfm and secondary dilution air ranges from 0-3 scfm.

3.6 Particle Sizing

3.6.1 Ejector Mini-Dilution Setup

The study employed an ejector mini-dilution tunnel for particle sizing along with a Scanning Mobility Particle Sizer (SMPS) and a Condensation Particle Counter (CPC) to determine particle size distribution. The mini dilution setup utilizes an Air Vac Engineering manufactured series TD110H ejector pump to dilute the raw exhaust. The ejector pump inlet is fitted with a critical flow orifice to admit raw exhaust of known constant volumetric flow rate. HEPA filtered dry compressed air is used as the dilution air and the subsequent vacuum induced by the flow of compressed air through the ejector pump creates enough vacuum to pull raw exhaust through the inlet of the ejector pump at critical flow conditions. The mixing induced in this type of system is extremely turbulent due to high flow velocities of raw exhaust and dilution air. The fact that various combinations of inlet flow orifice and compressed air pressure would

yield a wide range of dilution ratios makes this system versatile for looking into the effect of dilution ratio on the particle size distribution. The system can also reach very high dilution ratios of up to 1000, which is very close to atmospheric dilution conditions. However studies carried out by Kittelson and Khalek [26] predict that the event of nucleation would be suppressed in this type of dilution system as the residence time for particles are very less. However as every issue related to particle size measurement has been subject of ambiguity, so is the issue of sample dilution. A study undertaken by Jussy Lyyranen et al. [49] has cited that by use of an ejector dilution sampling system a noticeable nucleation trend is seen. And they attribute this trend to the fast mixing and cooling of raw exhaust.

Figure 3.5 Ejector dilution sampling setup

Figure 3.5 shows the sampling setup for the particle sizing test undertaken in this study. Raw exhaust was transferred through a heated line maintained at $375^{o}F$ into the inlet of the ejector dilutor. The temperature setting of the heated line is kept such that the unburned hydrocarbon compounds do not condense in the transfer tube itself. The dilution ratio is calculated by the following equation:

$$DR = \frac{(RawExhaustFlowRate + DilutionAirFlowRate)}{RawExhaustFlowRate}$$ **Equation 3.3**

Raw exhaust flow rate is denoted by the flow rate of the critical flow orifice and dilution air flow rate is obtained as the flow rate corresponding to the compressed air pressure (obtained from the chart supplied by the manufacturers of the ejector pump).

3.6.2 Scanning Mobitily Particle Sizer (SMPS)

The SMPS system is used to measure the particle size distribution of an aerosol stream. The SMPS consists of an Electrostatic Classifier (EC) and Condensation Particle Counter (CPC) which work together as one unit. The EC serves as segregation unit of the SMPS and the CPC functions as the counting unit. The study used a TSI model 3080 Electrostatic Classifier and a TSI model 3025A Condensation Particle Counter. The following section would elucidate the principle and working of the EC and CPC.
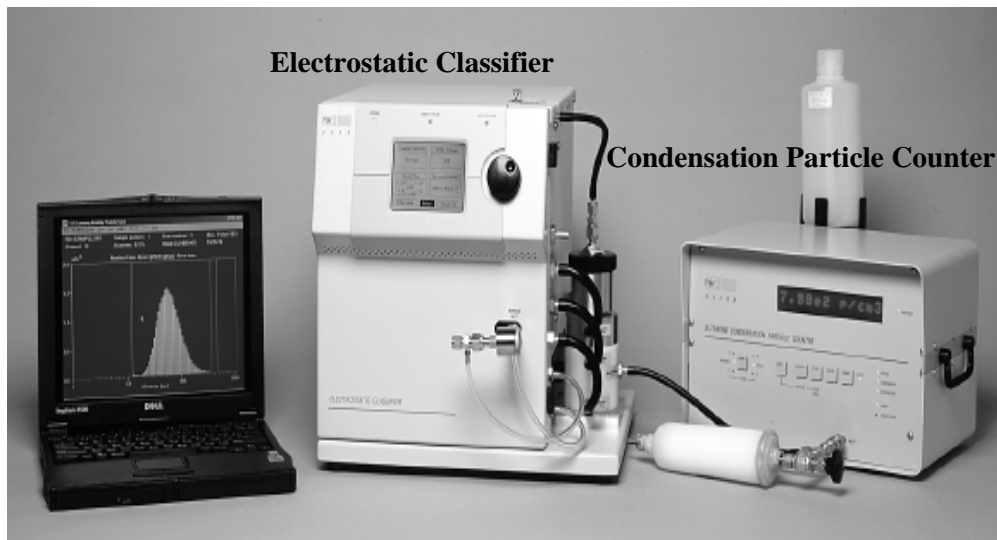
Figure 3.6 SMPS setup with EC TSI model 3080 and CPC TSI model 3025A [50]

3.6.2.1 Electrostatic Classifier

The working of the electrostatic classifier is based upon the electrical mobility property of the aerosol. Aerosol particles in general have some charge associated with them. And when these aerosol particles are subjected to an electric field while moving through an air stream, the drag force experienced by the particles would be that of the electric field. This tends the particles to reach a constant velocity known as the terminal settling velocity. The ratio of the velocity to the force is defined as the mobility of an aerosol and if this force happens to be an electric force the mobility is denoted as the electric mobility of an aerosol. Theoretically aerosol particles are considered to be spherical in nature, in real world aerosol particles specially combustion derived particles appear in complex geometrical shapes. Hence aerosol particles are either denoted by Stokes diameter or by Aerodynamic diameter. Stokes diameter is defined as the diameter of a

spherical particle with same density and terminal settling velocity of that of the aerosol particle. On the other hand Aerodynamic diameter is defined as the diameter of particle with density of $1g/cm^3$ and the same terminal settling velocity of the aerosol.

$$D_{pa} = D_{ps} \sqrt{\rho_p}$$
<div align="right">**Equation 3.4**</div>

Where

D_{pa}= Aerodynamic diameter in micrometer

D_{ps}= Stokes diameter in micrometer

ρ_p = Particle density in g/cm^3

The electrostatic classifier classifies particles based on its electrical mobility diameter which is basically the Stokes diameter of the particle [50]. The EC utilizes a Differential Mobility Analyzer (DMA) for the purpose of particle size classification. Poly disperse flow is defined as the aerosol stream for which the particle size distribution is to be characterized and mono disperse flow is defined as the size classified single diameter aerosol stream. The poly disperse flow enters the EC inlet through an impactor fitted at the inlet. The impactor filters out a certain aerodynamic diameter particles based on inertial impaction theory. The purpose of the impactor is to remove large particles which might carry multiple charges with it. Various size of orifice can be fitted prior to the impactor for using the classifier at different flow ranges. The aerosol flow enters the neutralizer which is Kr-85 Bipolar charger [50]. The bipolar charger consists of high concentration of ions and the frequent collision between aerosol particles and ions brings the aerosol charges to equilibrium. The aerosols from this point on would carry a bipolar charge distribution or would be known as singly charged particles. The singly charged particles enter the DMA where an electric field is applied based on the electric mobility of the particles. The DMA consists of two concentric cylinders with a central rod maintained at negative voltage and the outer cylinder grounded. This creates an electric field in the annular region. Poly disperse flow from the neutralizer and sheath air flow enters from the top of the DMA. The positively charged particles are attracted towards the negatively charged central rod and get precipitated along the length of the rod depending on their electrical mobility. Higher mobility particles get deposited at the top of the rod and less mobile particles get deposited towards the end of the rod. Particles which are not sufficiently attracted towards the rod exit the DMA as the mono disperse single size particles. The classifier voltage is changed to classify

particles from 2nm to 1000nm depending on the DMA model. The study utilized the TSI model 3081 Long DMA which has a size range of 10nm to 1000nm. The TSI model 3085 Nano DMA has a size range of 2nm to 150nm. The mono disperse flow exiting the classifier is transported to the CPC for determining the concentration of the aerosol stream. Figure 3.7 shows the construction of the electrostatic classifier with the DMA. The EC can be used in two modes namely the analog mode and the panel mode. The panel mode is chosen when the EC is used an SMPS unit and analog mode is chosen when the EC is used as a stand alone size classification instrument for other purposes [50].
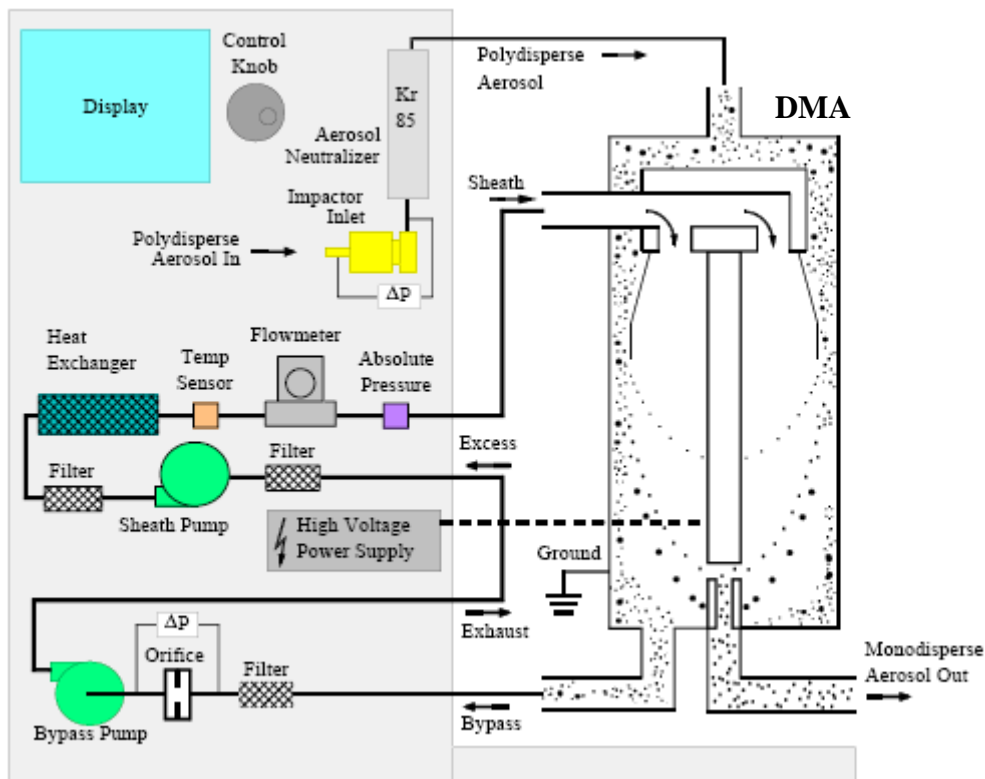
Figure 3.7 Schematic of Electrostatic Classifier with the DMA [50]

3.6.2.2 Condensation Particle Counter (CPC)

The CPC is an instrument to count the number of particles in a mono disperse aerosol stream. The CPC uses a process of heterogeneous growth of particles with alcohol vapor for the optical detector to count the particles. For this the CPC contains a heated Butanol saturated wick through which the aerosol stream passes [51]. This region is called the saturator as the region

within the wick is saturated with butanol vapor. The aerosol stream along with the butanol vapor travel with the air stream into a cooling condenser. The huge temperature differences causes condensation of alcohol vapor onto the particles due to which the particle size increases. The detection size limit of the CPC is specified in terms of the saturation ratio which is further dependent on the Kelvin diameter. It is defined as the droplet size of condensed vapor at a critical saturation ratio during which the particle neither evaporates nor continues to grow. In other words it is also the minimum diameter at which vapor condensation starts to take place at a given saturation ratio. The higher the saturation ratio in the condenser lesser is the Kelvin diameter. The particles typically grow to a size of 2 to 3 micrometer for optical detection [51]. The particles move through a light source thereby scattering it onto photo detectors which in turn produces electrical impulses proportional to the number of particles. The inlet flow rate of the CPC is 0.3lpm however it can also be operated at high flow modes at a flow rate of 1.5lpm in conjunction with the Long DMA. The CPC has a maximum particle concentration limit of 999×10^4 particles/cm^3 that it can count [51].
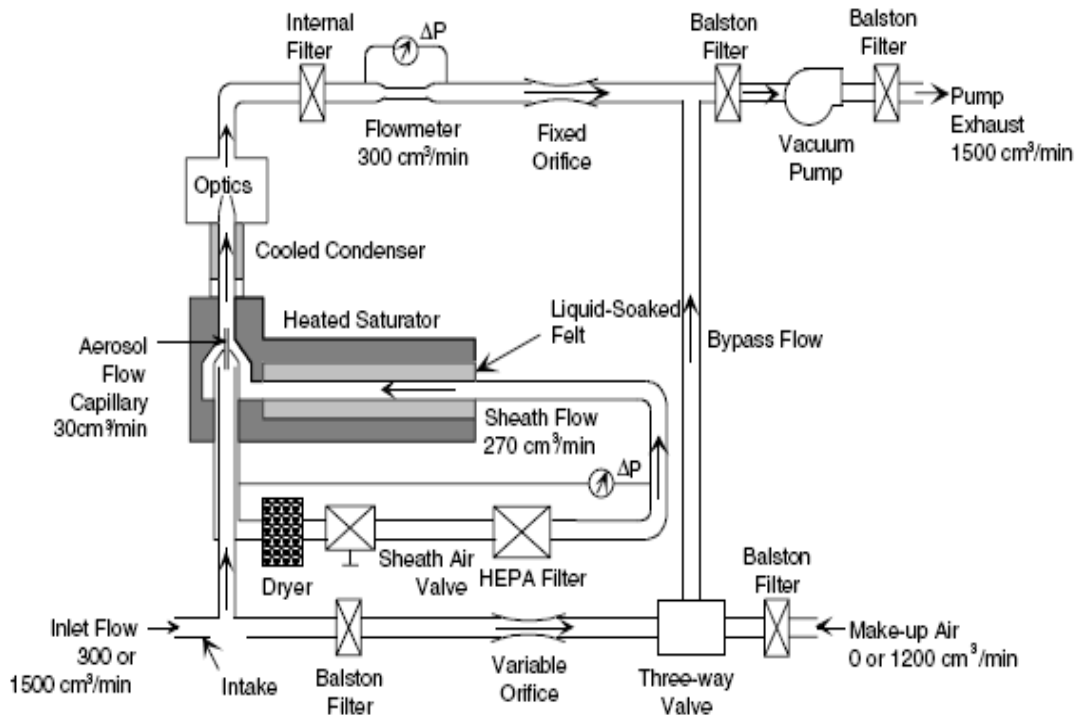
Figure 3.8 Schematic of construction and flow pattern of CPC [51]

The data acquisition system is the Aerosol Instrument Manager (AIM) software provided by TSI. The AIM software is responsible for the hardware control and data acquisition of the EC, CPC and the SMPS unit.

3.7   Gaseous Emission Sampling System

The gaseous emission sampling system consists of heated probes, heated transfer lines, temperature control units, and gas analyzers built into the analytical trailer. The design of the gaseous emission sampling system is in accordance with CFR40 regulations. The heated probes are flooded probe type for supplying zero and span gases to the analyzer. The probes are fitted at the sampling plane according to the 10 diameter rule from the mixing region. The gaseous emissions are sampled from the tunnel through 4 separate heated lines for CO/CO_2, NOx, THC, and aldehydes. The temperature of the heated lines and the probes are controlled by a temperature control module (TCM). Teflon heated lines are used for CO/CO_2, NOx, aldehydes and stainless steel heated lines are used for THC samples. The flows through the heated lines are controlled by calibrated rotameter and magnahelic pressure regulators. The pumps within the analyzers draws sample from the tunnel.

3.7.1   Regulated Emissions Sampling System

The regulated emissions sampling system consists of gas sampling systems (probes, heated lines), gas conditioning system (heated filters, chiller system), gas metering system (rotameter, magnahelic pressure gauges), calibration systems, two CO analyzers one used as low CO analyzer and the other used as high CO analyzer, one CO_2 analyzer, two NOx analyzer used for verification purposes and also perform NO/NO_2 split measurement, and one THC analyzer. The principle and working of the different analyzers will be discussed in the following sections.

3.7.1.1 CO/CO_2 Analyzer

The lab utilizes three Horiba model AIA-210 CO/CO_2 infra red analyzers. Two analyzers are for high CO and low CO measurements and one analyzer for CO_2 measurements. The high and low CO analyzers only differ in the range in which the analyzers operate. Low CO is used to measure low concentration of CO during the transient tests and high the CO analyzer measures

over a wider range of concentrations. Both CO and CO_2 are drawn from the same probe and transferred through a heated line maintained at 240^oF (115.5^oC) to avoid water condensation as it would affect the analyzer measurements. The gas sample is passed through a chiller and dryer unit to further reduce water content and then passed through heated filters to prevent particulate matter from entering the analyzer.

The CO/CO_2 analyzer works on the Non-Dispersive Infra Red (NDIR) principle. The outlined principle of this system is the infra red wavelength absorption capability of CO and CO_2 gases. Two equal infra red energy beams are sent through two optical chambers. One chamber is filled with a reference gas and sealed and the other chamber consists of the continously flowing sample gas. The IR beam is interrupted by a chopper at a given frequency. As the beam passes through the gas filled chambers it gets absorbed by the flowing gases and the detector placed on the far end of the chamber reads the reduced intensity of the beam. The quantity of the IR beam absorbed would be proportional to the concentration of the flowing gas. The detector measures the intensity of radiation from the reference cell and the sample cell and converts the difference in radiation as change in capacitance which in turn is converted to sample concentration.
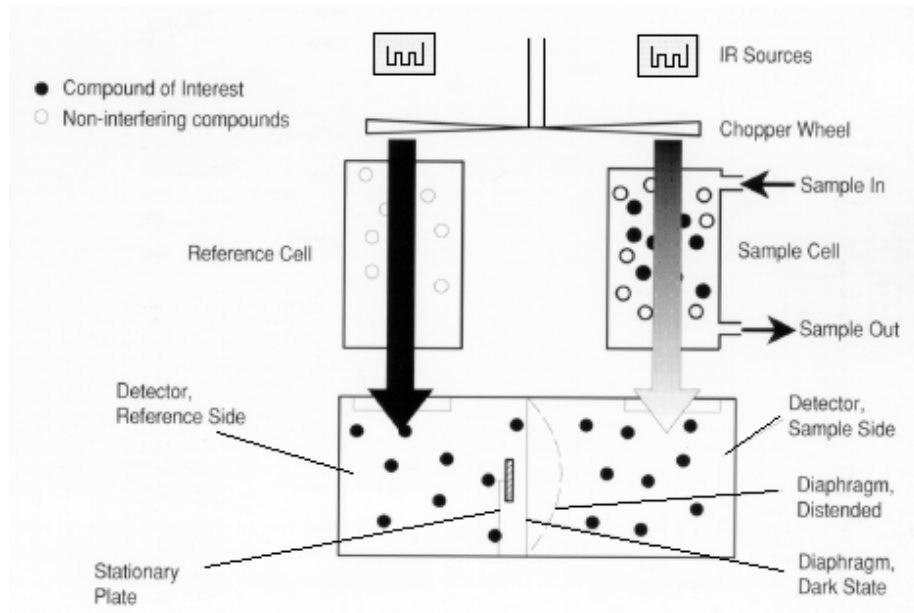
Figure 3.9 Illustration of the NDIR principle of CO/CO_2 analyzer [52].

The CO analyzer contains conditioning column containing ascarite which is used to remove CO_2 from the sample and the analyzer would read only concentration of CO.

3.7.1.2   NOx Analyzer

The lab utilizes two California Analytical Model 400 HCLD NOx analyzers. The primary purpose of two NOx analyzers is to verify the data between the two analyzers and also measure the NO/NOx split. The NOx sample is sampled from heated probe and transfer line maintained at $240^{o}F$ ($115.5^{o}C$) to avoid water condensation as presence water would absorb water soluble NO_2.

The analyzer works on the principle of chemiluminescence measurement technology. The analyzer consists of an ozone generator, NO converter, reaction chamber, photo electric diode and signal processing electronics. Chemiluminescence reaction is that in which two compounds react to emit photons. In the NOx analyzer it is the reaction between ozone and NO that leads to the formation of highly excited state NO_2 which returns to its ground state by emitting a photon.

$$NO + O_3 \longrightarrow NO_2^* + O_2 \qquad\qquad \textbf{Equation 3.5}$$

$$NO_2^* \longrightarrow NO_2 + photons(redlight) \qquad\qquad \textbf{Equation 3.6}$$
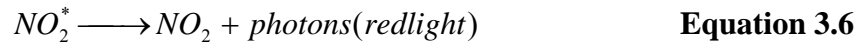
The intensity of photons emitted is measured by the photodiode and the signals are processed into the concentration of the sample gas.
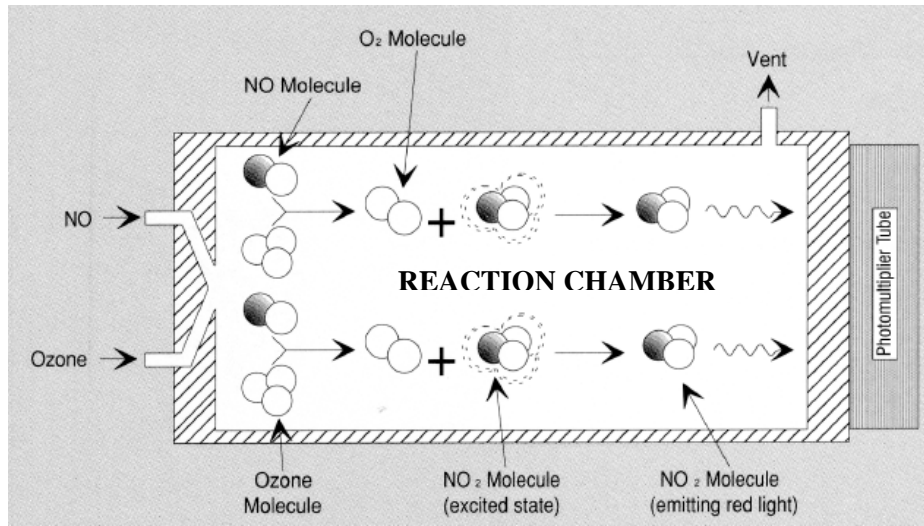
Figure 3.10 Illustration of the chemiluminescence principle of NOx analyzer [53].

For the NOx ($NO+NO_2$) measurement the analyzer employs a converter which converts all the NO_2 in the sample to NO on a heated vitreous carbon bed before passing through the reaction chamber. This step is bypassed if the analyzer is on NO mode.

3.7.1.3   Total Hydrocarbon (THC) Analyzer

The lab utilizes a Beckman model 402 which works on the Flame Ionization Detector (FID) principle. The hydrocarbon sample is drawn fro heated probes and stainless steel transfer lines maintained at $375^{o}F$ ($190.5^{o}C$) to prevent condensation of hydrocarbons in the transfer tubes.

The analyzer consists of a burner which is supplied with fuel (60% hydrogen and 40% helium) and air. The sample gas passes through the burning flame and undergoes a complex ionization process producing electrons and positive ions. These electrons are collected by an electrode, which causes a current to flow through the external circuit. The ionization current produced is proportional to the number of carbon atoms entering the burner which is a measure of the hydrocarbon content of the sample.
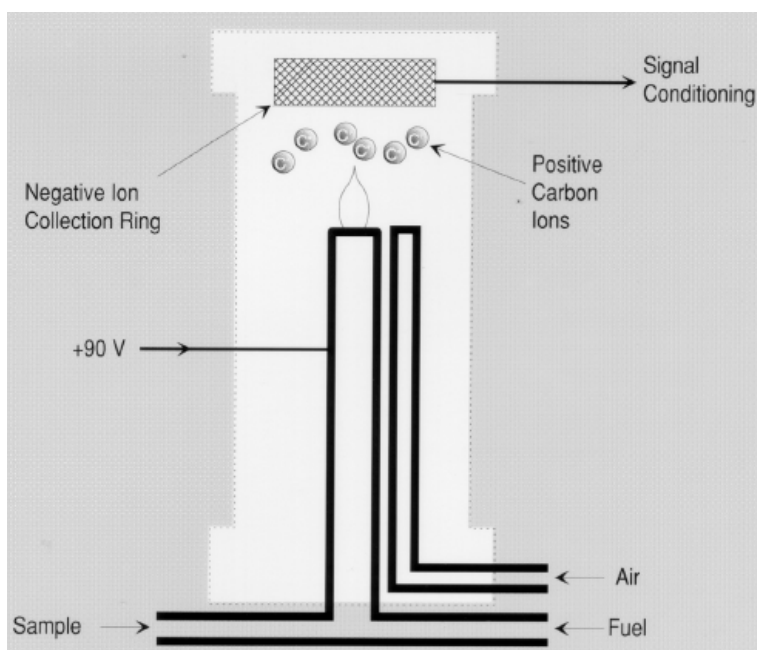
Figure 3.11 Illustration of the FID principle of the THC analyzer [54].

3.7.2   Unregulated Emissions Sampling Systems

The unregulated emissions sampling systems include sampling for carbonyls, Poly Aromatic Hydrocarbons (PAH), Volatile Organic Compounds (VOC), and Metals/EC/OC. The sampling devices for PAH and VOC and all unregulated media were supplied by DRI. The sampling systems for various species will be discussed in detail below.

3.7.2.1 Carbonyl Sampling

The carbonyl sample is drawn from the tunnel through heated probes and a transfer line maintained at 240°F (115.5°C) to avoid water condensation. The transfer line is connected to a vacuum manifold. A vacuum of 10 in Hg is maintained through 3 rotary vane pumps. The flow in the aldehydes transfer line is controlled through a mass flow controller set to operate at 1lpm. The carbonyl sample is passed through a 2,4 Dinitrophenylhydrazine (DNPH) cartridge fitted to the transfer line. The carbonyl compounds undergo a derivatization reaction forming 2,4 Dinitrohydrazones as shown in Figure 3.12 [55]. The hydrazones are then extracted from the cartridge using acetonitrile and analyzed through High Performance Liquid Chromatography (HPLC).
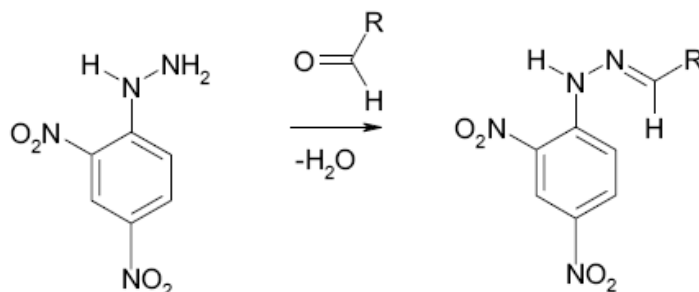
Figure 3.12 Derivatization reaction in DNPH cartridge for carbonyl sampling [55].

3.7.2.2 Volatile Organic Compound (VOC) sampling

The VOC sample was collected into a steel canister for laboratory analysis using a flow control system provided by DRI. The canister, which had a capacity of 6.0 L at atmospheric conditions, was pressurized to 20 psig in order to hold 12 L of sample. The system provided by DRI was built according to the EPA compendium method TO-15 for determination of toxic organic compounds in air. The system utilizes the pressurized sampling method developed in the standard. The steel canisters used to collect dilute exhaust were completely evacuated, and a vacuum of 10mm Hg was present inside the canister prior to the start of the test. The flow rate of the canister sampling system is adjusted manually, and verified with an electronic mass flow controller. The flow rate of the sampling is system is calculated by the following equation.

$$CanisterFlowrate = \frac{SampleVolume}{TestTime} \text{ "cc/min"} \qquad \textbf{Equation 3.7}$$

Where:
SampleVolume = Total Sample volume to be collected (12000 cc)

Figure 3.13 shows the flow diagram of the EPA TO-15 method for VOC canister sampling. The pump in the sampling system draws the sample from the tunnel and pushes the sample into the canister through a check valve. Two pressure gauges monitor the back pressure before the check valve and the canister pressure. The system is designed to operate optimally within a maximum back pressure of 22 psi. A pair of T60A20 filters contained in a filter holder placed upstream of the pump prevents PM from entering the system. The system is initiated manually with the start of the test. After the completion of the test the valves on the canister are closed and leak checked before packaging the canister for shipping.
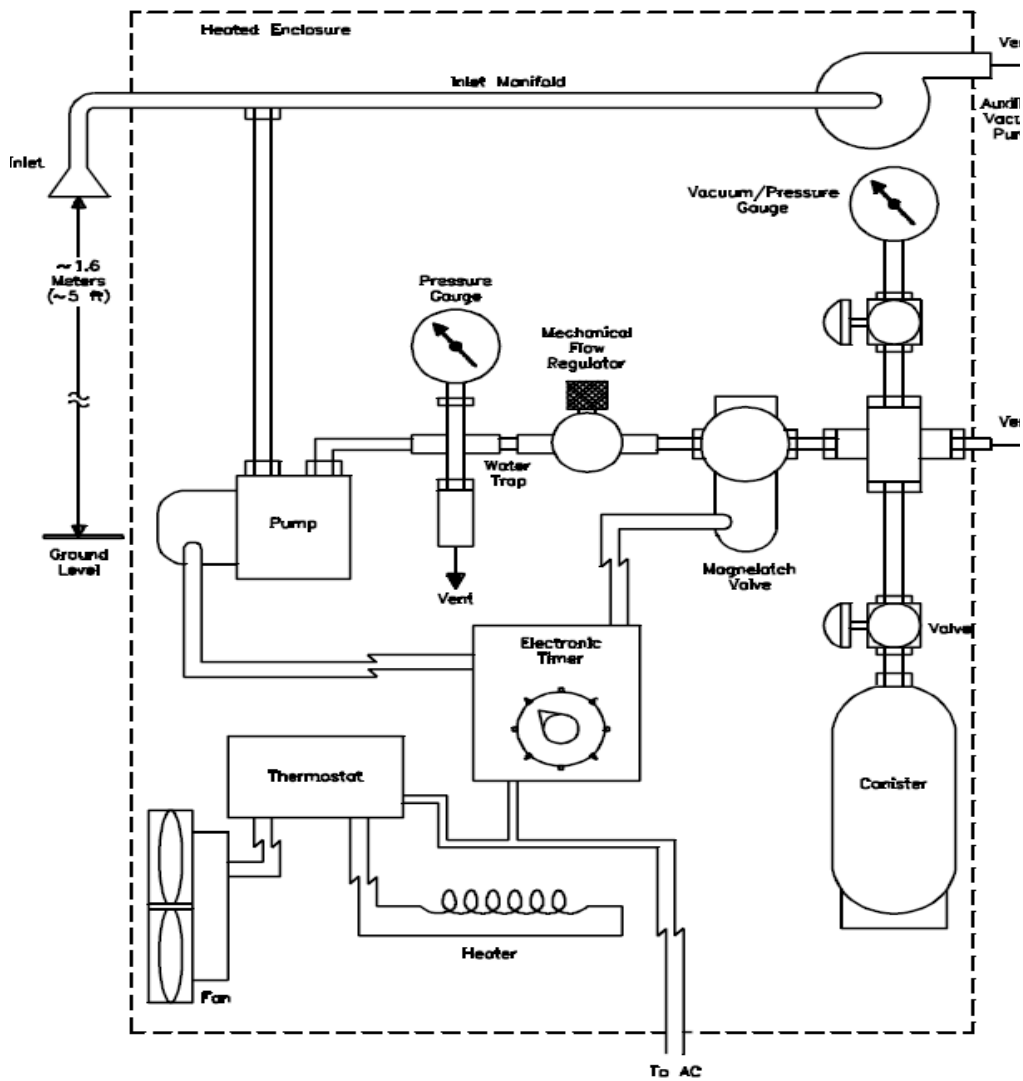
Figure 3.13 EPA TO-15 method for pressurized VOC canister sampling system.

Figure 3.14 DRI pressurized VOC sampling system

3.7.2.3 *Polycyclic Aromatic Hydrocarbon (PAH/n-PAH) Sampling System*

Polycyclic Aromatic Hydrocarbons and nitro-PAH were sampled from the tunnel into PUF/XAD cartridges. DRI's Fine Particulate/Semivolatile Organic Compounds (FPSVOC) sampling system was used for PAH collection. The tunnel sample is drawn at 113 lpm with the help of rotary vane pump. The sample is admitted into the sampler through a copper tube and into a manifold which contains the housing for the PUF/XAD cartridge. Figure 3.14 shows the schematic of the PUF/XAD cartridge housing. The housing holds the PUF/XAD cartridge and a 70mm T60A20 filter used to capture the PM bound organic compounds. A dummy cartridge and filter is loaded prior to the start of test and flow is set using a flow rotameter connected at the inlet. A flow adjustment is performed with the help of adjustment knob on the sampler. After setting the flow rate the PUF/XAD cartridge and filter pertaining to the test are loaded and the sampler transfer tube connected to the tunnel. The pumps are initiated manually with the start of the test.
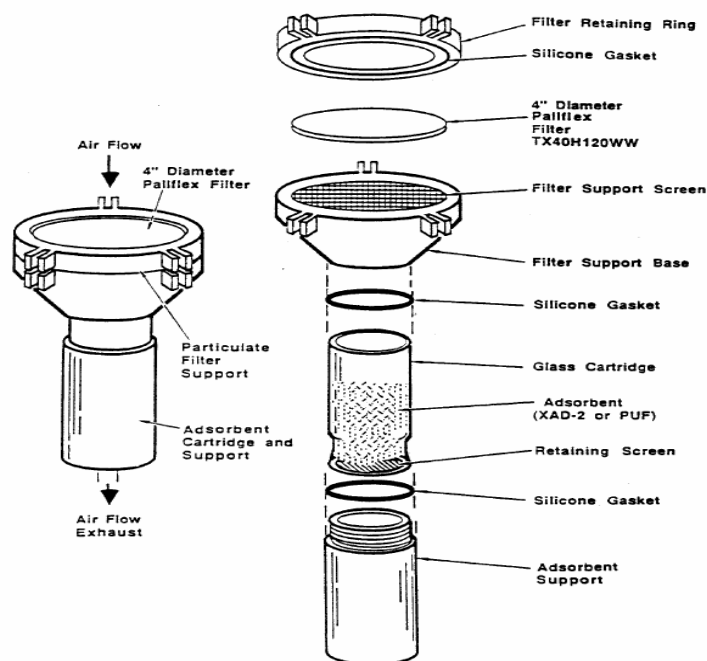
Figure 3.15 Schematic of DRI's PUF/XAD cartridge housing [56].

3.7.2.4   Unregulated Emissions Speciation On Filter Media

Gravimetric analysis of PM1, PM2.5 and PM10 require sample collection on T60A20 filters. In addition unregulated emissions speciation of metals/ions and EC/OC are to be collected on Teflon filters and Pre-fired Quartz filters respectively. For this purpose WVU utilized cyclonic particle classifiers fitted with filter holders to sample particles of different size fractions. URG manufactured Teflon coated aluminum cyclones were used. PM10 cyclone operates at 28.3lpm and PM1 and PM2.5 operate at 16.7lpm flow rate. Cyclones work on the principle of inertial separation of particles of different size fractions. A cyclone is usually specified by its flow rate and the cut-point diameter. The cut-point diameter denotes the size fraction of the PM that the cyclone would allow to pass through. Any particles larger than the specified size fraction would be filtered to the bottom of the cyclone. The working principle of the cyclone is based on the inertial properties of PM. A cyclone is designed in such a way that the air flow within it follows a vortex pattern before it exits out perpendicular to the direction of entry. The design is also in such a way that at specific flow rate only particles which fall within a certain diameter is able to exit out of the cyclone. The remaining heavier particles settle to the bottom of the cyclone and can be later removed. The efficiency of this segregation is dependent on the flow rate

through the cyclone. Hence it is necessary to keep the flow rate as close to cyclone specification for maximum efficiency.

The study required to collect PM2.5 metals/ions and PM2.5 EC/OC sample collection. The inlet of every cyclone was attached to the individual probes fitted to the primary tunnel. The outlet of the cyclone was fitted with a URG manufactured filter holders that were compatible with the cyclones used. Downstream of the filter packs were connected to the vacuum manifold through dedicated MFCs for each sample train. The MFC's flows were set according to the cyclones specification and sampling was initiated through the control computer. The MFC operation was monitored through the read back values obtained from them for data verification purposes.

3.7.3   NMHC Bag Sampling

Tedlar bags were used to collect bag samples of emissions after each test. One bag of dilute and one bag of dilution air samples were collected. The bags were then shipped to WVU for analysis of Non-Methane hydrocarbons using gas chromatography.

3.8   Gas Bag Sampling

Two large Tedlar bags are used to collect gaseous emissions during the test. These bags are later analyzed by passing the gases collected in the bags through the analyzers. This serves as data verification of the gas bench and is a required QA/QC procedure.

3.9   Temperature Control Module (TCM)

Dedicated temperature control modules were used to control the temperatures of the various probes and transfer lines as per CFR 40 regulations. The TCM functions as closed loop control system to maintain the various temperature set points. Omega model CNI-32 temperature controllers were used for this purpose. Individual temperature controllers were assigned set points and when the temperature feedback from the transfer line and probes fell below this set point value, the controllers send a signal to a solid state relay. The relay switches power to the respective heating unit to bring the temperature up to the set point and the controller disconnects the power through the relay once temperature set point has reached. J type thermocouples were

used to control the heated probes and both J and K type thermocouples were used to control the heated lines [47].

3.10 Instrumentation Control and Data Acquisition

The program for the instrumentation control and data acquisition is run from the control computer. A second reduction computer which interfaces with the control computer is used to setup tests and also to review the results of the tests. A third computer is dedicated to the logging of ECU data and media tracking software. The control computer interacts with the Dyne Loc systems to control the dynamometer loading and also with the data acquisition board for continuous logging of data at 10Hz. The control computer also contains the programs necessary for the calibration of various instruments of the transportable laboratory.

3.11 Emissions Species Collection Media

The transportable laboratory is capable of housing different media for sampling different emissions species. Media such as filters for gravimetric analysis of PM1, PM2.5, PM10 are preconditioned and preweighed in WVU before being shipped out to the test site. The list of unregulated species and their corresponding sample media are shown in the table below.

Table 3.1 List of species and sample media

Species	Media
VOC	Steel Canister (DRI)
Methane/NMHC	Tedlar Bags (WVU)
PAH	PUF/XAD (DRI)
Aldehydes	DNPH (DRI)
PM2.5 Elemental Carbon/Organic Carbon	47mm Pre-Fired Quartz filter (DRI)
PM2.5 Metals/Ions	47mm Teflon filter (DRI)
Total PM	47mm T60A20 double filter (WVU)

3.11.1 Media Conditioning and Weighing

All gravimetric media used are conditioned and pre-weighed at WVU's test facility in Morgantown before being shipped to the test site. The filters are placed in an environmental chamber maintained at $70^{o}F$ and 50% relative humidity for at least 1 hour and not more than 80 hours. The filters are then weighed according CFR 40 regulations and placed in sealed Petri

dishes and shipped to the test site. Prior to the weighing process three reference filters are kept in the environmental chamber. These reference filters must be weighed before weighing any test filters, so as to assess the stability conditions in the environmental chamber.

The filters were weighed using a Sartotius microbalance interfaced with a computer program which logs all test weight with the corresponding filter ID for future reference and data reduction.

3.11.2 Media Labelling

WVU uses a method of assigning unique identification numbers along with barcodes for each filter media. The barcodes are scanned and the characteristics of the filter media are entered. The bar coded stickers are pasted on the Petri dishes and the QA/QC sheet. The barcode stickers would have provisions for entering Test Number to identify used filters with the respective test runs. The media database would contain the pre-weight data of the filters. This study involved procuring certain media from DRI. And DRI used a similar system of media labeling through barcodes.

For easy tracking of filters with their corresponding sample train, color coding was employed for each sample train. Colored stickers were placed on filter holders for each sample train, so that it is easy to load and unload filters for different sample trains into appropriate filter holders.

3.11.3 Media Shipping and Tracking

A media tracking application was developed to associate different media with their respective sample trains. Barcodes on the respective media were scanned and the appropriate sample trains were entered in the application along with the test numbers. The used media were placed back in the Petri dishes and placed in padded pouches before being shipped overnight to WVU test facility at Morgantown. The QA/QC sheets placed along with the filters would also aided in the tracking of media. Special media that were to be shipped to DRI were placed in coolers with cold packs and shipped overnight to DRI facility at Reno, Nevada.

CHAPTER 4 - EMISSION TEST PROCEDURE

This chapter will discuss the steps involved in preparing the lab for emissions testing, which include calibration of instruments, system checks, and vehicle loading. The chapter would also deal with the method of calculation of distance specific emissions from raw lab data.

4.1   Lab Setup Procedures

The chassis dynamometer which is part of a flat bed trailer is lowered onto level ground with the help of the built in hydraulic jacks. The dynamometer surface is checked for flatness in order to prevent variation in vehicle loading due to inclination. The analytical trailer which houses the analyzer, control systems, dilution tunnel and data acquisition systems are placed close the dynamometer in order to reduce the length of exhaust transfer tube to the tunnel. The clean primary dilution tunnel used for this study was placed close to the trailer and dynamometer. The CFV-CVS blower unit was placed near the outlet section of the clean tunnel and connected via flexible air duct. The blower unit was powered by a Perkins diesel engine. The HEPA filter manifold is placed near the dilution air inlet section of the clean tunnel and connected via flexible air duct.

The pre-test preparation of the analytical trailer includes preparation of the gas bench and dynamometer controls. The heated probes for sampling the various gas species are fitted to the sampling plane of the tunnel through the available flanged ports. The probes are fitted facing upstream of the clean tunnel. The heated transfer lines were routed into the analytical trailer and connected to its respective ports. The clean tunnel covered with insulating material to prevent cold spots in the tunnel and thereby reducing thermophoretic loss of PM. The tubing for sampling of the unregulated species was installed to its respective sampling ports. Raw exhaust was planned to be sampled and diluted through ejector dilutor for particle sizing study. A 3/4 inch tubing was bent to form a J probe and fitted facing upstream at the raw exhaust inlet of the tunnel. The air compressor and zero air generators were powered prior to the trailer setup for storage of enough air for functioning of analyzers and air tools. The analyzers, heated lines and probes were all powered up for warm up and stabilization before further setup procedures were carried out. The laboratory utilizes a 100KW generator for power source if electrical power was

not available at the test location. Figure 4.1 shows the schematic of the sampling setup on the clean tunnel.
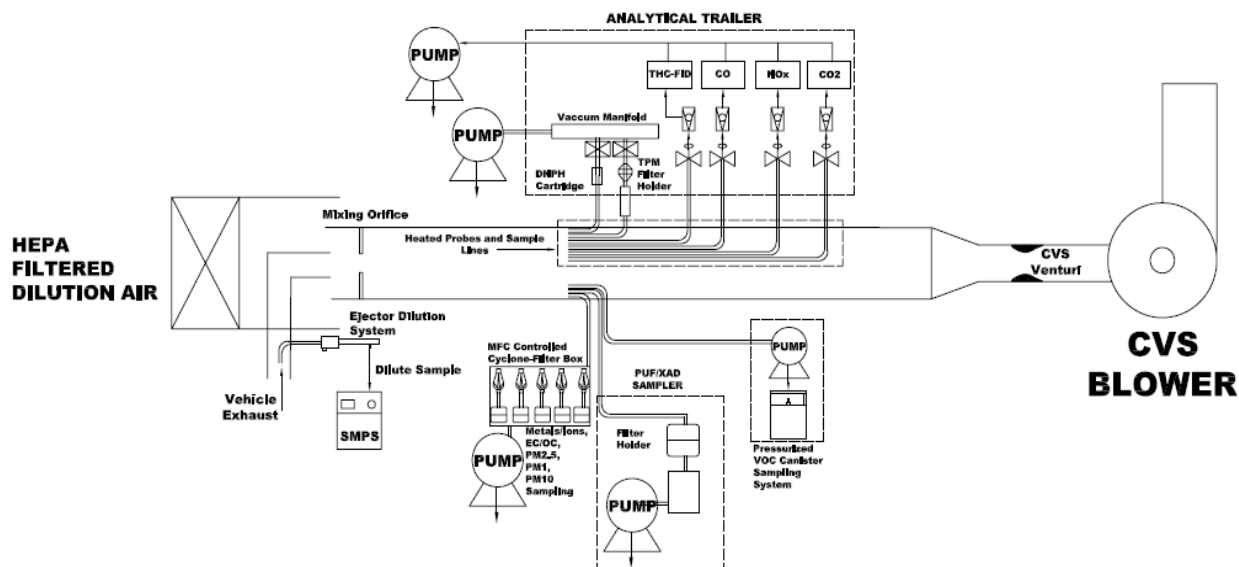
Figure 4.1 Schematic of clean tunnel sampling setup

4.2   Analyzer Setup and Calibration

Prior to the start of calibration procedures of the analyzers, various analyzer check procedure are carried out as stated in CFR 40, Part 86, subpart D, N. These checks are performed in order to assess the efficiency, interferences and response of the gas analyzers. NDIR analyzers experience interference from water vapor as it exhibits the same property towards infra red light as CO and CO_2. This test is performed by admitting span gases into the analyzer through a bubbling chamber and bypassing the bubbling chamber so as to asses the water vapor interference level. Water interference check denoted the efficiency of the chiller and dryer unit in removing water content from the gas sample. In a CO analyzer, a CO_2 interference check is performed to asses the efficiency of the conditioning column in removing CO_2 from the sample gas. Similarly CO_2 and water vapor interferes with the Chemiluminescence detector (CLD) of the NOx analyzer. Analyzer optimization tests such as on oxygen interference check for FID flame optimization and NOx converter efficiency for optimum working of the NOx analyzer in the NOx mode is performed. In addition methane response test is performed on the FID analyzer to check for the response of the flame towards methane gas in exhaust. The procedures for

performing these steps are given in CFR 40, Part 86, subpart D, N. These procedures are carried out periodically to ensure proper working of the analyzers. The following table lists the various preliminary checks on the analyzers.

Table 4.1 Analyzer optimization checks

Analyzer	Principle Of Operation	Checks	Purpose
CO2	Non-dispersive Infra Red (NDIR)	Water Interference check	Check efficiency of water removal unit
CO	Non-dispersive Infra Red (NDIR)	Water Interference check	Check efficiency of water removal unit
		CO2 interference check	Check CO2 removal unit
NOx	Chemiluminescence Detector (CLD)	Quench check for CO2 and water interference in reaction chamber	Check interferences in detector
		NOx converter efficiency check	Check NO2 to NO converter
THC	Flame Ionization Detector (FID)	Oxygen interference check for FID flame optimization	Check burner sensitivity
		Methane response test	Check response of FID to CH4

Analyzer calibrations are performed as prescribed in CFR 40, Part 86, and subpart N. The analyzers are calibrated between zero and full scale gas concentration readings expected during the tests. The span gas concentrations had an accuracy of 1% traceable to NIST, and the zero air was generated using a zero air generator incorporated into the analytical trailer. A 10 point calibration is performed on each analyzer using a gas divider which mixes a measured amount of span and zero gas to give sample concentrations varying in percentages of 10 between 0% and 100%. The analyzers are given a stabilization period at each calibration point before the data acquisition is initiated. The computer averages a 10 second reading at each point when data acquisition is initiated. Since the computer relates the concentration of calibration gases to ADC codes between 0 and 2000, a polynomial fit of the 10 point calibration is performed to convert ADC codes to engineering units. The span gases were chosen according to the level of emissions expected from a vehicle and also for greatest accuracy range. The decision is made from previous test experiences and vehicle configuration. If emission concentrations exceed the span gas value more than an allowable limit as stated in CFR 40 the analyzers are recalibrated with a higher span gas concentrations and tests repeated. The calibration files are always overwritten to avoid use of wrong calibration files. At the end of each test zero and span values of the analyzer are checked to estimate the analyzer drift. If the drift for THC analyzer was more than 3% and

for CO/CO_2, NOx more than 2% the analyzers were recalibrated. The NOx converter efficiency is checked for 90% or more efficiency in conversion else maintenance is performed on the analyzer.

4.3   Mass Flow Controller Calibration

Mass flow controllers are used for flow regulation for different sampling trains. This study utilized 5 MFCs for unregulated sampling and one MFC for TPM flow regulation. The 5 mass flow controllers used for the unregulated sample train were calibrated using Gilian flow standard device. A 10 point calibration was performed between fully closed and fully open conditions. The calibration curve was plotted and the slope and intercept of the curve was overwritten into the MFC calibration file. The TPM mass flow controller which was operated at a higher flow rate was calibrated using Laminar Flow Element (LFE) manufactured by Meriam Flow Measurement Devices. Meriam provides calibration coefficients and equations for each LFE which was obtained through calibration of LFE with NIST standard flow instruments. A five point calibration was performed. The flow rate was calculated using the following equation

$$\dot{V} = [B * \Delta P + C * \Delta P] * \left(\frac{\mu_{std}}{\mu_{flow}} \right) \qquad \textbf{Equation 4.1}$$

Where
B&C : LFE Coefficients
ΔP : Pressure differential across LFE
$\dfrac{\mu_{std}}{\mu_{flow}}$: Viscosity correction factor

The correction factor is calculated using the following equations:

$$CorrectionFactor = \left(\frac{529.67}{459.67 + T(^oF)} \right) * \left(\frac{181.87}{\mu_g} \right) \qquad \textbf{Equation 4.2}$$

$$\mu_g = \left(\frac{14.58 + \left(\dfrac{459.67 + T(^oF)}{1.8} \right)}{110.4 + \left(\dfrac{459.67 + T(^oF)}{1.8} \right)} \right) \qquad \textbf{Equation 4.3}$$

The differential pressure is measured using a Heise pressure reader and the temperature was measured using a fluke temperature calibrator. The LFE flow is expressed as standard flow using appropriate conversion to standard conditions of 20^oC and 101.1 KPa.

4.4 CFV-CVS Calibration

The CFV of the CVS system was calibrated using a subsonic flow meter and a flow restrictor as specified in CFR 40. The CFV calibration is performed once the lab is setup at the test site. The flow through the CFV is given by the following equation

$$Q_s = \left(\frac{K_v * P}{\sqrt{T}} \right)$$ **Equation 4.4**

Where
Qs : Venturi flow rate in cfm
P   : Absolute inlet pressure in Kpa
T   : Absolute inlet temperature in ^oK
Kv : Calibration coefficient

The calibration is system is leak checked and the blower is started with the flow restrictor in fully open conditions. Once flow is stabilized temperature and pressure at inlet are noted. Flow restrictor position is varied for eight readings in the critical flow range. The calibration coefficient is derived from the above equation knowing the flow rate and venturi inlet and temperature and pressure. Kv usually stays constant in the critical flow range and drops significantly with decrease in flow. The average of eight Kv readings and standard deviation is calculated. If the standard deviation exceeds 0.3% then recalibration is performed.

4.5 CFV-CVS Verification Procedure

WVU uses the method of Propane injection to verify the CFV-CVS operation and tunnel integrity. A propane injection kit is used to admit measured quantities of propane into the tunnel. The propane kit utilizes a critical flow orifice as a metering device, and the flow rate is calculated based on the inlet temperature and pressure reading obtained just prior to the orifice. The orifice is operated at critical flow conditions due to the high pressure inlet of gas and flow rate is not affected by any back pressure. Though the CFR prescribes a gravimetric method of calculating the amount of propane injected, WVU uses the propane injection kit manufactured by

Horiba for admitting know quantities of pure propane. The kit consists of a ruby orifice and the test gas is admitted into the CVS tunnel through a rosette for uniform mixing. A calibrated FID analyzer is used to measure the quantity of propane recovered from the tunnel. Percentage error is calculated between propane sample injected and propane recovered using FID analyzer value. The error should be within 2% else systematic trouble shooting is performed to asses the cause of loss of injected propane volume within the CVS system. Errors greater than 2% could be due to issues with CFV, leak in tunnel, THC analyzer calibration issues. The flow rate of propane through the kit is determined from the following equation.

$$q = \frac{A + (B*P) + (C*P^2)}{\sqrt{460 + T}}$$ **Equation 4.5**

Where
q   : Flow rate in SCFM at 20°C and 101.1 Kpa
A,B,C : Calibration coefficients supplied by Horiba
P   : Absolute orifice inlet pressure in psi
T   : Orifice inlet temperature in °F

Volume flow rate through the CVS-CFV is given by the following equation.

$$Q = \frac{V}{t} * 60$$ **Equation 4.6**

Where
V : Volume in SCFM as measured by the CFV.
t : Time interval in sec (300 sec)

Calculated sample concentration is determined by the following equation

$$C_{calc} = \left(\frac{q}{Q} * 10^6\right) * 3$$ **Equation 4.7**

The system error is obtained from the following equation, where C_{FID} is the measured concentration of the injected sample as read from the THC analyzer.

$$error = \left(\frac{C_{FID}}{C_{calc}} - 1\right) * 100$$ **Equation 4.8**

It is to be noted that propane injection is an end to end verifaction of the tunnel integrity, and the validity the check hold good only if the other individual sensory components, such as

temperature and pressure sensors, analyzer calibration have passed their respective verification procedures.

4.6 Test Procedure

As the first step in the test procedure the vehicle weight is measured and the respective flywheel setting is determined. For buses the equivalent inertia was calculated as the sum of the empty vehicle weight, half the passenger load, the driver and the equivalent weight of the non rotating wheel assemblies [46]. One set of rear wheels are removed and the dummy wheel rim is attached to connect the hub adapters for power transfer to the dynamometer components. The vehicle is backed on to the dynamometer and checked if the wheels are properly placed on the rollers. The vehicle is chained down on to the dynamometer bed for extra safety and the hub adapters are bolted to the dummy wheel rims attached to the vehicles. The necessary transfer line connections are made to route the exhaust from the vehicle into the dilution tunnel. Insulated flexible stainless steel transfer lines are used for this purpose.

Once the vehicle is placed on the dynamometer, the ECU connections are made to retrieve ECU broadcast engine speed and torque. The vehicle is run at a constant speed for the differential oils to warm up, as the viscosity of cold differential oil could add to significant load on the vehicle. While the differential warm up procedure is being undertaken the gas bench in the analytical trailer is prepared for the tests. Pre-test QA/QC checks on transfer line, heated probes and analyzer zero and span are performed. The two tedlar bags used for collection of integrated vehicle emission and background samples are evacuated using the GAST rotary vane pumps. The vacuum gauge indicating bag pressure should read 25 inches Hg indicating complete bag evacuation. All media are loaded and filters for PM are placed in the holder and fitted to the secondary dilution tunnel.

A coast-down operation of the vehicle is performed to evaluate the system loses in the dynamometer. The coast-down operation involves driving the vehicle to accelerate to 50mph and when initiated by the control computer letting the vehicle to coast to a stop with no external assistance such as braking or gear shifts. The computer performs a series of coast-down test to evaluate the frictional loses if any in the dynamometer system. The coast-down operation is performed based on SAE J1263 recommended practice of road load determination [57]. The coast-down program matches time taken in theoretical on road coast-down of a vehicle with the

time taken for coast-down of a similar vehicle on the dynamometer [58]. A lesser coast-down time on the dynamometer indicates less resistance from the dynamometer components and hence necessary power absorber braking is needed and a greater time on the dynamometer indicates more frictional resistance from the dynamometer components hence assistance from motor is needed to overcome the additional load due to friction of dynamometer components.

With the completion of the coast-down tests the vehicle is ready for chassis dynamometer testing. Since this study utilized additional sampling system from DRI, the flow rates of the sampling system are checked and the respective media are loaded and the field data sheets are filled out.

Once all the preliminary test procedures were completed the driver is provided with a monitor that displays the time and speed trace that vehicle needs to follow. With the initiation of the test sequence by the control computer the driver begins to drive the vehicle in accordance to the speed trace. Tests are repeated until repeatable data with COV of 5% or less is obtained for all emission constituents on three consecutive runs. Ambient temperature is monitored and if temperature exceeds 95°F testing is aborted.

Figure 4.2 Test vehicle mounted on the chassis dynamometer

4.7 Test Cycle

The test cycle that was used for this study was the Orange County Transit Authority (OCTA) cycle. The OCTA cycle was developed by WVU based on real bus operating data from the Orange County Transportation Authority. The OCTA cycle is an intermediate speed test cycle consisting of acceleration, deceleration, idle and cruise operations representing real world transit bus operation. Three back to back OCTA cycles were setup of which the first cycle was a warm-up cycle and the next to consecutive cycles were data taking cycles. The control computer initiated the pumps and mass flow controllers at the end of the first warm-up cycle to start the continuous data collection process. Samples were collected over a double length OCTA cycle so as to collect enough samples on the unregulated media for chemical characterization. The continuous data was recorded at 10Hz frequency. The driver is responsible for the control of vehicle speed according to the OCTA cycle speed trace and the control computer sends the calculated torque set point signals to the power absorbers Dyne-Loc systems for the vehicle loading. Unregulated media collection was done only on the second set of OCTA cycles. On completion of the cycle the vehicle is allowed for a 20 minute soak period before starting the next set of OCTA cycles. The study involved testing the vehicles with and without the after-treatment device hence the test procedures were repeated for these two vehicle configurations.
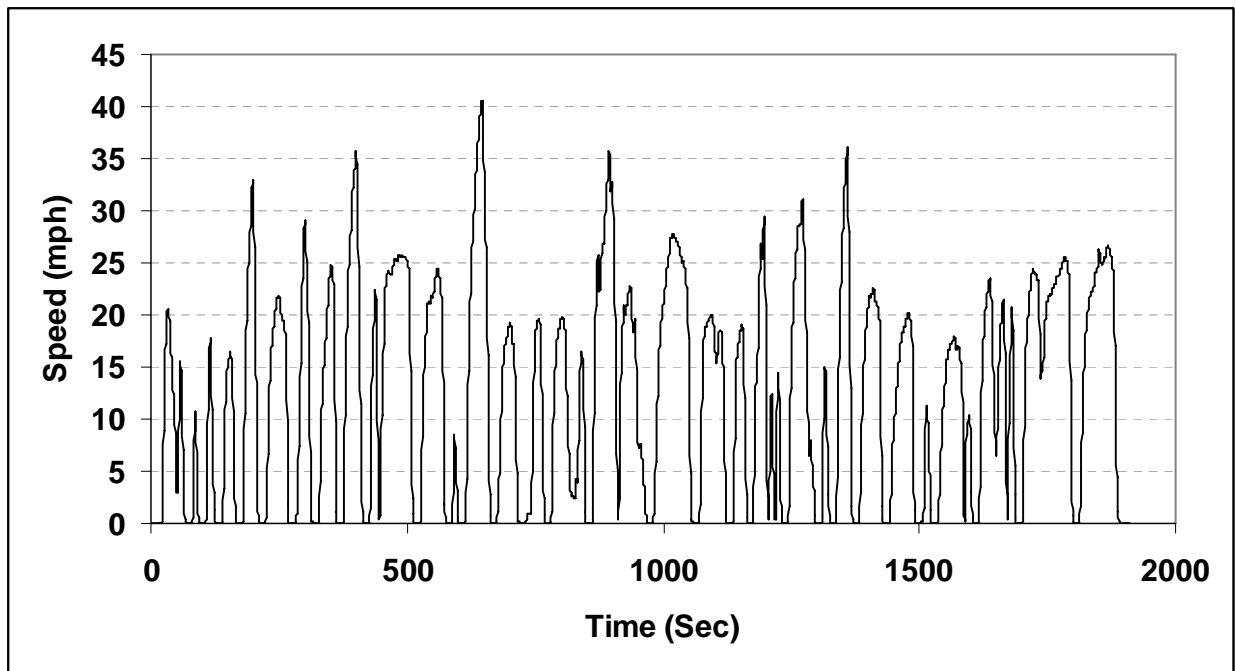
Figure 4.3 Speed Vs Time trace of OCTA cycle

For collecting the background emissions for the unregulated sample a similar double length OCTA cycle was setup and the vehicle was switched off and the control computer initiated all sampling devices during this tests. One background test was performed for each vehicle configuration. This method was followed so as to obtain background samples for the same length of time as that of the vehicle driven tests. Hence this would not bring about a discrepancy in test length while calculating distance specific emissions for background.

4.8 Emission Calculation

The data acquisition system consists of different modules for reading voltage signals from different sources. These modules are called as channels. Each channel receives analog voltage from the various analyzers, temperature and pressure monitoring systems. An analog to digital converter is used to convert the analog voltage signals to digital signals in the form of ADC codes. The ADC codes are converted to their respective engineering units with the help of the calibration files for each channel. The reduction computer uses data from different channels and substitutes the values in the respective equations to calculate the distance specific emissions. The equations used to calculate the different emissions are stated in this section.

For the calculation of the mass emissions of different exhaust constituents, it is necessary to calculate the flow through the tunnel (V_{mix}) and a factor known as the dilution factor (DF). Dilution factor is the ratio of theoretical amount of carbon-dioxide in the raw exhaust to the summation of the actual measured concentration of CO, CO_2, and HC. The total volume of dilute exhaust drawn through the tunnel for a test period is calculated using the following equation

$$V_{mix} = \sum_{1}^{n} \left(V_{(mix)i} * \Delta t \right) \qquad \text{[59]} \quad \textbf{Equation 4.9}$$

Where
V_{mixi} : Instantaneous tunnel flow rate through the CFV in ft^3/sec.

$$V_{(mix)i} = K_v * \frac{P_{vi}}{\sqrt{T_{vi}}} \qquad \text{[59]} \quad \textbf{Equation 4.10}$$

Where
Δt : Time interval between each instantaneous measurement point (sec)

n : Number of measurement points

K_v : Calibration coefficient of critical flow venturi

P_{vi} : Instantaneous pressure reading upstream of the CFV (inches Hg)

T_{vi} : Instantaneous temperature reading upstream of the CFV (^{o}R)

$$DF = \frac{13.4}{\left[(CO_{2e} + CO_{e} + HC_{e})*10^{-4}\right]}$$ [59] **Equation 4.11**

Where,

CO_{2e} : Carbon-dioxide concentration in dilute exhaust corrected for background (ppm).

CO_{e} : Carbon-monoxide concentration in dilute exhaust corrected for background
(ppm).

HC_{e} : Hydrocarbon concentration in dilute exhaust corrected for background (ppm).

4.8.1 Equations To Calculate Distance Specific Mass Of Regulated Emissions

For the calculation of distance specific mass emissions of regulated exhaust constituents, the data in the units of ppm is converted to mass units of grams. The resulting mass of emissions over a test cycle is divided by the total distance in miles traveled by the vehicle during the cycle to derive the distance specific mass emissions. The equations used to derive the mass of emissions are as follows.

$$CO_{mass} = \sum_{i=1}^{n}\left[\frac{(CO_{e})_{i}}{1*10^{6}}*V_{(mix)i}*\rho co*\Delta t\right] - \frac{CO_{d}}{1*10^{6}}*\left(1-\frac{1}{DF}\right)*V_{mix}*\rho co \quad [59]$$

Equation 4.12

Where,

$(CO)_{e}$: Instantaneous CO concentration of dilute exhaust obtained from the CO
analyzer readings (ppm).

V_{mixi} : Instantaneous dilute exhaust flow through CFV from Equation 4.10 (scfm).

ρ_{co} : Density of CO 32.97 g/ft^3 STP.

Δt : time interval between instantaneous measurement points (sec).

CO_{d} : Concentration of CO in dilution air corrected for water vapor (ppm).

$$CO_{d} = (1-0.000323*R)*CO_{dm}$$ [59] **Equation 4.13**

R : Relative humidity (%)

CO_{dm} : Concentration of CO in dilution air as obtained from CO analyzer readings (ppm).

V_{mix} : Total volume dilute exhaust drawn through the tunnel in a test period from Equation 4.9 (scf).

DF : Dilution factor from Equation 4.11.

$$CO_{dis\,tan\,ceSpecific} = \frac{CO_{mass}}{TotalDis\,tan\,ce}(g\,/\,mile)$$ **Equation 4.14**

CO_2 emissions are calculated using the following equation

$$CO_{2mass} = \sum_{i=1}^{n}\left[\frac{(CO_{2e})_i}{1*10^6}*V_{(mix)i}*\rho co_2*\Delta t\right] - \frac{CO_{2d}}{1*10^6}*\left(1-\frac{1}{DF}\right)*V_{mix}*\rho co_2 \quad [59]$$

Equation 4.15

Where,

$(CO)_{2e}$: Instantaneous CO_2 concentration of dilute exhaust obtained from the CO_2 analyzer readings (ppm).

V_{mixi} : Instantaneous dilute exhaust flow through CFV from Equation 4.10 (scfm).

ρ_{co2} : Density of CO_2 51.81 g/ft^3 STP.

Δt : time interval between instantaneous measurement points (sec).

CO_{2d} : Concentration of CO_2 in dilution air as obtained from CO_2 analyzer readings (ppm).

V_{mix} : Total volume dilute exhaust drawn through the tunnel in a test period from Equation 4.9 (scf).

DF : Dilution factor from Equation 4.11.

$$CO2_{dis\,tan\,ceSpecific} = \frac{CO2_{mass}}{TotalDis\,tan\,ce}(g\,/\,mile)$$ **Equation 4.16**

NOx emissions calculations are performed with the following equations.

$$NO_{Xmass} = K_H * \left[\sum_{i=1}^{n} \left[\frac{(NO_{Xe})_i}{1*10^6} * V_{(mix)i} * \rho_{NOx} * \Delta t \right] - \frac{NO_{Xd}}{1*10^6} * \left(1 - \frac{1}{DF}\right) * V_{mix} * \rho_{NOx} \right] [59]$$

Equation 4.17

Where,

NOxe : Instantaneous NOx concentration of dilute exhaust obtained from the NOx analyzer readings (ppm).

V_{mixi} : Instantaneous dilute exhaust flow through CFV from Equation 4.10 (scfm).

ρ_{NOx} : Density of NOx 54.16 g/ft^3 STP.

Δt : time interval between instantaneous measurement points (sec).

NOxd : Concentration of NOx in dilution air as obtained from NOx analyzer readings (ppm).

V_{mix} : Total volume dilute exhaust drawn through the tunnel in a test period from Equation 4.9 (scf).

DF : Dilution factor from Equation 4.11.

K_H : Humidity correction factor

$$K_H = \frac{1}{(1 - 0.0026 * (H - 75))} \qquad [59] \quad \textbf{Equation 4.18}$$

$$H = \frac{(43.478 * R_i * P_d)}{\left(P_b - \frac{(P_d * R_i)}{100}\right)} \qquad [59] \quad \textbf{Equation 4.19}$$

Where,

H : Absolute humidity of the engine intake air (grains of water/lb of dry air).

R_i : Relative humidity of the engine intake air (%).

P_d : Saturated vapor pressure at engine intake air dry bulb temperature (mm of Hg).

P_b : Barometric pressure (mm of Hg).

$$NOx_{dis\,tan\,ceSpecific} = \frac{NOx_{mass}}{TotalDis\,tan\,ce} (g/mile) \qquad \textbf{Equation 4.20}$$

THC emissions are calculated using the following equations.

$$THC_{mass} = \sum_{i=1}^{n}\left[\frac{(HC_e)_i}{1*10^6}*V_{(mix)i}*\rho_{HC}*\Delta t\right] - \frac{HC_d}{1*10^6}*\left(1-\frac{1}{DF}\right)*V_{mix}*\rho_{HC} \quad [59]$$

Equation 4.21

Where,

HC_e : Instantaneous HC concentration of dilute exhaust obtained from the HC FID
analyzer readings (ppm).

V_{mixi} : Instantaneous dilute exhaust flow through CFV from Equation 4.10 (scfm).

ρ_{HC} : Density of HC for CNG fueled vehicles 18.85 g/ft^3 STP.

Δt : Time interval between instantaneous measurement points (sec).

HC_d : Concentration of HC in dilution air as obtained from HC FID analyzer readings
(ppm).

V_{mix} : Total volume dilute exhaust drawn through the tunnel in a test period from
Equation 4.9 (scf).

DF   : Dilution factor from Equation 4.11.

$$THC_{dis\,tan\,ceSpecific} = \frac{THC_{mass}}{TotalDis\,tan\,ce}(g/mile)$$

Equation 4.22

The PM emission collected on filters from the secondary dilution tunnel is calculated using the following equation.

$$P_{mass} = (V_{mix}+V_{sf})*\left[\frac{P_f}{V_{sf}}-\left(\frac{P_{bf}}{V_{bf}}*\left(1-\frac{1}{DF}\right)\right)\right] \quad [59] \quad \text{**Equation 4.23**}$$

Where,

Vmix : Total volume dilute exhaust drawn through the tunnel in a test period from
Equation 4.9 (scf).

Vsf   : Total sample volume of dilute exhaust drawn through the secondary dilution
tunnel (scf).

Pf   : Actual mass of PM collected on the sample filter (grams).

Pbf : Actual mass of PM collected on the background filter (grams).

DF   : Dilution factor from Equation 4.11.

4.8.2 Equations To Calculate distance Specific Emissions of Unregulated Species

The unregulated species analysis was carried out at Desert Research Institute (DRI), Reno, Nevada. Preliminary data processing was performed by DRI and the concentrations were reported in the units of g/m^3 to WVU. Final data reduction involved similar calculations as in regulated emissions to derive the distance specific emissions of unregulated species.

The data reduction does not involve background correction. Hence concentrations are reduced as tunnel concentration and background concentrations separately. This methodology is followed to eliminate negative emissions value if background emissions happen to be greater than the test emissions. For the calculation of the emission concentration in the tunnel, the total flow through the tunnel is calculated.

$$V_{Tunnel} = (V_{mix} + V_{mini} + V_{PUF/XAD} + V_{DNPH} + V_{voc} + V_{PM2.5} + V_{PM10} + V_{PM1.0} + V_{EC/OC} + V_{Metals})$$

Equation 4.24

Where,

V_{Tunnel} : Total flow through the tunnel in a test period (scf)

V_{mini} : Total flow through the secondary dilution tunnel in a test period (scf)

$V_{PUF/XAD}$: Total flow through the PUF/XAD cartridge in a test period (scf)

V_{DNPH} : Total flow through the DNPH cartridge in a test period (scf)

V_{VOC} : Total flow into the VOC canister in a test period (scf)

$V_{PM2.5}$, V_{PM10}, V_{PM1}, $V_{EC/OC}$, V_{Metals} : Total flow through the respective filters in a test period (scf)

The tunnel flow was calculated from integrating actual flows of all sample trains from the read back value of the MFCs.

4.8.2.1 *Carbonyl Sample Analysis*

The carbonyl sample train was consisted of a silica gel Sep-Pak cartridge coated with DNPH. The exhaust was sampled through this cartridge at 0.5lpm, with the flow controlled through a MFC. The reactions of the DNPH with exhaust carbonyls create hydrazones in the cartridge which are further extracted and analyzed using High Performance Liquid Chromatography (HPLC) method. The procedures followed by DRI in the analysis of carbonyls

81

involve the extraction of hydrazones by eluting the cartridge with acetonitrile. And transferring part of the eluted sample into a 2-ml septum vial and injecting it into high performance liquid chromatograph through an auto sampler. The chromatogram used in DRI was Waters 2690 Alliance System with 996 Photodiode Array Detector for separation and quantization of the hydrazones. DRI analyzed C_1 through C_7 carbonyl compounds. HPLC system used in DRI was equipped with the photodiode array detector, which makes the identification of carbonyl compounds much more accurate than the standard UV/VIS detector. More detailed description of the carbonyl analysis procedure followed by DRI is explained in APPENDIX A-1.

The tunnel concentration of carbonyl compounds is calculated by the following equation.

$$Carbonyl_{TestUncorrected} = V_{tunnel} * Carbonyl_{sample} * 10^{-6} \qquad \textbf{Equation 4.25}$$

Where,

$Carbonyl_{TestUncorrected}$: Tunnel concentration of individual carbonyl compounds
without correcting for background concentration (grams).

$Carbonyl_{Sample}$: Concentration obtained by HPLC analysis with preliminary
data processing from DRI ($\mu g / m^3$).

V_{tunnel} : As calculated in Equation 4.24 (m^3)

$$Carbonyl_{TestUncorrected}^{Dis\tan ceSpecific} = \frac{Carbonyl_{TestUncorrected}}{TotalDis\tan ce} \left(g / mile \right) \qquad \textbf{Equation 4.26}$$

4.8.2.2 *Poly Aromatic Hydrocarbons/Nitro-Ploy Aromatic Hydrocarbon (PAH/n-PAH) Sample Analysis*

The PAH compounds were categorized as particle bound PAH, gas phase PA Hans semi-volatile PAH. The PAH compounds were collected with a PUF/XAD sampling train. The sampling train is explained in *Section 3.7.2.3*. The samples from the PUF/XAD cartridge and TIGF filters were extracted and prepared for analysis. The sample preparation and analysis method is explained in detail in APPENDIX A-2. n-PAH analysis was carried out by HPLC method and the filters and PUF/XAD extracts were done using a Gas Chromatography and Mass Spectrometry (GC/MS) technique. A Varian CP-3800 GC equipped with a CP8400 auto sampler

and interfaced to a Varian Saturn 2000 Ion Trap operating in electron impact (EI) ionization mode was used for this purpose. The n-PAH analysis was carried out using the Varian 1200 triple quadruple Gas Chromatograph/Mass Spectrometer (GC/MS) system with CP-8400 auto sampler.

The tunnel concentrations of PAH/n-PAH were obtained from the following equation.

$$PAH_{TestUncorrected} = V_{tunnel} * PAH_{sample} * 10^{-9}$$ **Equation 4.27**

Where,

$PAH_{TestUncorrected}$: Tunnel concentration of individual PAH/n-PAH compounds

without correcting for background concentration (grams).

PAH_{Sample} : Concentration obtained by HPLC/GC/MS analysis with preliminary

data processing from DRI (ng/m^3).

V_{tunnel} : As calculated in Equation 4.24 (m^3)

$$PAH_{TestUncorrected}^{Dis\tan ceSpecific} = \frac{PAH_{TestUncorrected}}{TotalDis\tan ce}(g/mile)$$ **Equation 4.28**

4.8.2.3   Volatile Organic Compound Sample Analysis

The Volatile Organic Compound sample was obtained by sampling with a VOC canister sampling system, supplied by DRI. A detailed description of the sampling system is discussed in *Section 3.7.2.2.* The sealed canister samples were preconditioned and analyzed with the help of GC with flame ionization detector and GC with mass spectrometry. A detailed description of the preparatory steps before GC analysis and GC calibration procedures employed in DRI are stated in APPENDIX A-3.

The tunnel concentrations of the various VOC compounds were obtained from the following equations.

$$VOC_{TestUncorrected} = V_{tunnel} * VOC_{sample} * 10^{-6}$$ **Equation 4.29**

Where,

$VOC_{TestUncorrected}$: Tunnel concentration of individual VOC compounds

without correcting for background concentration (grams).

VOC$_{Sample}$: Concentration obtained by GC analysis with preliminary

                           data processing from DRI (ng/m^3).

V$_{tunnel}$: As calculated in Equation 4.24 (m^3)

$$VOC_{TestUncorrected}^{Dis\tan ceSpecific} = \frac{VOC_{TestUncorrected}}{TotalDis\tan ce}\left(g/mile\right)$$
         Equation 4.30

4.8.2.4   *Elemental/Organic Carbon (EC/OC) Sample Analysis*

The sample for analysis of EC/OC was collected on 47mm pre-fired Quartz filter. Particles of 2.5 micron cut size segregated using a cyclone was collected on the filters. DRI employed the thermal/optical reflectance (TOR) method for the analysis of EC and OC. The TOR method is based on the principle that different types of carbon-containing particles are converted to gases under different temperature and oxidation conditions. The TOR method helps to distinguish 7 different carbon fractions. A detailed description of the methodology and procedure of analysis are described in APPENDIX A-4.

The tunnel concentrations of EC/OC are obtained from the following equation.

$$EC/OC_{TestUncorrected} = \frac{V_{tunnel}}{V_{EC/OC}}*2*EC/OC_{sample}*10^{-6}$$
         Equation 4.31

Where,

EC/OC$_{TestUncorrected}$: Tunnel concentration of individual EC/OC compounds

                         without correcting for background concentration (grams).

EC/OC$_{Sample}$: Concentration obtained by TOR analysis with preliminary

                         data processing from DRI ($\mu g/filter$).

V$_{tunnel}$: As calculated in Equation 4.24 (m^3)

V$_{EC/OC}$: Total flow rate through pre-fired Quartz filter (m^3)

$$EC/OC_{TestUncorrected}^{Dis\tan ceSpecific} = \frac{EC/OC_{TestUncorrected}}{TotalDis\tan ce}\left(g/mile\right)$$
         Equation 4.32

4.8.2.5 Metals Sample Analysis

Samples were metal analysis was collected on 47mm Teflon filters. Particles of 2.5 micron cut size segregated using a cyclone was collected on the filters. The Teflon filters were pre-conditioned for 24 hours before analysis. X-Ray Fluorescence (XRF) method was used to identify the different metals in the sample. A Kevex Corporation Model 700/8000 Energy Dispersive X-Ray Fluorescence (EDXRF) analyzer using a side-window, liquid-cooled, 60 keV, 3.3 milliamp rhodium anode x-ray tube and secondary fluorescers was used for this purpose. A detailed description of the analysis methodology, instrument resolution and mimium detection limit are stated in APPENDIX A-5.

The tunnel concentrations of different metals are obtained from the following equation.

$$Metals_{TestUncorrected} = \frac{V_{tunnel}}{V_{Metals}} * 2 * Metals_{sample} * 10^{-6} \qquad \textbf{Equation 4.33}$$

Where,

$Metals_{TestUncorrected}$: Tunnel concentration of individual Metals compounds
without correcting for background concentration (grams).

$Metals_{Sample}$: Concentration obtained by XRF analysis with preliminary
data processing from DRI ($\mu g / filter$).

V_{tunnel} : As calculated in Equation 4.24 (m^3)

V_{Metals} : Total flow rate through Teflon filter (m^3)

$$Metals_{TestUncorrected}^{Dis\tan ceSpecific} = \frac{Metals_{TestUncorrected}}{TotalDis\tan ce} \left(g / mile \right) \qquad \textbf{Equation 4.34}$$

CHAPTER 5 - RESULTS AND DISCUSSION

The two natural gas transit buses were tested on the WVU transportable chassis dynamometer laboratory. Regulated emissions from both vehicles with and without the after-treatment devices were measured and a complete characterization of exhaust from the RTA natural gas bus was successfully carried out. The after-treatment device which was a two-way oxidation catalyst was manufactured by Engine Control Systems. The vehicles were subjected to a double length OCTA cycle. This chapter discusses the results obtained and the effectiveness of the catalyst in reducing regulated and unregulated constituents of vehicle exhaust. The regulated emission constituents measured in this study were CO, NOx, THC and PM. The regulated emission results presented here are an average of multiple runs and the error bars plotted as maximum and minimum value in the multiple runs. The unregulated category which includes, VOC, PAH, Carbonyls, Metals and EC/OC were characterized and quantified by DRI. The unregulated data presented here are not corrected for background and presented as test non-corrected and background values for that corresponding test configuration. As part of the study particle size measurements were performed using the SMPS. A particle sizing study was conducted to study the variation in particle size distribution in vehicle exhaust during the catalyst warm-up period in cold starts.

5.1   Regulated Emissions Results

The results of the regulated emissions obtained from the testing of the RTA transit bus are shown in Figure 5.1. The oxidation catalyst was effective in reducing the concentration of CO by 98.9%. The THC emissions were reduced by 62.4% with the use of the oxidation catalyst. The effectiveness of an after-treatment device in reducing hydrocarbon emissions from natural gas vehicles is limited only to the Non-Methane Hydrocarbon (NMHC) portion of the total hydrocarbon emissions. This is due to the fact that NMHC is the only environmental concern, due to its smog forming capabilities. Methane, which forms the major portion of hydrocarbon emissions from natural gas vehicles, is considered not to be phototoxic. The PM emissions from natural gas vehicles is usually extremely low and often below quantifiable limits. This is due to the gaseous nature of the combusting fuel combined with spark ignition. The only source of PM

from natural gas vehicle could be as a result of lube oil combustion. The PM value seen from the vehicle without the after-treatment device could be as a result of the lube oil combustion.

RTA CNG TRANSIT BUS
REGULATED EMISSIONS
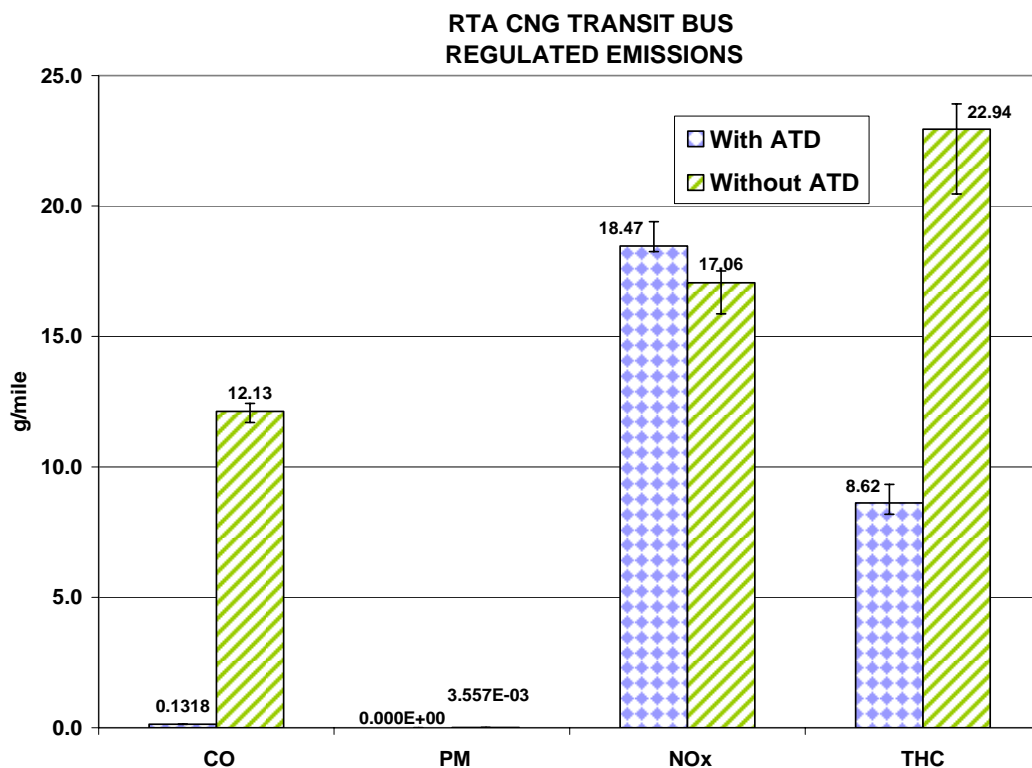
Figure 5.1 Regulated Emissions Result from RTA Transit Bus.

Figure 5.2 shows the methane and NMHC split in the exhaust of the RTA natural gas vehicle. The methane concentration was obtained from the VOC analysis of DRI. The methane analysis of the exhaust showed that 63.8% of the exhaust from the baseline configuration consists of methane. This is due to the fact that the natural gas vehicles are more prone to incomplete combustion and consequently higher levels of hydrocarbon emissions consisting predominantly of methane is seen. The NMHC portion of the hydrocarbon emissions were reduced by 72.4%. Most oxidation catalysts are not efficient in reducing methane concentration in exhaust. This is due to the fact that methane oxidation requires higher light off temperatures in the exhaust around $500^{o}C$ [45]. And in order to increase the exhaust temperatures to suitable levels engine designers would have to sacrifice thermal efficiency of the engine. Though on regulatory stand point methane reduction is not of major concern as it is not phototoxic, factors such as its contribution to global warming and the formation of additional formaldehyde due to impartial oxidation in the oxidation catalyst warrants after-treatment device manufacturers to

consider the reduction of methane in the exhaust of natural gas vehicles. Certain platinum group metals in the right ratio are able to achieve considerable reduction in methane concentration in the exhaust at lower light off temperatures [45]. This particular oxidation catalyst that was fitted to the RTA transit bus tested in this study was effective in reducing the methane concentration by 57%.

Note: Methane concentration obtained from DRI VOC analysis
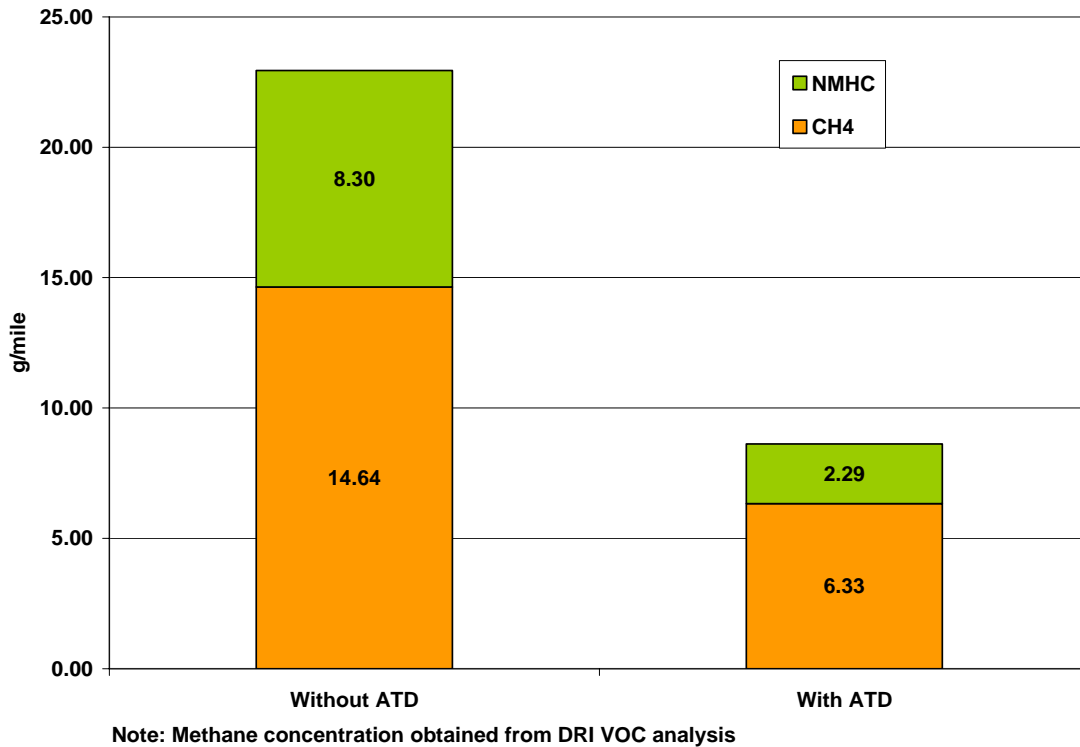
Figure 5.2 Methane/NMHC Results from RTA Transit Bus

The results of the regulated emissions from the LACMTA transit bus are shown in Figure 5.3. The results showed a 99.3% reduction in CO concentration. The CO concentrations with the after-treatment device was reduced to below detectable limits in most of the test runs. The PM values were very low in number. The THC levels in the exhaust from the LACMTA transit bus was only reduced by 29.1% with the after-treatment device. It is also to be noted that the NMHC speciation was not performed on this vehicle. Therefore it could be possible that majority of the THC composition could be methane and the catalyst that was retrofitted to the LACMTA transit bus was not effective in reducing methane and as a result it reflects as higher hydrocarbon emissions in the exhaust without the after-treatment device.

The catalyst being a two-way catalyst did not show any effect on the NOx concentrations in the exhaust of both the vehicles.

LACMTA CNG TRANSIT BUS
REGULATED EMISSIONS
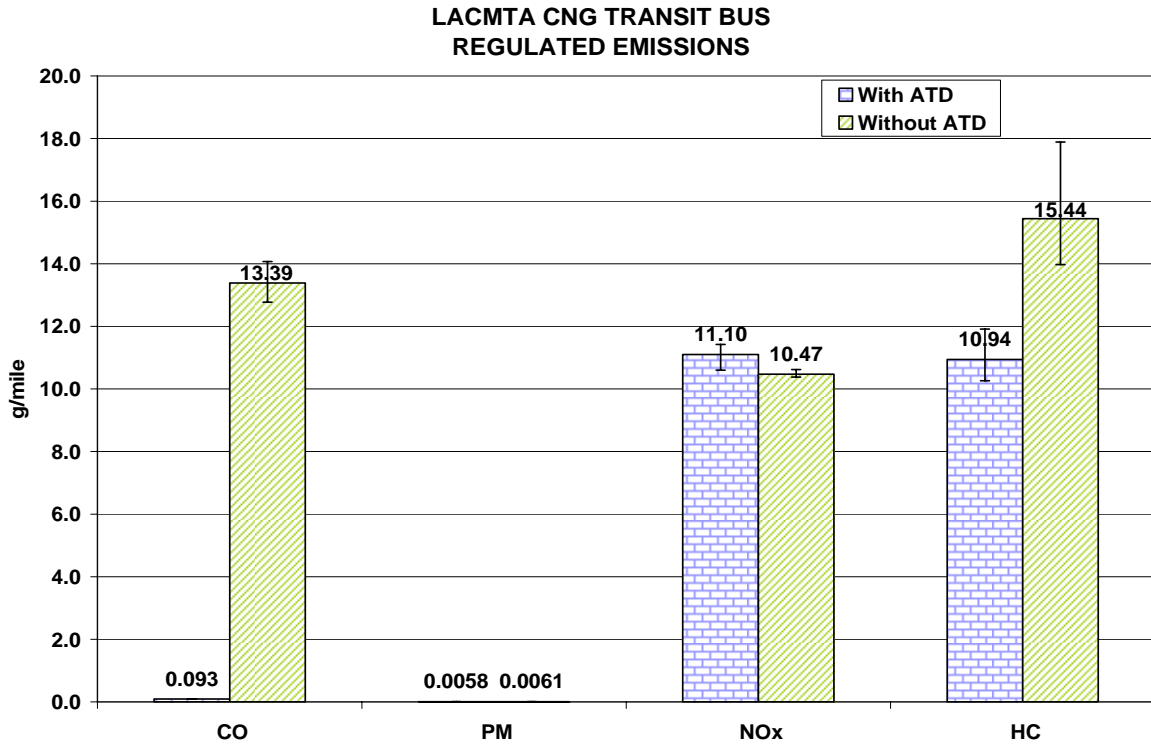
Figure 5.3 Regulated Emissions Result from LACMTA Transit Bus.

5.2   Unregulated Emissions Results

The unregulated emissions sample with special sampling media and analyzed by DRI. The categories of unregulated emissions analyzed in this study include, carbonyls, Poly Aromatic Hydrocarbons (PAH), Volatile Organic Compounds (VOC), metals, Elemental Carbon/Organic Carbon (EC/OC) fraction. The unregulated emissions results are presented as test non-corrected values and background values for the respective tests separately. This is to avoid the occurrence of negative emissions values in the case of the background being higher than the test values. Unregulated emissions results have uncertainty values associated with each species detected. This uncertainty value depicts the measurement error associated with each species. The calculation of this uncertainty is discussed in APPENDIX V. DRI's data reduction program takes into account uncertainty in sample volume flows also.

5.2.1   Carbonyl Emissions Result

The carbonyl emissions were sampled onto DNPH cartridges and later extracted and analyzed by DRI using high performance liquid chromatography method. Carbonyl emissions characterization involved the identification of 14 different carbonyl compounds. The results of carbonyl emissions are shown in Figure 5.4.
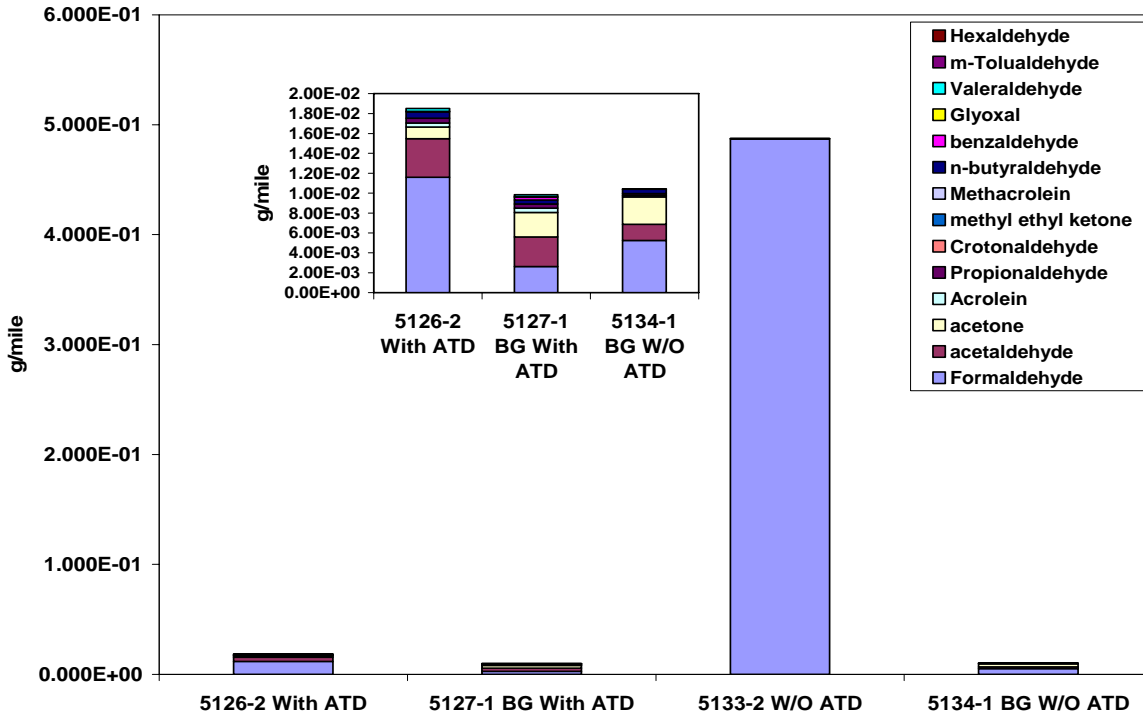
Figure 5.4 Carbonyl Emissions Results from RTA Transit Bus.

The after-treatment device was effective in reducing the carbonyl emissions by 96%. Total carbonyl emissions with the after-treatment device were reduced close to levels found in tunnel background concentration. The compounds that are shown in the legend but not visible in the chart were below detectable limits. Figure 5.5 and Figure 5.6 shows a detailed classification of the various carbonyl compounds found in the exhaust and their percentage contribution to the total carbonyl emissions.
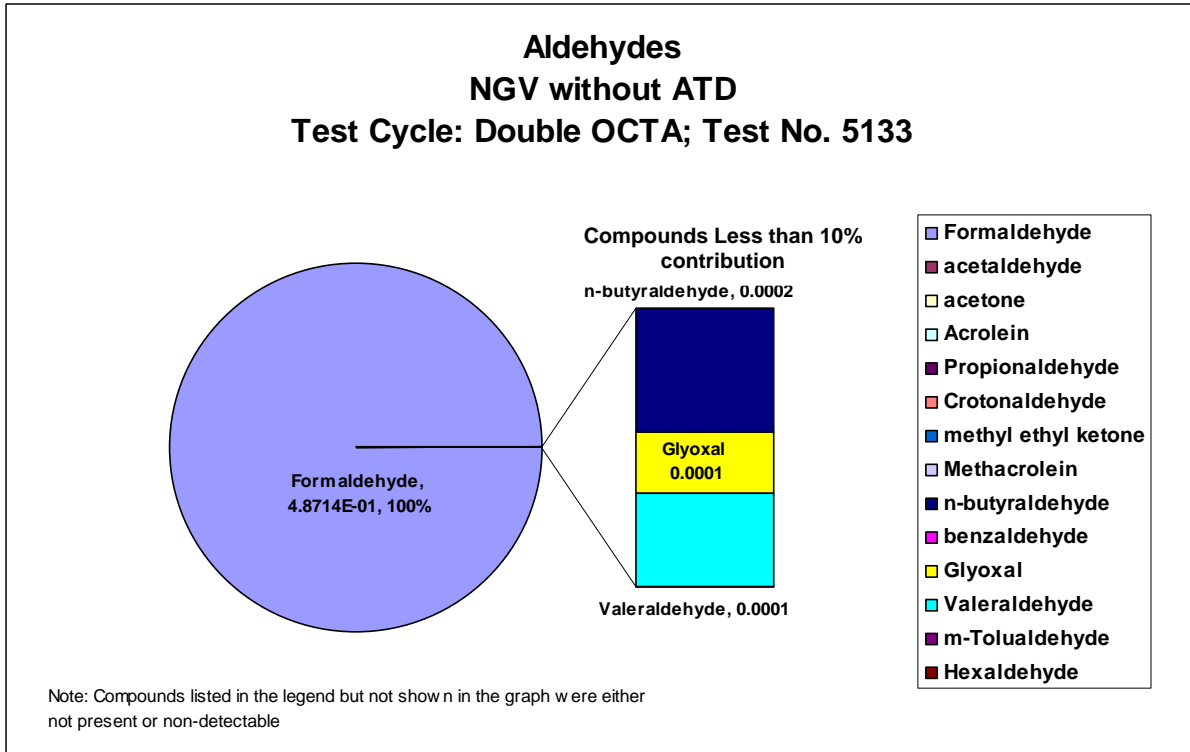
Figure 5.5 Carbonyl Compounds Concentration Without After-treatment Device.
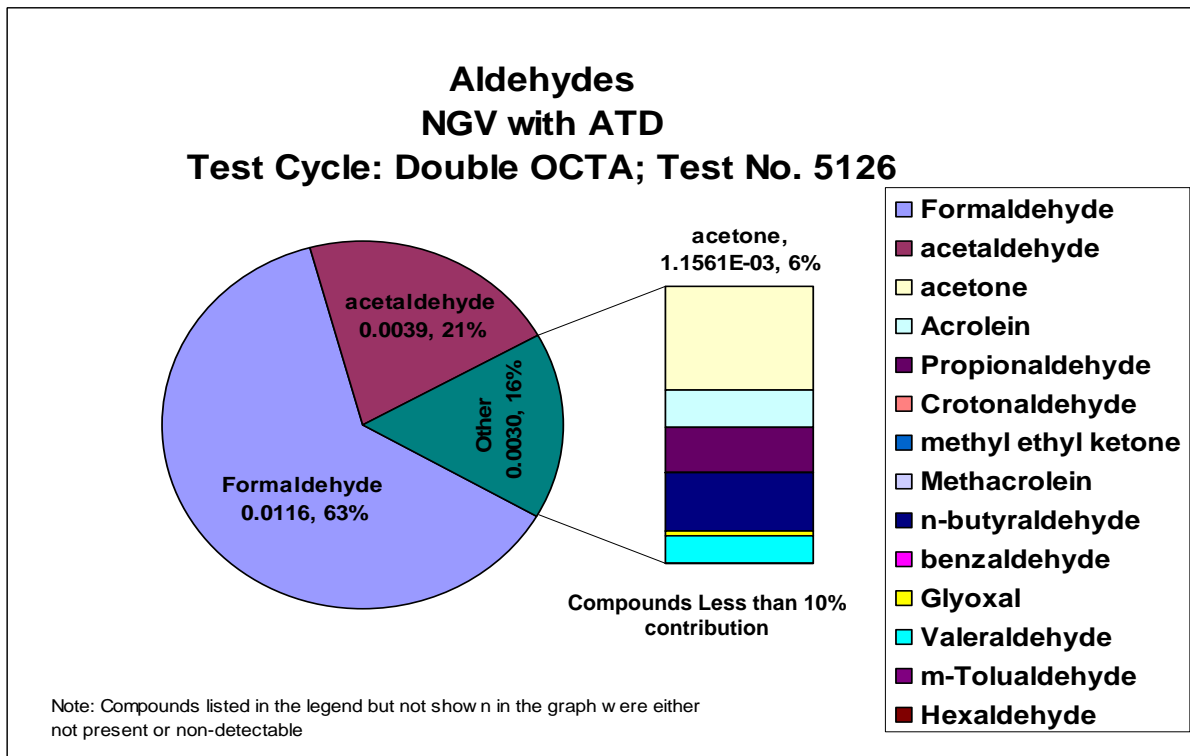
Figure 5.6 Carbonyl Compounds Concentration With After-treatment Device.

The results from Figure 5.5 and Figure 5.6 show that formaldehyde was the major contributor towards carbonyl emissions in natural gas vehicles. The growth of natural gas vehicles and the formaldehyde emissions associated with them have forced regulatory authorities to enforce regulations on formaldehyde. Emission regulations of EPA for the clean fuel vehicles place the cap on formaldehyde emissions at 0.025 g/bhp-hr. Formaldehyde being the major product of incomplete oxidation of methane is a target species for catalyst manufacturers. The results from the transit bus configurations with the after-treatment device shows that formaldehyde reduction of 97.5% was achieved and subsequently concentrations were reduced close to background levels. The result also indicated the presence of acetaldehyde in the configuration with the after-treatment device while the same not being identified in the baseline configuration of the transit bus. Though the level of acetaldehyde was low it could have formed due to the impartial oxidation of the unburned methane within the oxidation catalyst. Study conducted by Sakai et al. has shown that with the presence of NO in the exhaust inhibits the oxidation of methane and increases the formation of formaldehyde [60, 61]. Although the experiments conducted by Sakai et al. did not establish the formation of other carbonyl compounds, acetaldehyde also known as ethanal is one step higher than formaldehyde in the carbonyl compound hierarchy. Hence presence of acetaldehyde in the exhaust with the after-treatment device present might hint the acetaldehyde formation mechanism similar to the formaldehyde formation mechanism illustrated by Sakai et al.

Figure 5.7 shows the total carbonyl emissions with the total uncertainty in the measurement involved. The results show that with the after-treatment device the concentrations of carbonyl compounds were very low such that the uncertainty in the measurement was close to the analyte concentration values indicating higher error in measurement for very low concentrations of compounds detected.
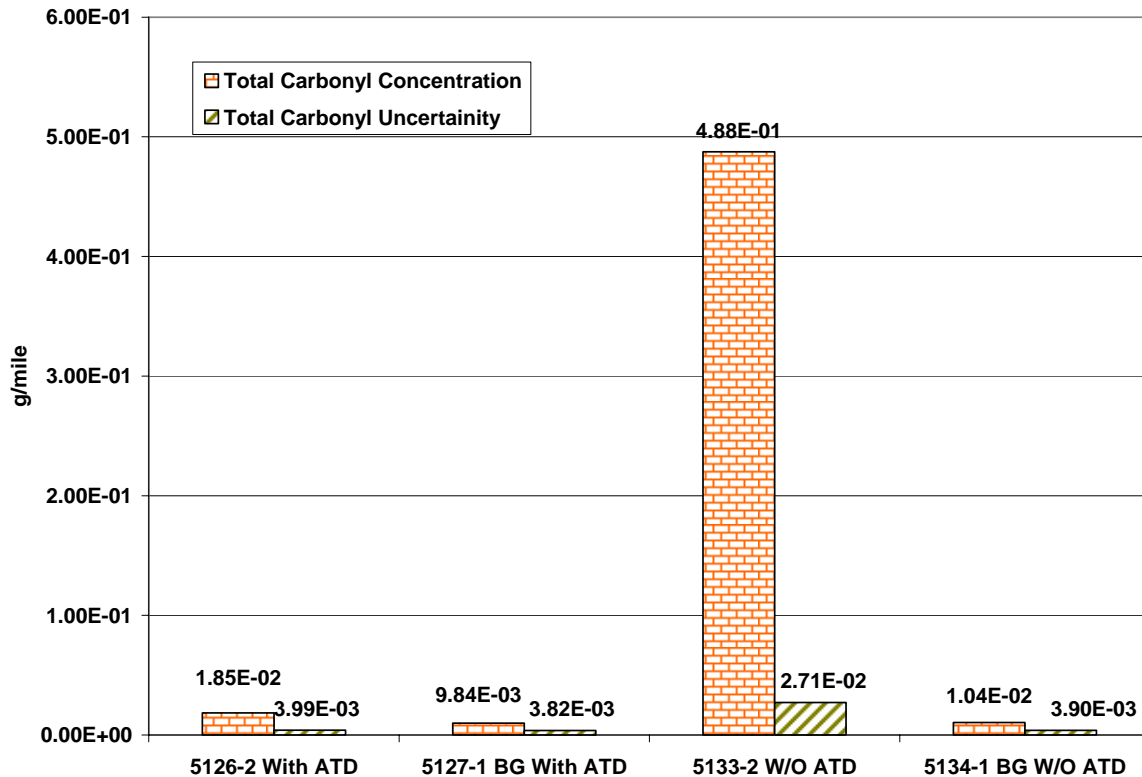
Figure 5.7 Total Carbonyl Concentration and Measurement Uncertainty

5.2.2 Poly Aromatic Hydrocarbons/ nitro- Poly Aromatic Hydrocarbons (PAH/n-PAH) Result

The samples for the analysis of PAH/n-PAH compounds were collected on PUF/XAD cartridge and later extracted and analyzed by DRI using GC/MS techniques. DRI caharcterized 93 different PAH compounds and 29 different nitro-PAH compounds. PAH are usually believed to be as result of combustion of aromatic fuels such as diesel. The aromatic fraction of CNG fuel is very negligible as seen from the fuel analysis report attached in APPENDIX A. Hence the source of PAH emissions from CNG vehicles could be from the combustion of lubrication oil. The PAH analysis obtained from DRI are subdivided into particle phase PAH, semi-volatile phase PAH, and gas phase PAH. The semi-volatile and gas phase PAH are obtained from extraction of sample from the PUF/XAD cartridge and the particle phase PAH are obtained from the extraction of sample from the TIGF filter placed upstream of the cartridge holder. Figure 5.8 and Figure 5.9 and Figure 5.10 show the results of the different categories of PAH emissions.
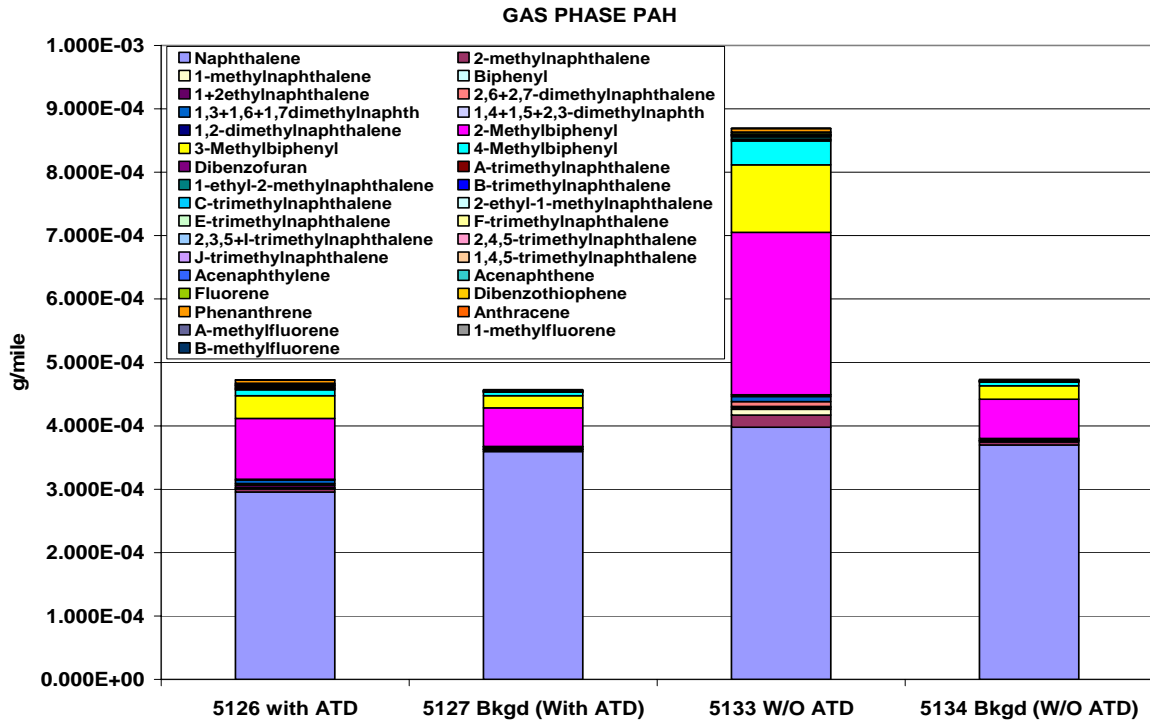
GAS PHASE PAH

Figure 5.8 Results of Gas Phase PAH Emissions from RTA Transit Bus.
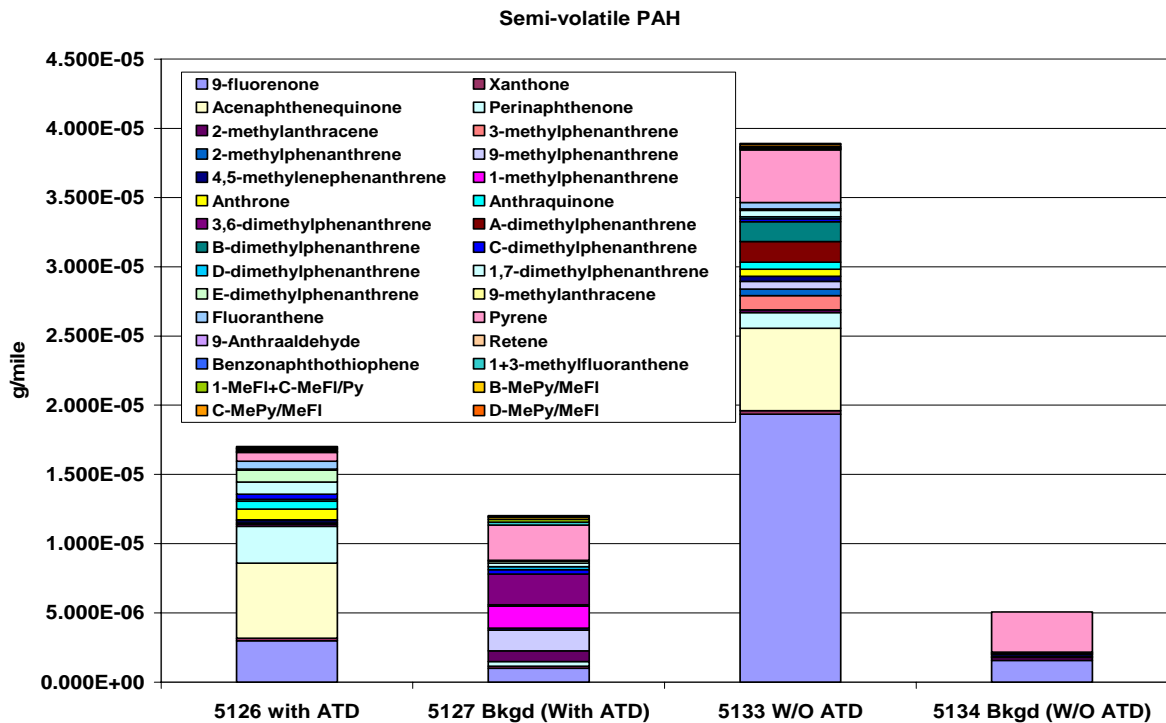
Semi-volatile PAH

Figure 5.9 Results of Semi-Volatile Phase PAH Emissions from RTA Transit Bus.
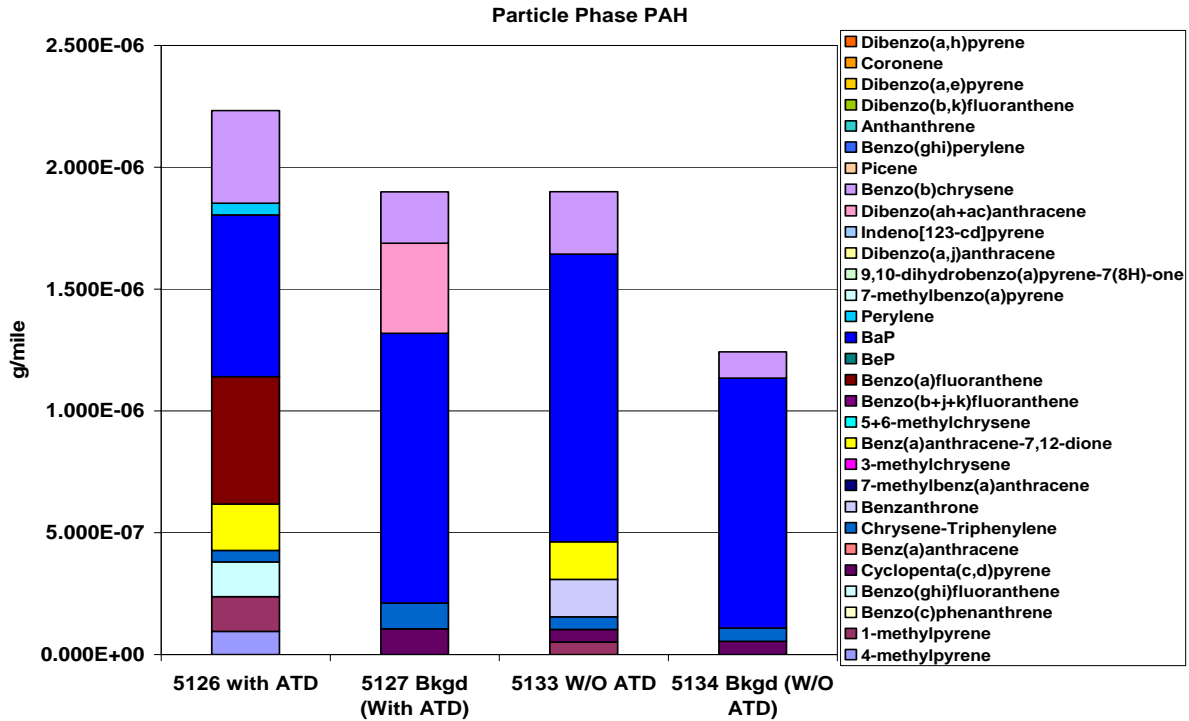
Particle Phase PAH

Figure 5.10 Results of Particle Phase PAH Emissions from RTA Transit Bus.

The results show that the after-treatment device was effective in reducing the total gas phase and total semi-volatile PAH emissions by 45.6% and 56.2% respectively. However there was a 17% increase in particle phase PAH, and this could attributed to measurement uncertainty as the detected concentrations were very close to background levels. Figure 5.11 and Figure 5.12 show the contribution of individual PAH compounds to the total PAH emissions. The results show naphthalene as the major contributor in the gas phase PAH portion of emissions , but it also to be noted that the naphthalene concentrations are close background value that were seen. And the detected concentrations were very low hence the effect of uncertainty on the data is higher. The reasons for high background concentrations could be the operation of heavy earth moving machinery adjacent to the test site during the test period. And as WVU transportable lab does not have means of removing volatile contaminants from the dilution air. As seen in many previous studies isomers of methyl-biphenyl seem to contribute significantly to the PAH emissions. The after-treatment device was effective in reducing isomers of methyl-biphenyl by 66.4%.
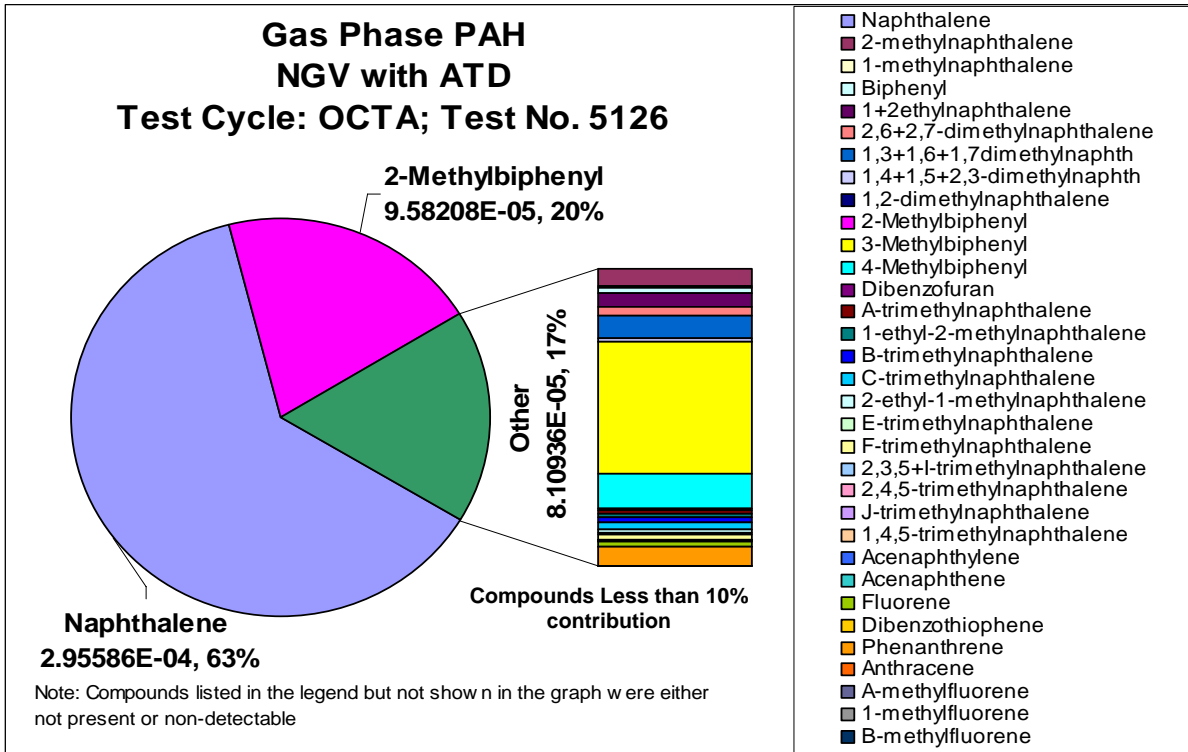
Figure 5.11 Gas Pahse PAH Compounds in the Exhaust from RTA Transit Bus With After-treatment Device.
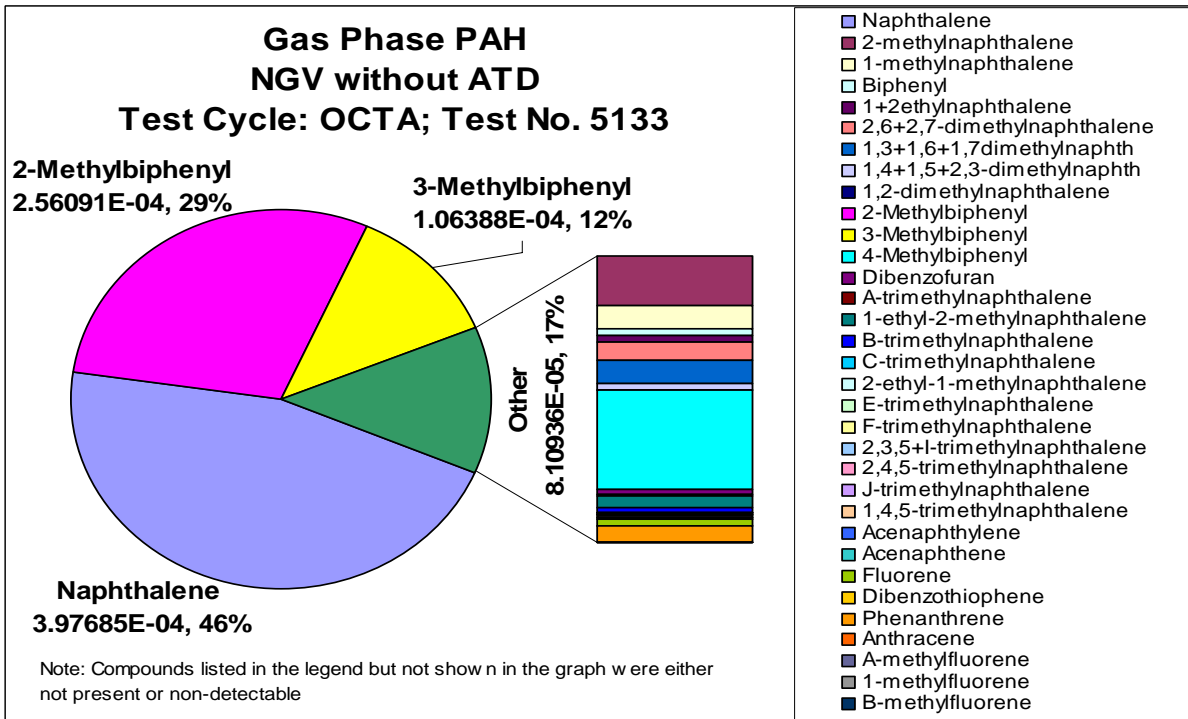
Figure 5.12 Gas Pahse PAH Compounds in the Exhaust from RTA Transit Bus Without After-treatment Device.

Figure 5.13 and Figure 5.14 show the percentage contribution of the semi volatile phase PAH compounds to the total PAH emissions under different vehicle configuration. The after-treatment device was effective in removing only 9-flourenone and Perinaphthenone. The total semi volatile phase PAH was reduced by 56%.

The concentrations of particle phase PAH were very low and close to background levels. This increases the uncertainty error associated with them and the data is quite insignificant to correlate with engine operation and catalyst performance.
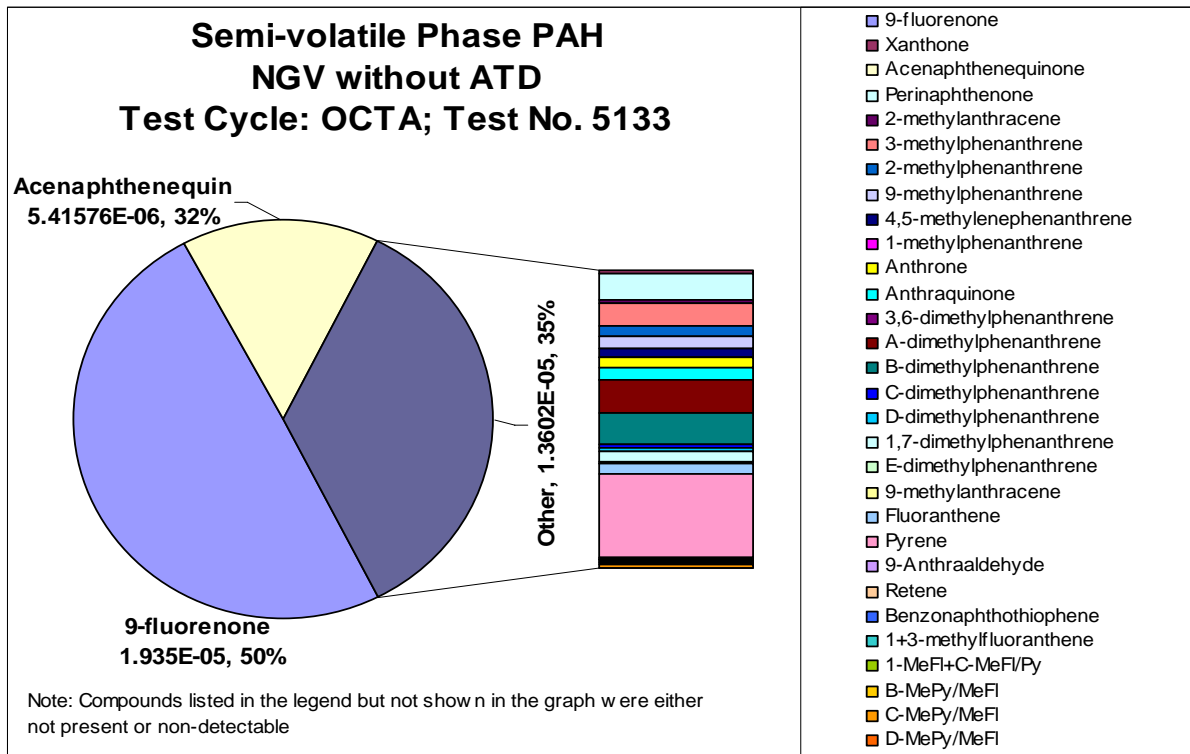
Figure 5.13 Semi Volatile PAH Compounds in the Exhaust from RTA Transit Bus Without After-treatment Device.
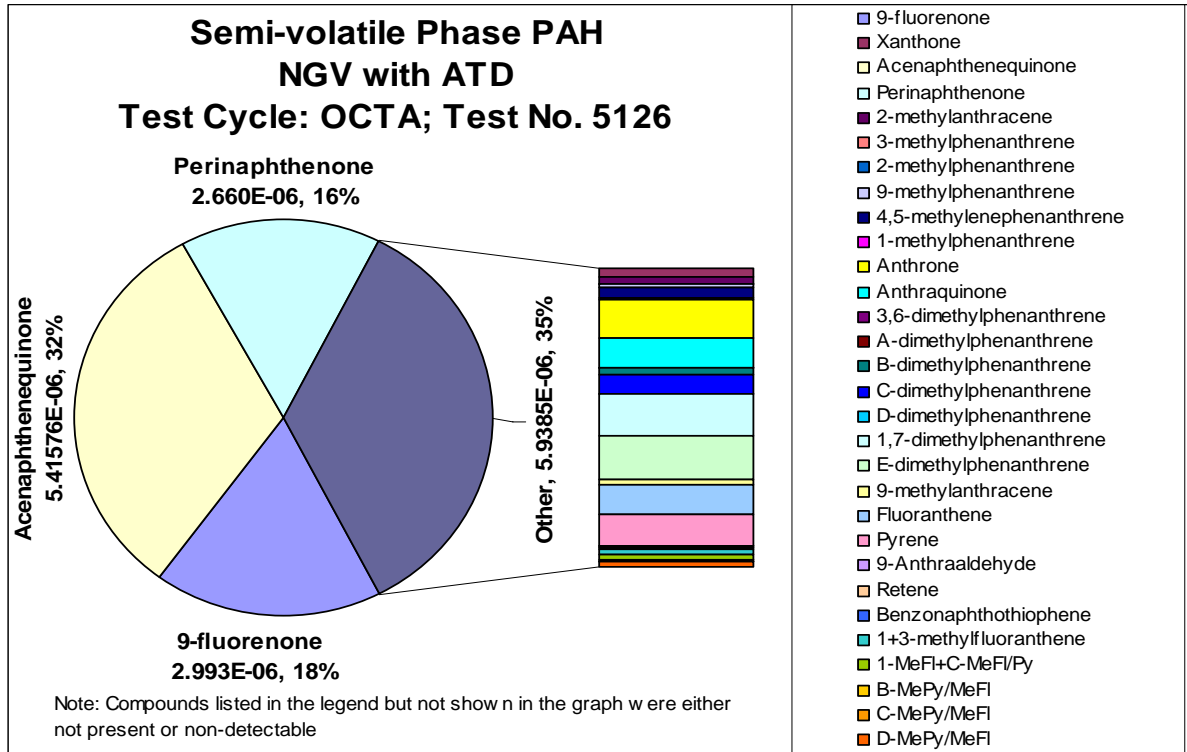
Figure 5.14 Semi Volatile PAH Compounds in the Exhaust from RTA Transit Bus With After-treatment Device.
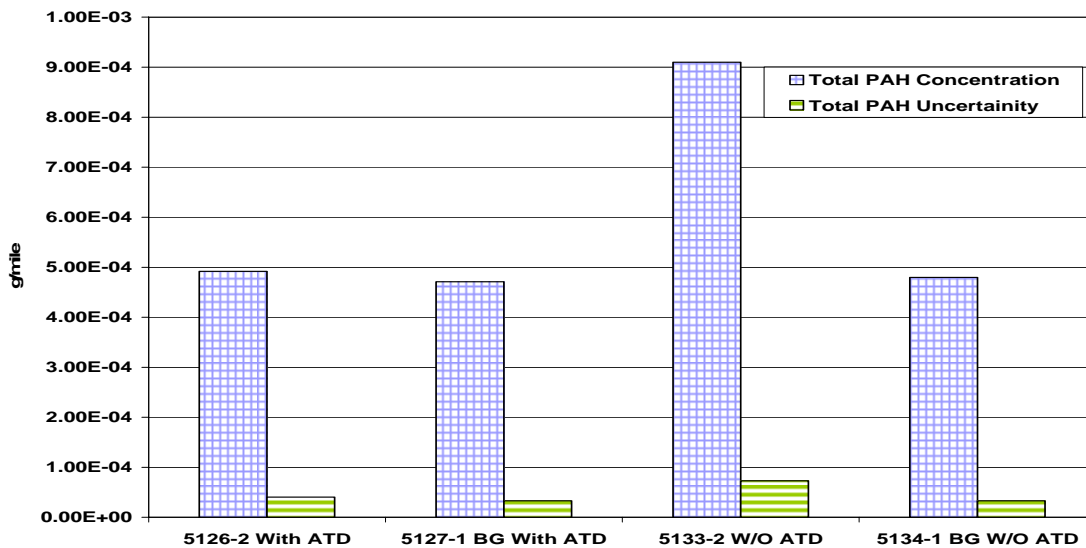
Figure 5.15 Total PAH Emissions and Uncertainty Values from RTA Transit Bus.

The above shown uncertainty levels for the total PAH emissions were greatest for particle phase PAH as they were most often below detectable limits. The uncertainty for gas phase and

semi volatile PAH compounds were on the whole less with exception of certain species which were reduced to below detectable limits the catalyst.

Figure 5.16 shows the nitro-PAH results obtained from the RTA transit bus. N-PAH compounds are believed to be formed from the reaction of PAH compounds with atmospheric nitrogen. The concentration of n-PAH compounds were very low and the most dominant species was found to be nitronaphthalene. The after-treatment device was effective in reducing n-PAH emissions by 60%.
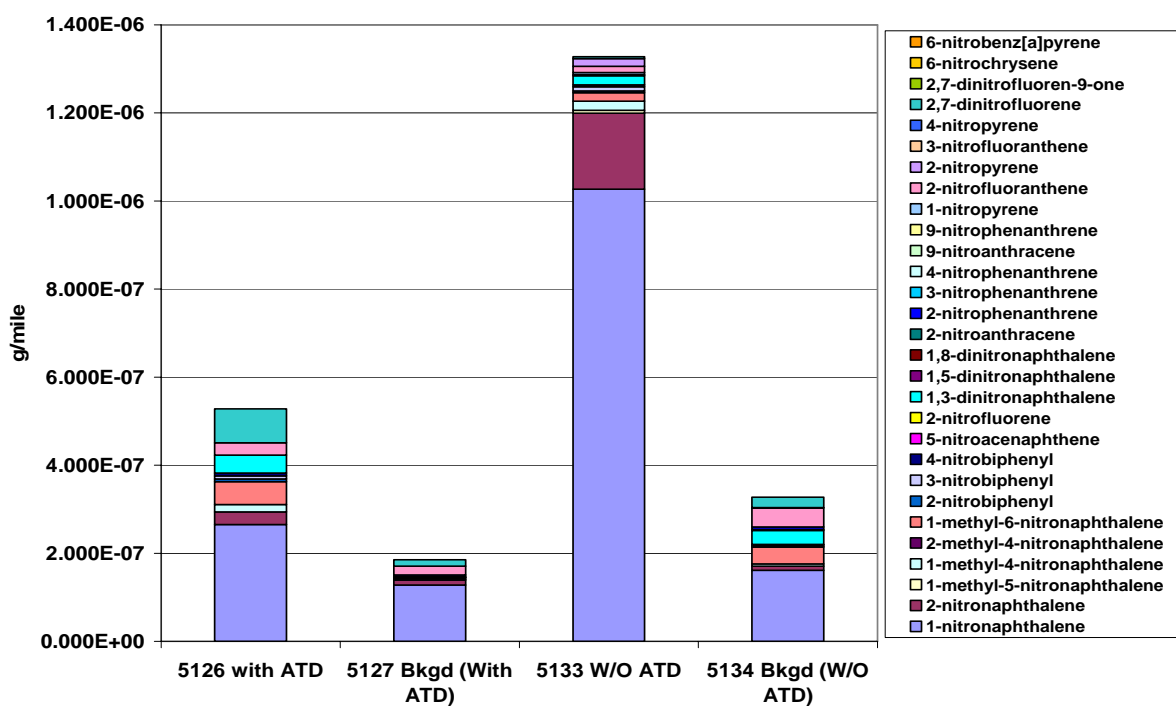
Figure 5.16 Results of n-PAH Emissions From RTA Transit Bus.

5.2.3 Volatile Organic Carbon (VOC) Emissions Results

The VOC speciation was carried out by analyzing the sample collected into the canisters. The pressurized canister samples were analyzed by GC/MS technique to identify the various VOC species. The VOC species can be further classified as alkanes, alkynes, olefins, and aromatics and can be further sub divided based on number of carbon atoms. The results of the VOC speciation are classified according to the carbon-carbon bonds and the number of carbon atoms. By this method it is easier to point out the segment of the VOC in which the catalyst was most effective.

5.2.3.1 *Alkanes Fraction of VOC Emissions*

The results of the VOC speciation indicated that the after-treatment device was effective in reducing the total VOC emissions by 92.6%. Figure 5.17 shows the results of the C2-C5 alkanes emissions.
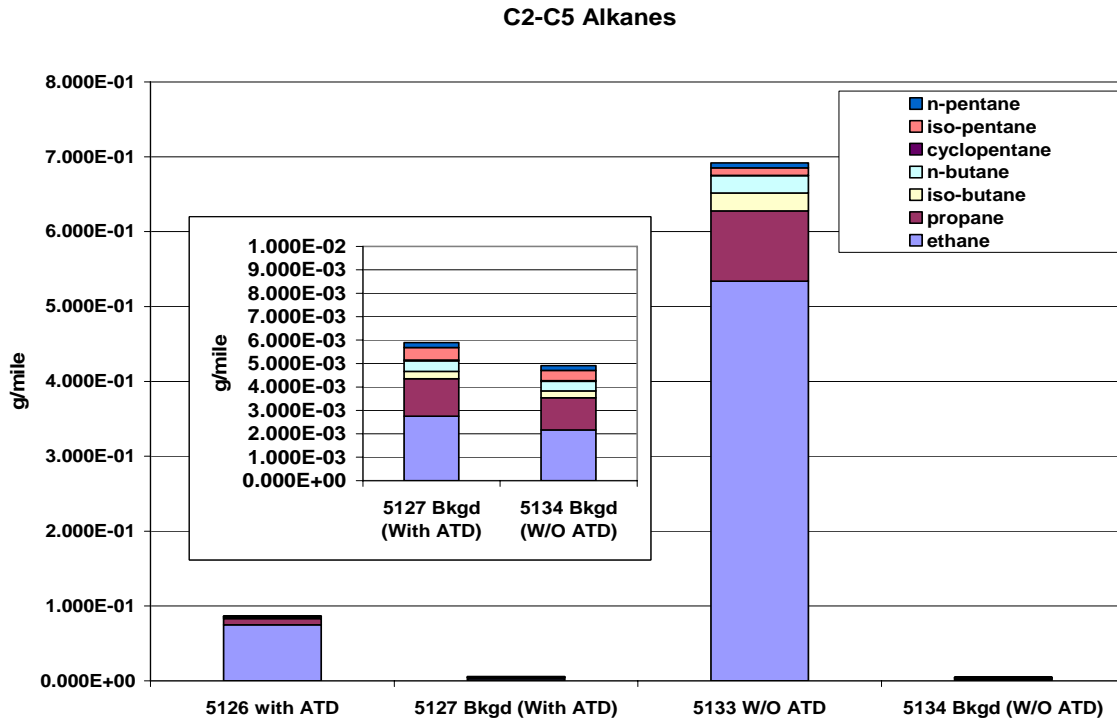
Figure 5.17 C2-C5 Alkanes Emissions Results from RTA Transit Bus

The results show that the major contributor to the VOC emissions in the C2-C5 alkanes segment was ethane without the after-treatment device. The source of ethane is directly related to the 2% ethane present in the natural gas test fuel. The concentration of ethane was reduced by 86% with the use of after-treatment device. In comparison to background levels of ethane the concentrations even after the oxidation catalyst is two orders of magnitude higher. This is again attributed to the fact that hydrocarbons with lesser carbon atoms have higher light off temperatures. The reduction in concentration higher carbon number alkanes was more predominant.

Figure 5.18 shows the results of C6 and greater carbon number alkane fraction of the VOC emissions. The after-treatment device was effective in reducing the total VOC emissions in this segment by 85.6%.
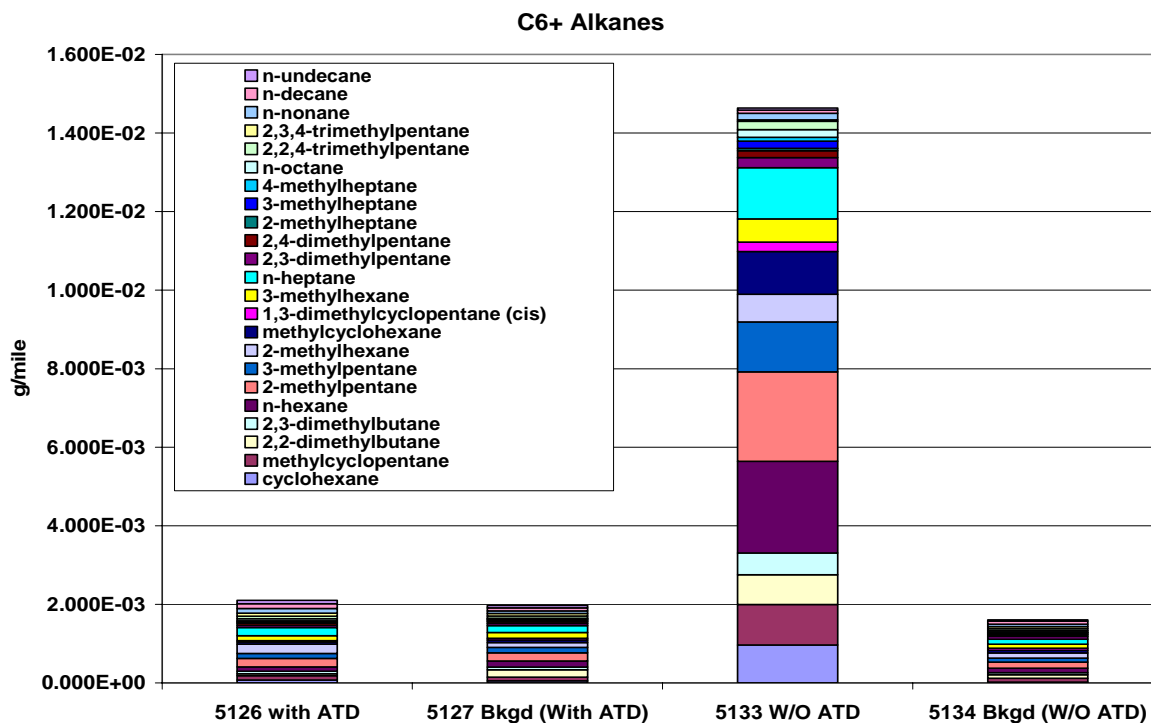
Figure 5.18 C6+ Alkanes Emissions Results from RTA Transit Bus

The results show that the after-treatment device reduced the concentration of C6 and greater alkane compounds to background concentration levels. The results indicate that the after-treatment device is very efficient in reducing higher chain volatile hydrocarbon compounds. Species such as 2-methylpentane, n-heptane, and n-hexane were reduced to below detection limits with the use of the after-treatment device.

5.2.3.2 Olefins Fraction of VOC Emissions

Olefins are hydrocarbon compounds which consist of carbon-carbon double bonds. Ethene is usually formed due to the cracking of higher hydrocarbon compounds. However the formation of ethene from natural gas fueled vehicles with very less higher chain hydrocarbons present in the fuel is unclear. The formation of ethane could be attributed to the partial oxidation of ethane or higher hydrocarbons present in trace quantities in the fuel.
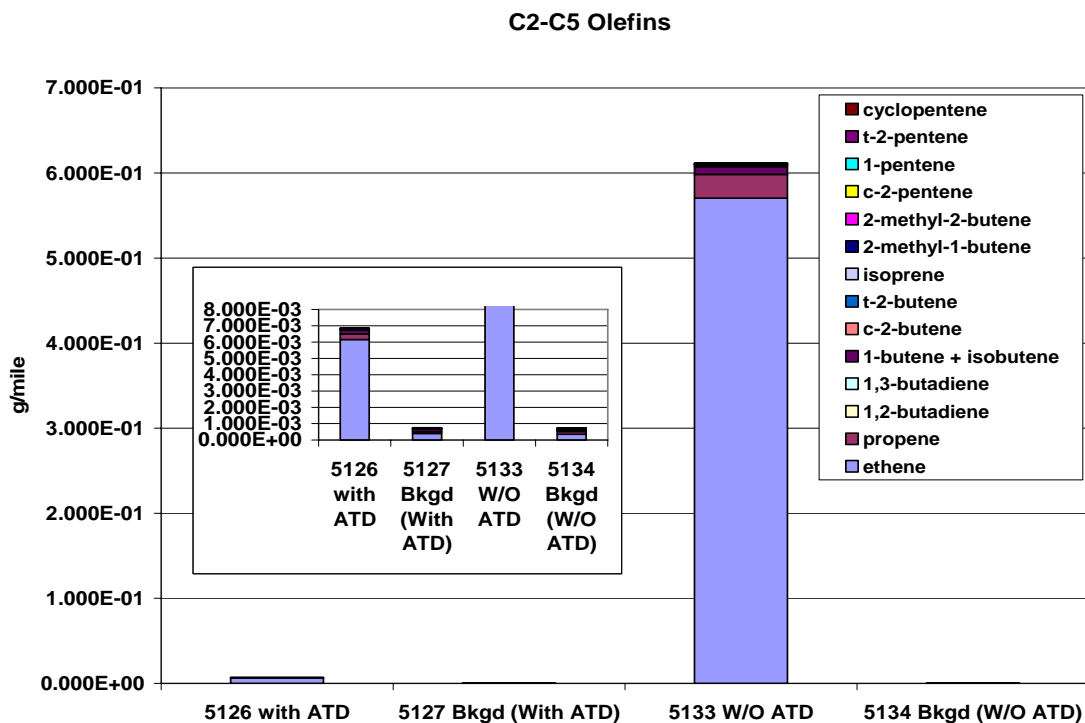
Figure 5.19 C2-C5 Olefins Emissions Results from RTA Transit Bus

The results showed that the concentration of ethene in the exhaust was reduced by 98% with the use of after-treatment device. One interesting trend is to be noted in comparing ethene reduction and acetaldehyde formation in the exhaust with the after-treatment device present. As stated earlier in the carbonyl emission result there was the appearance of acetaldehyde with the presence of after-treatment device which was not present in the baseline configurations. This trend could be attributed to the oxidation of ethene. The production of acetaldehyde from ethene in the presence of catalyst containing platinum group metals is a well documented process [62]. This process has also been used for the industrial production of acetaldehyde. The results obtained from the current study also show sharp contrast to this acetaldehyde formation mechanism. The presence of platinum group metals in the oxidation catalyst might have aided the oxidation of ethene to acetaldehyde, which resulted in decrease of ethene concentration and subsequent increase in acetaldehyde concentration.

Figure 5.20 shows the C6 and higher carbon number Olefin compounds. There was a 84% reduction in this fraction of Olefins emission with the presence of after-treatment device. Emission concentrations with after-treatment device were reduced to background levels.
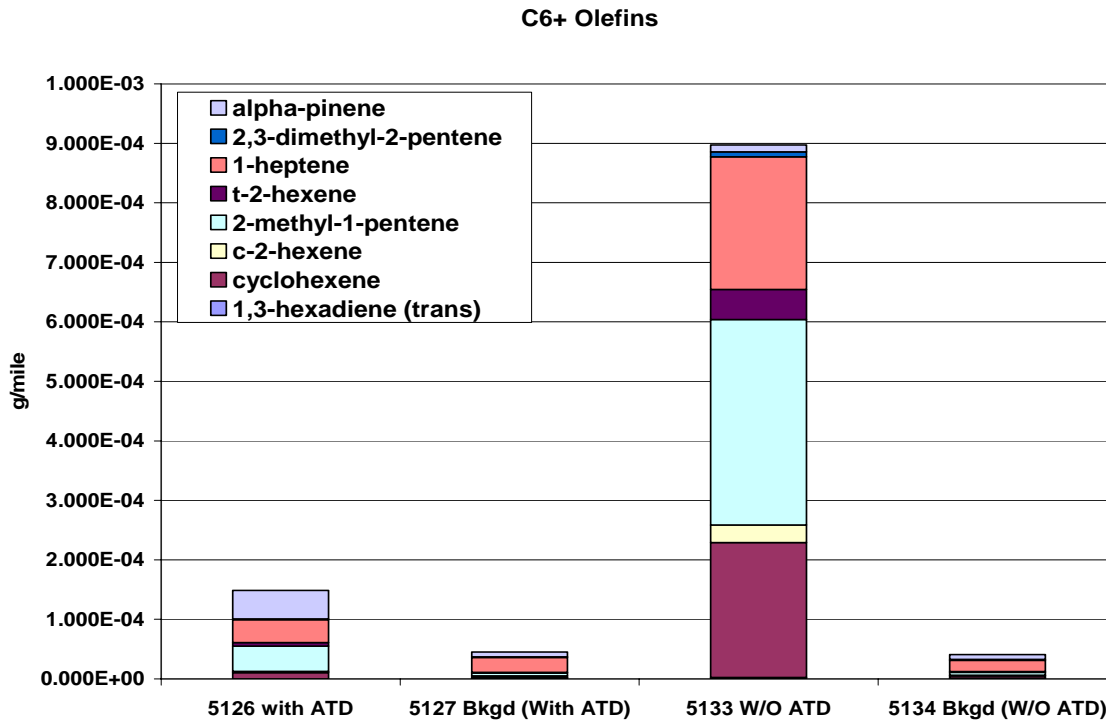
Figure 5.20 C6+ Olefins Emissions Results from RTA Transit Bus

5.2.3.3 Alkynes Fraction of VOC Emissions

Alkynes are hydrocarbon compounds that have carbon-carbon triple bond. Figure 5.21 shows the alkynes fraction of the VOC emissions from the RTA transit bus. The results of alkynes emissions showed the presence of only propyne and acetlyne. The results show a 96% reduction in alkyne fraction with acetylene being reduced by 96%. Propyne was reduced to below detection limits with the after-treatment device. A study conducted by Shigeru et al. has shown that methane undergoes pyrolitic reaction using a pulse of direct current discharge to form C2 hydrocarbons readily. Acetylene has the greatest potential for formation with this mechanism [63]. This could be the case for the formation of many C2 hydrocarbons including acetylene in natural gas engines where spark ignition is used as the combustion initiator. Hence in the region around the spark plug electrode in which the electric pulse from the spark plug could induce pyrolitic reaction of methane which in turn produces C2 hydrocarbons in addition to acetylene.
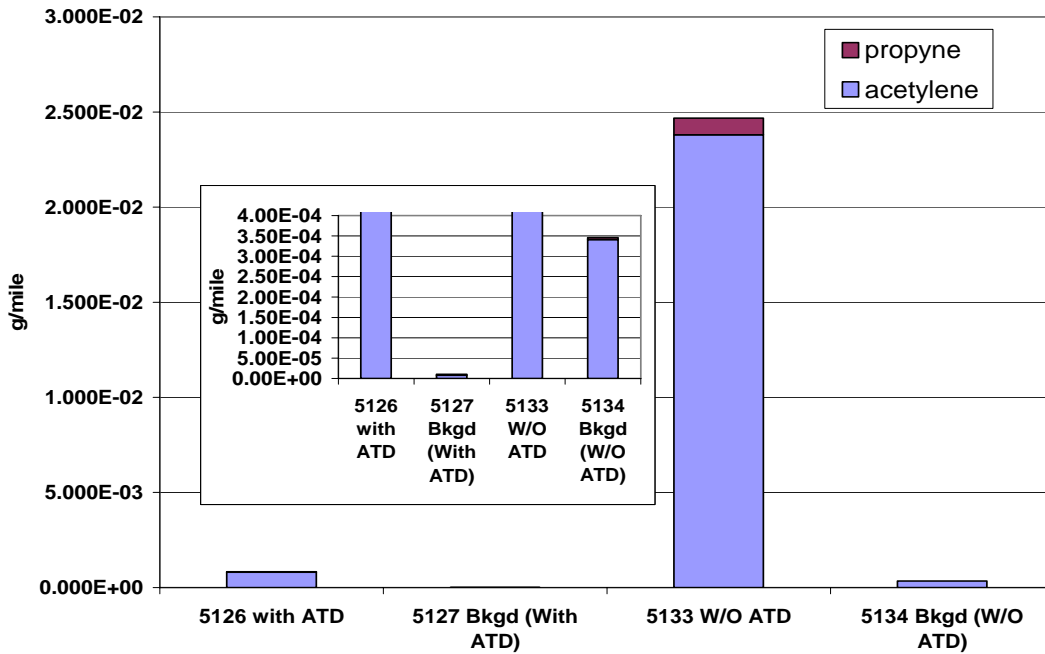
Figure 5.21 Alkynes Emissions Results from RTA Transit Bus

5.2.3.4 *Aromatic Fraction of VOC Emissions*

Aromatics are hydrocarbons which consist of benzene rings attached to them. Aromatic fractions are basically dominant in emissions from diesel engines as diesel contains higher fraction of aromatic compounds. Source of aromatic hydrocarbons in natural gas vehicle emissions is unclear and could be attributed to pyrolitic reaction of natural gas fuel. The total aromatic fraction of VOC was reduced by 53.4% with the use of after-treatment device. Figure 5.22 shows the results of the aromatic fraction of the VOC emissions. One of the main contributors of emissions in this category was benzene which is extremely toxic and considered to be carcinogenic in nature. Benzene concentration was reduced by 86% with the after-treatment device and the levels that were found with the after-treatment device was equivalent to those found in background samples. Similarly toluene which is closely associated with benzene in its aromatic properties was also reduced by 48% and reduced to levels found in background sample.
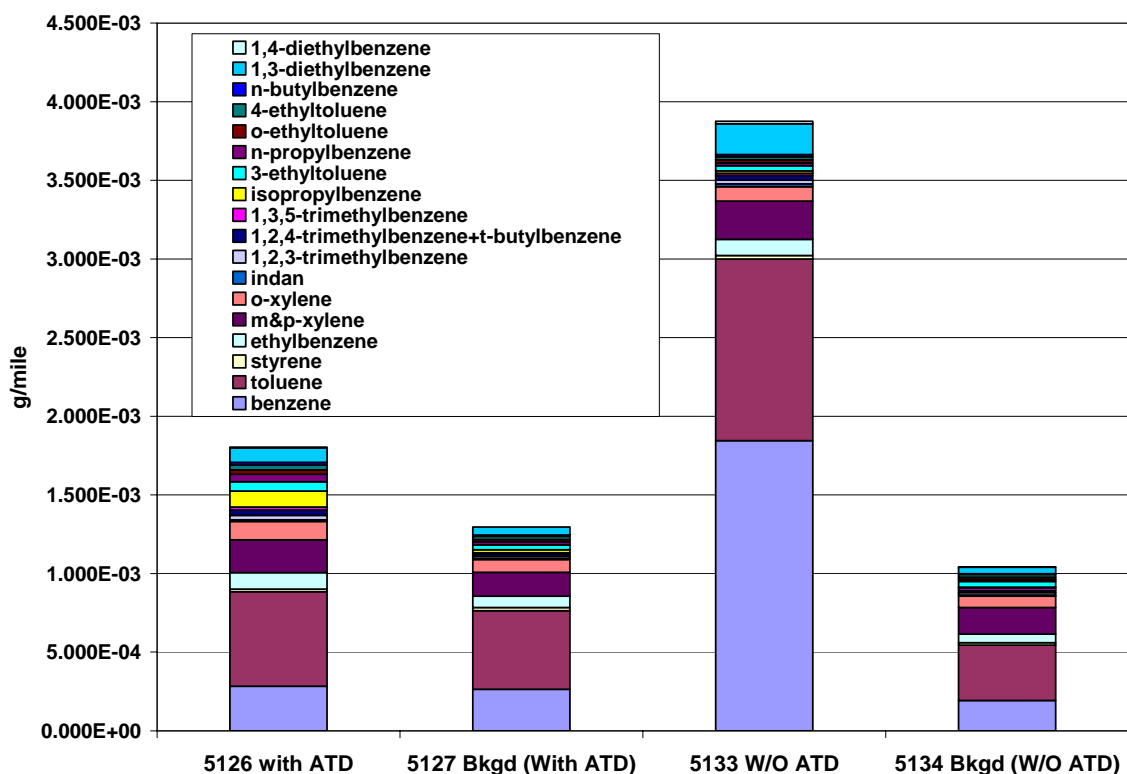
Figure 5.22 Aromatic Emissions Results from RTA Transit Bus

5.2.4 Metals Emission Results

The samples for the metals analysis of the vehicle emission was collected on 47mm Teflon filters. The particulates were classified using a PM 2.5 cyclone before collecting them on the filters. DRI used XRF spectrometry method for the analysis of the various metallic elements present in the exhaust. The source of metal emissions could be due to engine wear, lubrication oil additives, and even shedding of material by the oxidation catalyst. Figure 5.23 shows the metallic elements emissions from the RTA transit bus.

The results of the emissions showed very high concentration of metals in the background sample and were consistent with both vehicle configurations. The results showed higher emissions of metals with after-treatment device than the baseline configuration. Concentration of iron had increased by 50% and elements such as tantalum, indium, tin and cadmium were seen with the after-treatment device present. The source of these metals could be from the catalytic converter itself. More concrete conclusion could be derived only by reviewing the catalyst

chemistry and design. Most of the other metals concentraions were consistent in their concentrations before and after the catalyst.
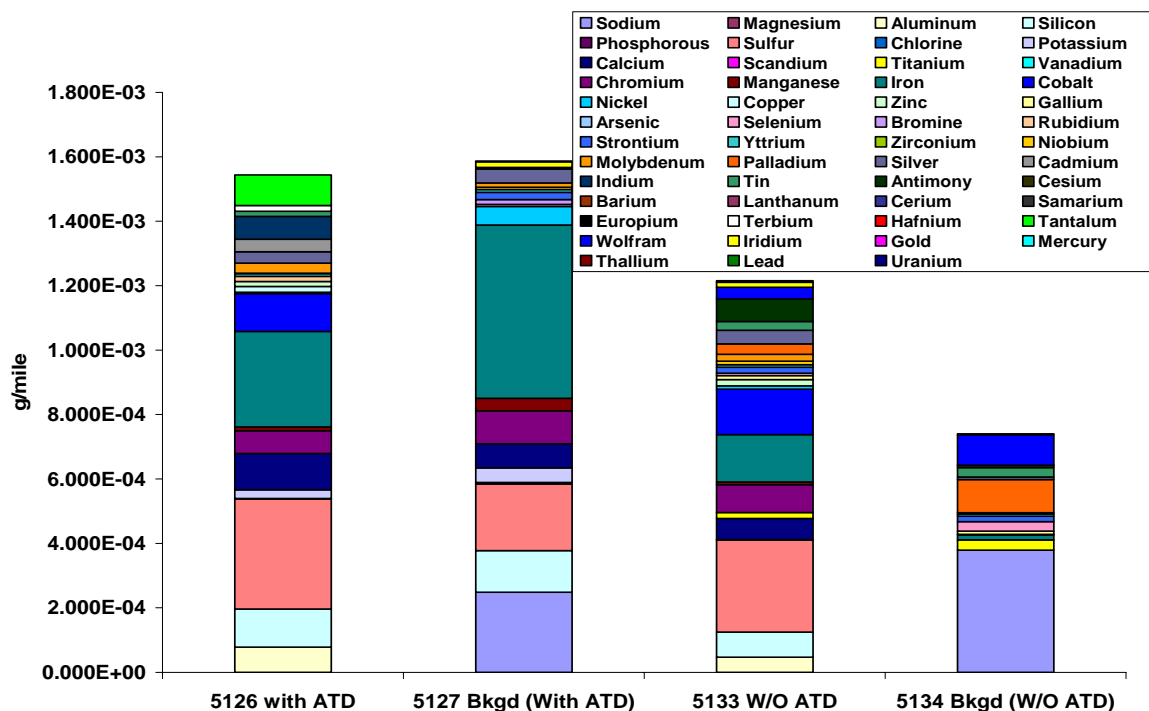
Figure 5.23 Metals Emissions from RTA Transit Bus.

5.2.5 EC/OC Emissions Results

The samples for the analysis of EC/OC fractions were collected on pre-fired quartz filters. The particles were sized classified using a PM2.5 cyclone before collecting them on the filter. The samples were later subjected to Thermal Optical Reflectance analysis by DRI to quantify EC/OC emissions

Carbon fractions found in the exhaust of CNG vehicles are usually organic in nature with very minimal or no elemental carbon fractions. This is due to the gaseous nature of fuel which upon combustion does not produce elemental carbon, which is a characteristic of liquid fuels. Figure 5.24 shows the EC/OC emission fractions from the exhaust of the RTA transit bus.
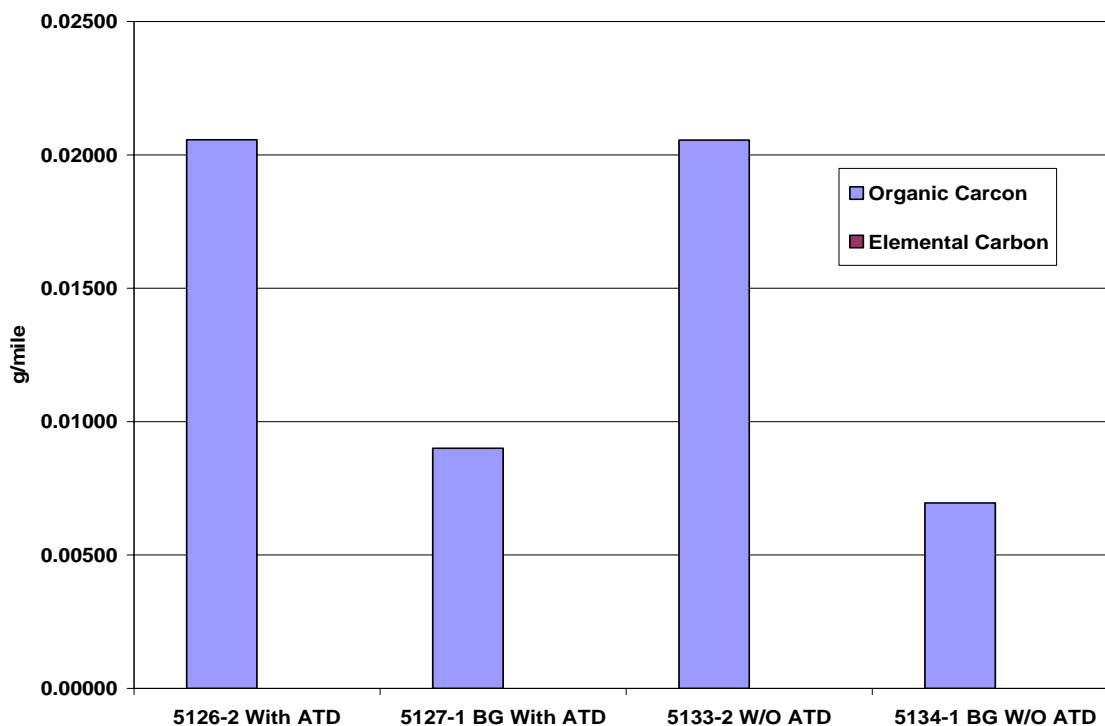
Figure 5.24 EC/OC Emissions from RTA Transit Bus

The results show the after-treatment device had no effect on the concentrations of organic carbon fraction in the exhaust. This could be due to the fact that the catalytic converter was a flow through type device which had minimal effect on the particle matter stream.

5.3 Particle Sizing Results

A particle sizing study was carried out to assess the effect of the catalyst on the particle size distribution during the warm up period of the catalyst from early a cold start. In addition to this study concentrations of particles of certain diameter were tracked during the course of the entire double length OCTA cycle. Raw exhaust was sampled and diluted using the ejector dilution setup and particle size distribution was measured using the SMPS.

For the cold start particle size distribution study the vehicle was operated at steady state conditions starting with 20mph, followed by idle, followed by 30mph, followed by 40mph vehicle speeds. The tests were setup as quickly as possible without letting the vehicle cool down so as to establish a proper trend in the particle size distribution during the warm up period of the catalytic converter. This test procedure was followed for two vehicle configurations

with and without the after-treatment device. A dilution ratio of 20 was chosen so as to produce maximum nucleation as prescribed by Kittelson et al in their study with respect to dilution ratio and saturation vapor pressure of volatile hydrocarbons to produce nucleation mode particles [48]. Higher dilution ratios were avoided due to the fact that it would end up in lesser particle concentrations and higher aerosol flow velocity from the ejector dilutor which in turn would increase the error in concentration measurement.

The results of the particle size distribution from the baseline configuration of the vehicle showed a distinctive nucleation mode peak which is characteristic of natural gas vehicle particle distribution. The distribution peaked consistently at CMD of 22.5nm. The nucleation mode seen here is a result of the sudden cooling of hydrocarbon compounds upon dilution to undergo homogenous nucleation to form nano particles. The results were consistent in showing a decreasing overall particle concentration with increasing vehicle speeds, which is in direct correlation with the fact that hydrocarbon emissions would decrease with increasing vehicle speed in Otto cycle engines.
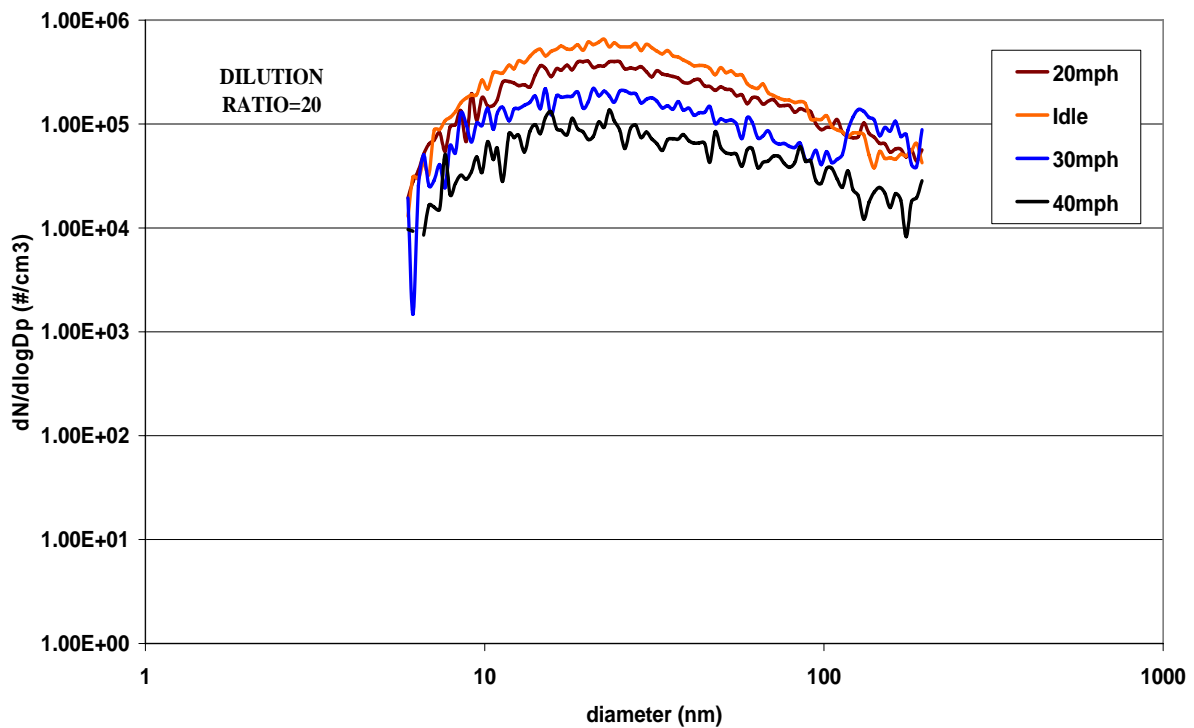
Figure 5.25 Particle Size Distribution From RTA Transit Bus Without the After-treatment Device During Cold Start Operations

Figure 5.26 shows the particle size distribution from the RTA transit bus with the after-treatment device present.
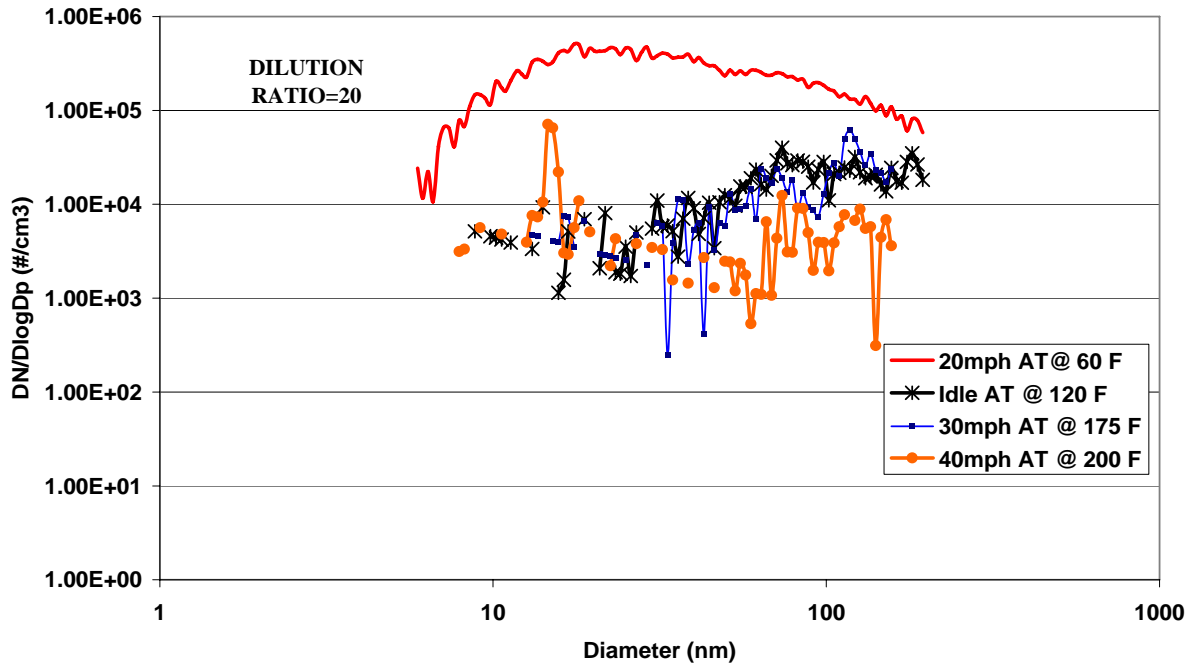
Figure 5.26 Particle Size Distribution from RTA Transit Bus With the After-treatment Device During Cold Start Operations.

The results showed that with the first vehicle operation at the steady state speed of 20mph the particle size distribution was equivalent to that of baseline configuration distribution. As the test progressed the catalytic converter temperature increased and subsequent decrease in particle size distribution is seen. The temperature seen in the chart is the exterior temperature of the converter shroud and not the temperature of the catalyst surface. This temperature was recorded to get a broad prospect on the correlation between temperature increase of the catalytic converter and the subsequent decrease in particle concentration. The results show a complete removal of the nucleation mode seen earlier in the baseline configuration; this is due to the operation of the catalytic converter in oxidizing the unburned hydrocarbons and preventing nucleation.

The particle size distribution for the 40mph steady state operation shows a distinctive nucleation mode spike at 15.1nm. This spike could not be attributed as measurement error as it was consistent during all the 6 consecutive samples. Upon review of literature this phenomenon could be attributed to the storage effect of catalytic converter. Every catalytic converter

undergoes a phase during the warm up period where it absorbs the volatile compounds onto its cold catalyst surface. This effect is known as the storage effect of catalyst [41]. And when the catalyst warms up it starts to shed these absorbed hydrocarbons without oxidizing them [41]. And this sudden release of volatile hydrocarbons undergoes homogenous nucleation to produce nano particles and appear as a sharp nucleation mode spike in the particle size distribution.
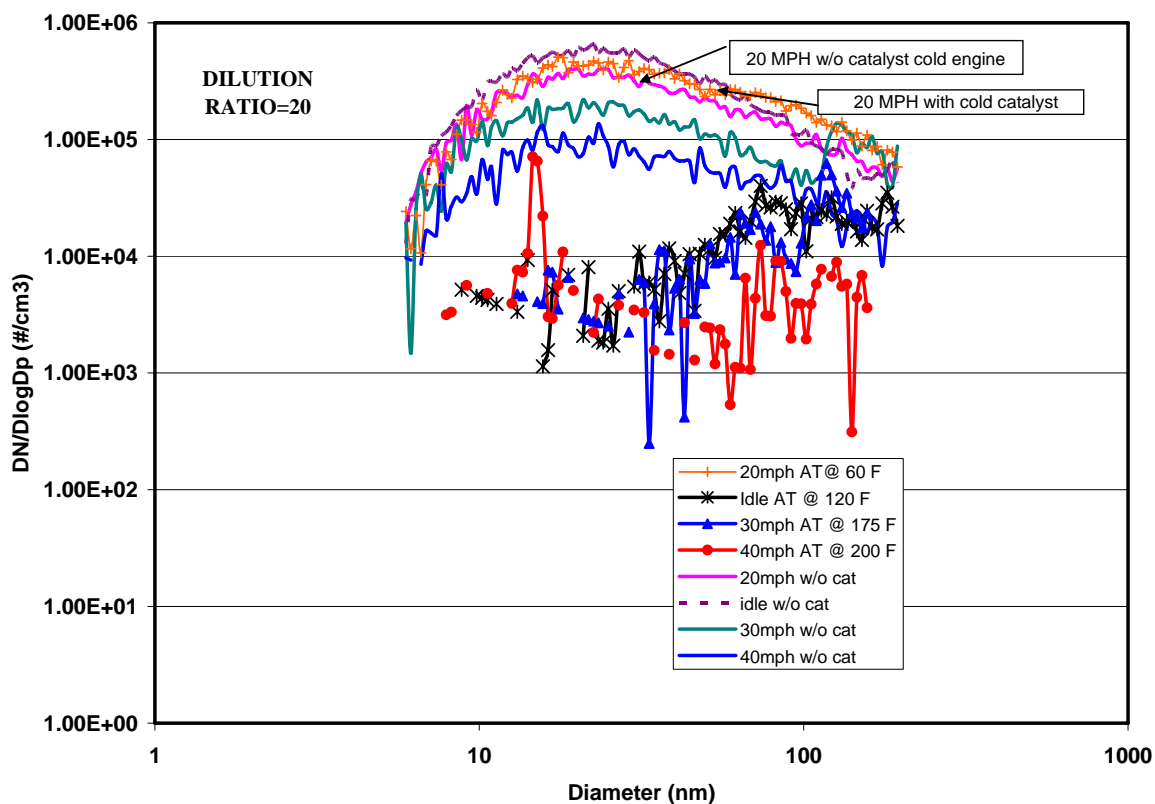
Figure 5.27 Particle Size Distribution Comparison With and Without the After-treatment Device with Continuously Warming Catalytic Converter.

Figure 5.27 shows a good match in the particle size distribution curve with and without the after-treatment device at 20mph and coldest catalyst temperature. The particle size distribution seen in the figure above shows that the catalyst was very effective in oxidizing volatile hydrocarbons immediately after catalyst warm up so as to completely eliminate the nucleation mode.

The study also involved the tracking of concentration of particle of three different diameters over the entire length of the double OCTA cycle. The diameters chosen were 20nm, 35nm and 55nm. Figure 5.28, Figure 5.29 and Figure 5.30 shows the concentration of particles of three different diameters in two vehicle configurations.
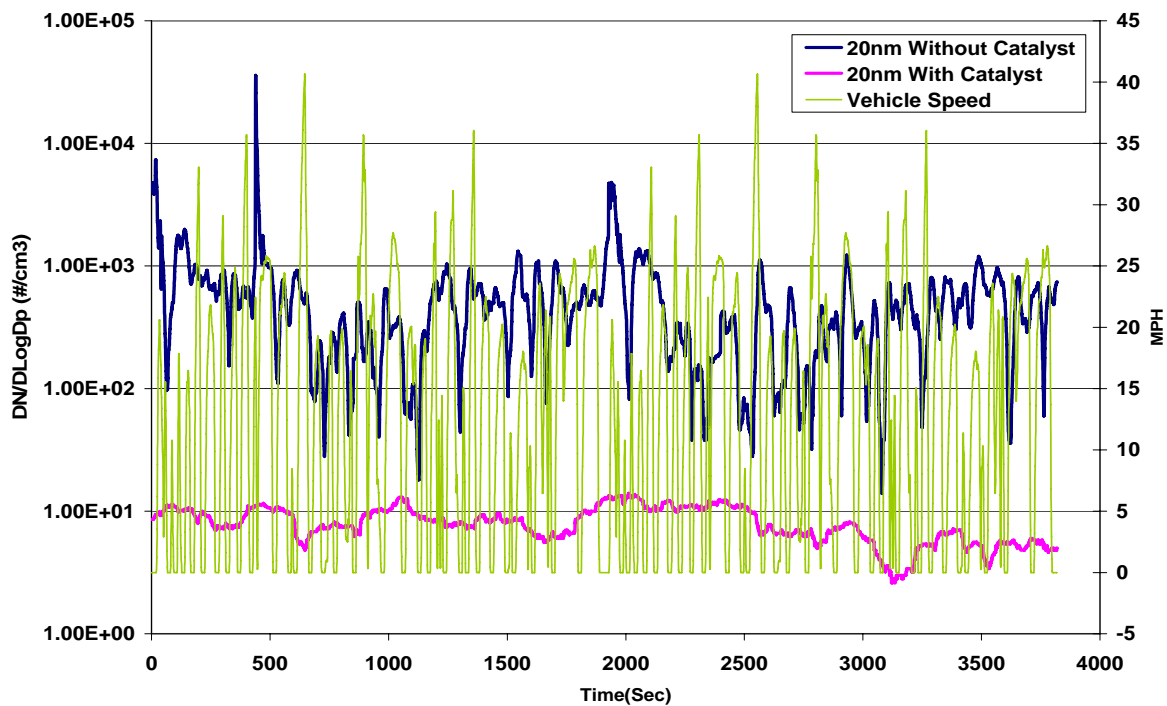
Figure 5.28 20nm Particle Concentration With and Without the After-treatment Device
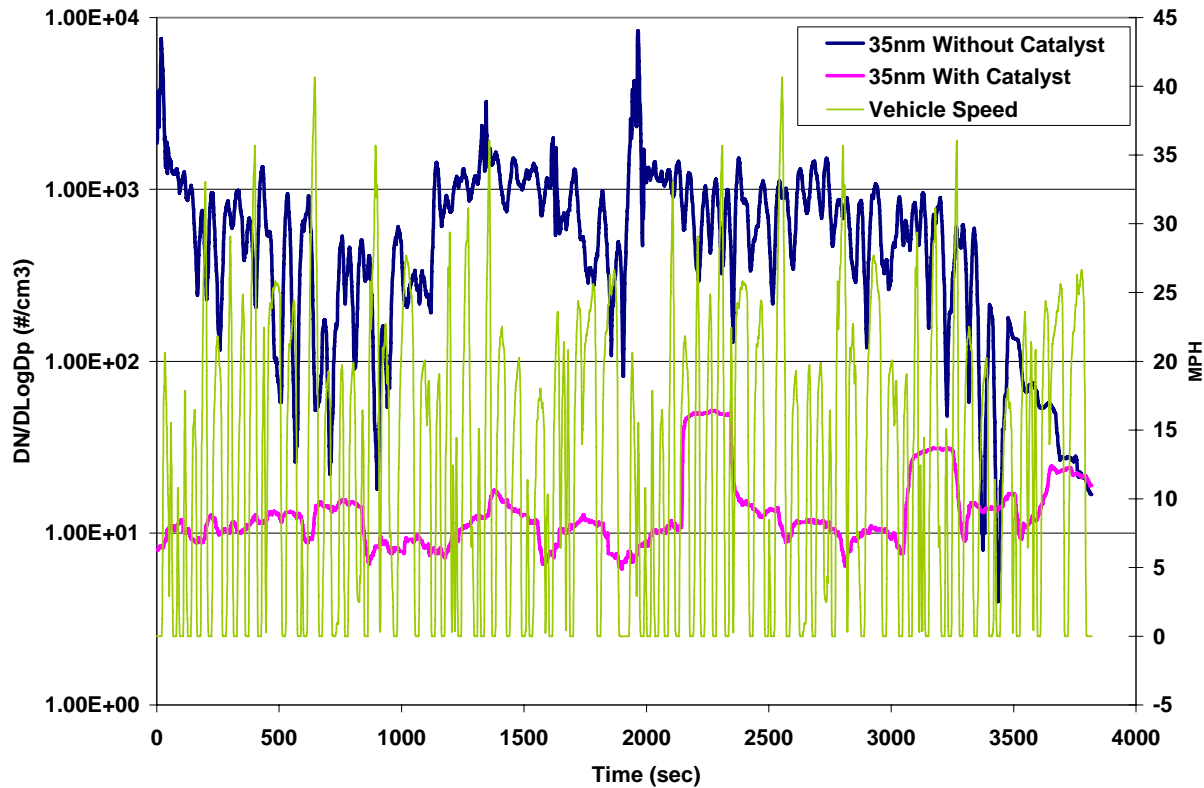
Figure 5.29 35nm Particle Concentration With and Without the After-treatment Device
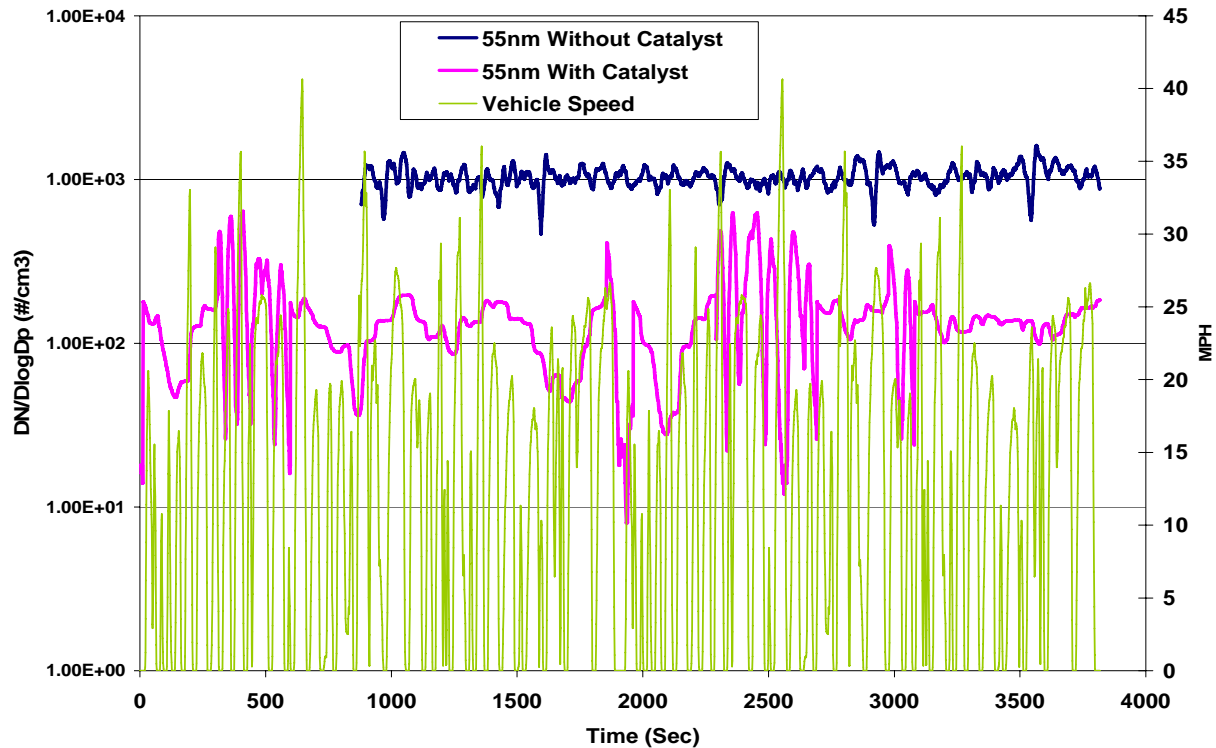
Figure 5.30 55nm Particle Concentration With and Without the After-treatment Device

Results of the particle concentration at three different diameter show that with the after-treatment device present particle concentrations had decreased by two orders of magnitude in all three particle diameters. The results also show more of a constant particle concentration with the after-treatment device present for the 20nm and 35nm particles. This is due to the oxidation of hydrocarbon compounds by the after-treatment device, which in turns lowers nucleation and produces a low particle concentration which does not vary much with the vehicle speed. The 55nm data taking process was started 800sec late hence it does not show particle concentration for the first period of the cycle.

CHAPTER 6 - CONCLUSIONS

The chassis dynamometer testing on the two CNG fueled heavy duty transit authority busses powered Detroit Diesel Series 50 engines were successfully carried out as per the work plan. All tests were carried out in accordance with regulations given in CFR40 part 86. The studies aim of evaluating the effectiveness of an all palladium catalyst formulation retro-fitted on natural gas transit bus was successfully carried out.

The results of the regulated emissions test conducted on the RTA and LACMTA busses showed that with the after-treatment device with present CO emissions were reduced to non-detectable levels from both busses and HC emissions were reduced by 62% from the RTA bus and by about 29% from the LACMTA bus. The methane speciation of the exhaust from the RTA bus also showed that the catalyst was effective in reducing methane emissions by 57% and the NMHC fraction was reduced by 72%.

The results of the unregulated emissions speciation carried out on the RTA bus showed and overall decrease in concentration of all compounds with the after-treatment device present. With the presence of after-treatment device the total emissions of carbonyl compounds were reduced by 96%, Poly Aromatic Hydrocarbons were reduced by 46% and Volatile Organic compounds were reduced by 92%. The metals emission results showed an increase in concentration of certain metals. The after-treatment device had no effect on the organic carbon fraction of the exhaust.

6.1 Recommendations

This study has clearly shown that natural gas fueled vehicle is a cleaner alternative to heavy duty vehicles only in the presence of suitable after-treatment device. The unregulated emission results illustrate the fact that natural gas vehicles exhaust contains many toxic air pollutants which necessitates the need for after-treatment devices. The recommendations that can be suggested from this study are,

- Vehicle engine strategy plays a very important role in the tail pipe emissions; hence the effectiveness of the catalyst over engines from different engine manufacturers must be studied.

- Stripping the dilution air from VOC with the use of activated charcoal is necessary to reduce background interference in measuring toxic air contaminants of very low concentrations.

- Difference in concentration of toxic air pollutants in ambient air and within the tunnel should be studied in order to better understand the background contribution of unregulated emissions to the test value.

References

1. R. K. Schubert and S. Fable, "Comparitive Costs of 2010 Heavy-Duty Diesel and Natural Gas Technologies," TIAX LLC,D0286/D0288, July2005.

2. J. S. Cannon, "Greening Garbage Trucks: Trends in Alternative Fuel Use, 2002-2005," INFORM INC, New York,2006.

3. Ayala, N. Y. Kado, R. A. Okamoto, B. A. Holmen, P. A. Kuzmicky, R. Kobayashi, and K. E. Stiglitz, "Diesel and CNG Heavy-duty Transit Bus emissions over Multiple Driving Schedules: Regulated Pollutants and Project Overview," *SAE Paper 2002-01-1722*, Feb.2002.

4. "Fleet Rule for Transit Agencies"*, CCR Title 13, 2000, p. 1956.1-1956.4.

5. "International Energy Outlook 2007," Energy Information Administration,DOE /EIA-0484/2007, 2007.

6. "Specifications for Alternate Motor Vehicle Fuels,"*, CCR Title 13, 1998, pp. 2290-2293.5.

7. T. J. Callahan, T. W. Ryan, and S. R. King, "Engine Knock Rating of Natural Gases-Methane Number," *Journal of Engineering for Gas Turbines and Power*, vol. 115, no. 4, pp. 769-776, Oct.1993.

8. Weaver C S, "Gaseous Fuels for Engines: Natural Gas and Liquified Petroleum Gas," in *Automotive Fuels Reference Book* Society of Automotive Engineers, 1995, pp. 551-588.

9. B. Challen and R. Baranescu, *Diesel Engine Reference Book*, II edition, Society of Automotive Engineers, 1999.

10. M. Kamel, "Development of a Cummins Westport SI-EGR Natural Gas Engine at 0.2 gr/bhp-hr," NREL, Colorado,NREL/SR-540-40757, 2006.

11. T. C. Lekar and T. J. Martin, "Natural Gas Engine Development," NREL, Colorado, NREL/SR-540-40816, 2006.

12. J. P. Mello, D. Bezaire, S. Sriramulu, and R. Weber, "Perfomance and Economics of Catalytic Glow Plugs and Shields in Direct Injection Natural Gas Engines for the Next Generation Natural Gas Vehicle Program," NREL, Colorado,NREL/SR-540-34286, 2003.

13. J. B. Heywood, *Internal Combustion Engine Fundamentals,* McGraw-Hill Inc, 2002.

14. J. A. Raub, "Health effects of exposure to ambient carbon monoxide," *Chemosphere. Global change science*, vol. 1, no. 1, pp. 331-351, 1999.

15. P. L. Burk, J. K. Hochmuth, D. R. Anderson, S. Sung, S. J. Tauster, C. O. Tolentino, J. Rogalo, G. Miles, M. Niejako, A. Punke, and U. Dahle, "Cold start hydrocarbon emissions control," *SAE Paper 950410*, Mar.1995.

16. R. C. Yu, T. W. Kuo, S. M. Shahed, and T. W. Chang, "the effect of mixing rate, end of injection, and sac volume on hydrocarbon emissions from a D.I. diesel engine," *SAE Paper 831294*, 1983.

17. H. Geiger, J. Kleffmann, and P. Wiesen, "Smog chamber studies on the influence of diesel exhaust on photosmog formation," *Atmospheric Environment*, vol. 36, no. 11, pp. 1737-1747, 2002.

18. Z. A. Mansurov, "Soot formation in combustion processes," *Combustion, Explosion, and Shock Waves*, vol. 41, no. 6, pp. 727-744, 2005.

19. H. Yokota, T. Kamimoto, H. Kosaka, and K. Tsujimura, "Fast burning and reduced soot formation via ultra-high pressure diesel fuel injection," *SAE Technical Paper Series*, 1991.

20. R. B. Laurence, V. W. Wong, and A. J. Brown, "Effects of lubrication system parameters on diesel particulate emission characteristics," *SAE Paper 960318*, 1996.

21. B. A. Buchholz, R. W. Dibble, D. Rich, and A. S. Cheng, "Quantifying the contribution of lubrication oil carbon to particulate emissions from a diesel engine," *SAE Paper 2003-01-1987*, 2003.

22. K. J. Baumgard and J. J. Johnson, "The effect of fuel and engine design on diesel exhaust particle size distributions," *SAE Paper 960131*, 1996.

23. D. Kittelson, J. Johnson, W. Watts, Q. Wei, M. Drayton, D. Paulsen, and N. Bukowiecki, "Diesel Aerosol Sampling in the atmosphere," *SAE Paper 2000-01-2212*, 2000.

24. H. Burtscher, "Literature Study: Tailpipe particulate emission measurement for diesel engines," Fachhochschule Aargau, University of Applied Science, Switzerland,2001.

25. U. Mathis, R. Kaegi, M. Mohr, and R. Zenobi, "TEM analysis of volatile nanoparticles from particle trap equipped diesel and direct-injection spark ignition vehicles," *Atmospheric Environment*, vol. 38, pp. 4347-4355, 2004.

26. D. Kittelson and I. A. Khalek, "Formation of nanoparticles during exhaust dilution," 1999.

27. B. R. Graskow, D. Kittelson, M. R. Ahmadi, and J. E. Morris, "Exhaust particulate emissions fro two port fuel injected spark ignition engines," *SAE Paper 1999-01-1144*, 1999.

28. M. Tainio, J. T. Tuomisto, O. Hanninen, P. Aarni, K. J. Koistinen, M. J. Jantunen, and J. Pekkanen, "Health effects caused by primary fine particulate matter (PM2.5) emitted from buses in the Helsinki metropolitan area, Finland," *Risk Analysis*, vol. 25, no. 1, pp. 151-160, 2005.

29. "Understanding the health effects of components of the particulate matter mix: Progess and next steps," Helath Effects Institute, 2002.

30. W. K. C. Morgan, R. B. Reger, and D. M. Tucker, "Health effects of diesel," *Ann. occup. Hyg.*, vol. 41, no. 6, pp. 643-658, 1997.

31. C.-C. Lin, S.-J. Chen, K.-L. Huang, W.-I. Hwang, G.-P. Chang-Chien, and W.-Y. Lin, "Characteristics of of Metals in Nano/Ultrafine/Fine/Coarse Particles Collected Beside a Heavily Trafficked Road," *Environmental Science and Technology*, vol. 39, no. 21, pp. 8113-8122, 2005.

32. Y. Kitamura, A. Mohammadi, T. Ishiyama, and M. Shioji, "Fundamental Investigation of NOx Formation in Diesel Combustion Under Supercharged and EGR Conditions," *SAE Paper 2005-01-0364*, 2005.

33. D. Satcher, "Toxicological Profile for Polycyclic Aromatic Hydrocarbons," Agency for Toxic Substance and Disease Registry,1995.

34. Storey John M, S. A. Lewis, B. H. West, S. P. Huff, S. C. Sluder, R. M. Wagner, N. Domingo, J. Thomas, and M. Kass, "Hydrocarbon Species in the Exhaust of Diesel Engines Equipped with Advanced Emission Control Devices," Fuels,Engines and Emissions Research Center, Oak Ridge National Laboratory, Tennessee,CRC Project No.AVFL-10b-2, Jan.2005.

35. H. K. Kappanna, "Reduction of Toxic Air Contaminants (TACs) and Particulate Matter Emissions from Heavy Duty Natural Gas Engines." Master's Thesis, Department of Mechanical and Aerospace Engineering, West Virginia University, 2006.

36. A. Ayala, N. Y. Kado, R. A. Okamoto, M. Gebel, P. Rieger, R. Kobayashi, and P. A. Kuzmicky, "CNG and Diesel Transit Bus Emissions in Review," Newport, Rhode Island: 2003.

37. A. Holmen and A. Ayala, "Ultrafine PM Emissions from Natural Gas, Oxidation-Catalyst Diesel, and Particle-Trap Diesel Heavy-Duty Transit Buses," *Environmental Science and Technology*, vol. 36, pp. 5041-5050, 2002.

38. T. L. Ullman, L. R. Smith, J. W. Anthony, W. J. Slodowske, B. Trestrail, A. L. Cook, W. B. Bunn, C. A. Lapin, K. J. Wright, and C. R. Clark, "Comparison of Exhaust Emissions, Including Toxic Air Contaminants, from School Buses in Compressed Natural Gas, Low

Emitting Diesel, and Conventional Diesel Engine Configurations," *SAE Paper 2003-01-1381*, 2003.

39. N. O. Nylund, K. Erkkila, M. Lappi, and M. Ikonen, "Transit Bus Emission Study: Comparison of Emissions from Diesel and Natural Gas Buses," VTT Processes,PRO3/P5150/04, 2004.

40. M. Lev-On, C. LeTavec, J. Uihlein, K. Kimura, T. L. Alleman, D. R. Lawson, K. Vertin, M. Gautam, G. J. Thompson, S. Wayne, N. Clark, R. Okamato, P. Rieger, G. Yee, B. Zielinska, J. Sagebiel, S. Chatterjee, and K. Hallstrom, "Speciation of Organic Compounds from the Exhaust of Trucks and Buses: Effect of Fuel and After-Treatment on Vehicle Emission Profiles," *SAE Paper 2002-01-2873*, 2002.

41. M. Melendez, J. Taylor, J. Zuboy, W. S. Wayne, and D. Smith, "Emission Testing of Washington Metropolitan Area Transit Authority (WMATA) Natural Gas and Diesel Transit Buses," NREL, Colorado,NREL/TP-540-36355, 2005.

42. P. Eastwood, *Critical Topics in Exhaust Gas After Treatment* Research Study Press Ltd, 2000.

43. J. E. Johnson and D. B. Kittelson, "Physical Factors Affecting Hydrocarbon Oxidation in a Diesel Oxidation Catalyst," *SAE paper 941771*, 1994.

44. P. Zelenka, K. Ostgathe, and E. Lox, "Reduction of Diesel Exhaust Emissions by Using Oxidation Catalyst," *SAE paper 902111*, 1990.

45. A. Mizutani, T. Okawa, H. Matsuzaki, H. Kubota, and S. Hosogai, "Oxygen Sensor for CNG Application as ULEV or Tighter Emission Vehicle," *SAE paper 980264*, 1998.

46. K. H. Gluck, E. Lox, S. A. Schafer, T. Kreuzer, and R. S. Muniz, "Catalyst Development for Stoichiometric and Lean Burn Natural Gas Engines," *SAE Paper 942419*, 1994.

47. D. H. Ferguson, "Design, Fabrication and Testing of an Emissions Measurement System for a Transportable Heavy-Duty Vehicle Emissions Testing Laboratory." Master's Thesis, Department of Mechanical and Aerospace Engineering, West Virginia University, 1993.

48. T. S. Burlingame, "Reduction of Natural Gas Engine Emissions Using a Novel Aftertreatment System." Master's Thesis, Department of Mechanical and Aerospace Engineering, West Virginia University, 2004.

49. J. Lyyranen, J. Jokiniemi, E. I. Kauppinen, U. Backman, and H. Vesala, "Comparison of Different Dilution Methods for Measuring Diesel Particle Emissions," *Aerosol Science and Technology*, vol. 38, pp. 12-23, 2004.

50. "Model 3080 Electrostatic Classifier-Instruction Manual," TSI Inc., 2002.

51. "Model 3025A Ultrafine Condensation Particle Counter-Instruction Manual," TSI Inc., 2002.

52. "Non-Dispersive Infrared Analyzer (NDIR) Module," Rosemount Analytical, 1999.

53. "CLD NO/NOx Analyzer Module," Rosemount Analytical, 2006.

54. "FID Hydrocarbon Analyzer Module," Rosemount Analytical, 2006.

55. K. Nord, "Particles and Unregulated Emissions from CI Engines Subjected to Emssion Control." Department of Chemical Engineering and Geosciences, Lulea University of Technology, 2005.

56. "Standard Operating Procedure for PM2.5 Organic Sampling Using PUF Cartridges during Intensive Operating Periods in CRPAQS," Desert Research Institute, Reno, Nevada,1-750.4, 1997.

57. "Road Load Measurement and Dynamometer Simulation Using Coast-Down Techniques-SAE Recommended Practice," SAE, Warrendale, Pennsylvania,SAE J1263, 1991.

58. W. G. Wang, D. W. Lyons, N. N. Clark, and J. D. Luo, "Energy Consumption Analysis of Heavy-Duty Vehicles for Transient Emissions Evaluation on Chassis Dynamometer," *Proc Instn Mech Engrs*, vol. 213, no. D 1999.

59. "Code of Federal Regulations," CFR 40 Part 86 Sub-Part D,N ed 2004.

60. T. Sakai, B. C. Choi, R. Osuga, Y. Ko, and E. Kim, "Unburned Fuel and Formaldehyde Purification Characteristics of Catalytic Converters for Natural Gas Fueled Automotive Engine," *SAE Paper 920596*, 1992.

61. B.-C. Choi and T. Sakai, "Characteristics of Formaldehyde Formation from Catalytic Reaction of Methane in the Presence of NO," *SAE Paper 942008*, 1994.

62. F. R. Hartley, "Chemistry of the Platinum Group Metals: Recent Developments," *Platinum Metals Rev.*, vol. 36, no. 1, pp. 34-38, 1991.

63. S. Kado, Y. Sekine, and K. Fujimoto, "Direct Synthesis of Acetylene from Methane by Direct Current Pulse Discharge," *The Royal Society of Chemistry*, pp. 2485-2486, 1999.

APPENDIX A - UNREGULATED SPECIES ANALYSIS PROCEDURE
(Source: Desert Research Institute, 2007)

A.1   Gaseous Carbonyl Compound Analysis Procedure

C_1 through C_7 carbonyl compounds were collected with Sep-Pak cartridges, which have been impregnated with an acidified 2,4-dinitrophenylhydrazine (DNPH) reagent (Waters, Inc). When ambient air was drawn through the cartridge, carbonyls in the air sample are captured by reacting with DNPH to form hydrazones, which are separated and quantified using HPLC in the laboratory. Depending on the type of sorbent (C18, or silica gel, (Si) in the cartridge, the ambient measurement results are subject to various artifacts due to interaction with ozone. However, since ozone is not present in the vehicle exhaust, this is not a concern, and commercial Si cartridges from Waters are adequate for this project.

After sampling, the cartridges were eluted with acetonitrile. An aliquot of the eluent was transferred into a 2-ml septum vial and injected with an autosampler into a high performance liquid chromatograph (Waters 2690 Alliance System with 996 Photodiode Array Detector) for separation and quantization of the hydrazones. The carbonyl concentrations, in ppb, were computed from the amounts measured after blank correction and the volume of air sampled using the following equation:

$$\text{ppb}_i = \frac{m_i - b_i}{f \times t} \times 1000 \times \frac{24.45}{MW_i} \qquad (1)$$

where ppb_i= concentration in ppb of carbonyl species, i,

m_i = ug of i measured in the sample,

b_i = average ug of i in the blank,

t = sampling duration, in minutes,

f = sampling flow rate, in liters/min,

MW_i = molecular weight of i.

Since our HPLC system was equipped with the photodiode array detector, the identification of carbonyl compounds was much more accurate than with standard UV/VIS detector. Also, the sensitivity of the analysis was enhanced by using the photodiode array detector.

A.2 Polyaromatic Hydrocarbon/nitro-Polyaromatic Hydrocarbon Analysis Procedure

For each sample, PUF/XAD/PUF cartridges and TIGF filters were extracted and analyzed together. Prior to extraction, the following deuterated internal standards were added to each filter and PUF/XAD sorbent (Table 3-1).

Table A.1 List of Deuterated Internal Standards

PAH	Alkanes	N-PAH
naphthalene-d_8	dodecane-d_{26}	2-nitrodiphenyl-d_9
biphenyl-d_{10}	hexadecane-d_{34}	1-nitropyrne-d_9
acenaphthene-d_{10}	eicosane-d_{42}	
phenanthrene-d_{10}	octacosane-d_{58}	
anthracene-d_{10}	tetracosane-d_{50}	
pyrene-d_{12}	hexatriacontane-d_{74}	
benz(a)anthracene-d_{12}		
chrysene-d_{12}		
benzo[k]fluoranthene-d_{12}		
benzo[e]pyrene-d_{12}		
benzo[a]pyrene-d_{12}		
benzo[g,h,i]perylene-d_{12}		
coronene-d_{12}		

Filters and XAD-4 were extracted with dichloromethane using the Dionex ASE followed by acetone extraction under the same conditions. Since PUF media degrades when extracted with dichloromethane, the PUF were extracted twice with acetone using the Dionex ASE. This method gives good recovery for PAH.

All extracts were then concentrated by rotary evaporation at 35°C under gentle vacuum to ~1 mL and filtered through 0.2 μm PTFE disposal filter device (Whatman Pura disc^{TM} 25TF), rinsing the flask 3 times with 1 ml dichloromethane (DCM) and acetone (50/50 by volume) each time. The extract was concentrated to 1 ml and split into two fractions, as follows:

The first fraction was precleaned by the solid-phase extraction technique, using Superclean LC-SI SPE cartridges (Supelco) with sequential elution with hexane, and hexane/benzene (1:1). The second fraction was utilized for the polar compound analysis without precleaning. It was derivatized using a mixture of bis(trimethylsilyl)trifluoroacetamide and pyridine to convert the polar compounds into their trimethylsilyl derivatives for analysis of organic acids and diacids, cholesterol, sitosterol, and levoglucosan.

The samples collected for nitro-PAH analyses were extracted with dichloromethane as described above. The extracts were precleaned by the solid-phase extraction technique, using Aminopropyl (NH2) SPE cartridges, with sequential elution with hexane/DCM, 98/2 v/v and hexane/DCM 80/20 v/v. For nitro- and dinitro-PAH analysis, these fractions were combined and further cleaned by semi-preparative normal-phase high performance liquid chromatography (HPLC) technique. The Chromegabond Amino Cyano 25 cm x 9.6 mm column (ES Industries, West Berlin, NJ) and isocratic elution with 20% DCM in hexane was used. The fraction corresponding to nitro- and dinitro-PAH was collected and analyzed by negative ion chemical ionization GC/MS.

The filters and PUF/XAD extracts were analyzed by gas chromatography/mass spectrometry (GC/MS), using Varian CP-3800 GC equipped with a CP8400 autosampler and interfaced to a Varian Saturn 2000 Ion Trap operating in electron impact (EI) ionization mode. Injections (1 µL) were made in the splitless mode onto a 30m long 5% phenylmethylsilicone fused-silica capillary column (DB-5ms, J&W Scientific or equivalent). Quantification of the individual compounds was obtained by selective ion storage (SIS) technique, monitoring the molecular (or the most characteristic) ion of each compound of interest and the corresponding deuterated internal standard. Calibration curves for the GC/MS quantification were made for the most abundant and characteristic ion peaks of the compounds of interest (Table 3-1) using the deuterated species most closely matched in volatility and retention characteristics as internal standards. National Institute of Standards and Technology (NIST) Standard Reference Material (SRM) 1647 (certified PAH) with the addition of deuterated internal standards and of those compounds not present in the SRM (i.e., oxy-PAH, nitro-PAH, hopane, sterenes, carpanes, hydrocarbons, cycloalkanes) were used to make calibration solutions. A six- to eight-level calibration was performed for each compound of interest and the calibration check (using median calibration standards) was run every 10 samples to check for accuracy of analyses. If the relative accuracy of measurement (defined as a percent difference from the standard value) was less than 20%, the instrument was recalibrated.

The nitro-and dinitro-PAH were analyzed using the Varian 1200 triple quadrupole gas chromatograph/mass spectrometer (GC/MS/MS) system with CP-8400 autosampler. The tandem MS/MS system allowed for structural elucidation of unknown compounds with precursor, product and neutral loss scan. The GC interface allowed for sensitive analyses of complex

mixtures in electron impact (EI) as well as positive and negative chemical ionization (CI) mode. Negative CI offered a superior sensitivity for the analysis of nitro-PAH (approximately 100 times higher than EI or positive CI) that could be emitted from combustion sources, including motor vehicle engines. For negative CI, 10 fg/ul of octafluoronaphthalene gave S/N of 20:1. This superior sensitivity offered the advantage of analyzing small samples collected during a short sampling time. Injections (1 µL) were made in the splitless mode onto a 30m long x 0.25 mm id 50% phenylmethylsilicone fused-silica capillary column (DB-17ms, CP-Sil-24ms or equivalent). Quantification of the individual compounds was obtained by multiple ion detection (MID) technique, monitoring the molecular ion of each compound of interest and the corresponding deuterated internal standard. Calibration curves for the GC/MS quantification were made for the most abundant and characteristic ion peaks of the compounds of interest using the deuterated species most closely matched in volatility and retention characteristics as internal standards and the authentic standards of quantified nitro-PAH. A six- to eight-level calibration was performed for each compound of interest and the calibration check (using median calibration standards) was run every 10 samples to check for accuracy of analyses. If the relative accuracy of measurement (defined as a percent difference from the standard value) was less than 20%, the instrument was recalibrated.

Diesel fuel and lubrication oil samples were obtained from the vehicles immediately after emissions sampling and were analyzed for PAH and hopanes/steranes. The oils were cleaned and fractionated prior to analysis. Clean up was conducted on a 12ml Supelco solid phase extraction (SPE) cartridge packed with 2g of SiOH. Cartridges were placed on a vacuum manifold and conditioned prior to cleanup with 14ml of hexane. Prior to cleanup, fuels and oils were diluted in hexane (300 and 150 µl/1ml). Three hundred microliters of the diluted fuel or oil was spiked onto a SPE cartridge along with ten microliters of tetrocosane-d_{50} (internal standard) and the PAH internal standard mixture described above. Samples were eluted and fractionated with 8ml of hexane followed by 10ml of benzene/hexane (1:1).

A.3 VOC Analysis Procedure

For the analysis of all VOC, a 2D-chromatography method was employed. Gaseous sample is preconcentrated on the three stages of Entech preconcentrator (glass beads with Tenax, Tenax and capillary tube) and injected into the head of a DB-1 type column (60 m long 0.32 mm

i.d., 1 μm film thickness) at room temperature. This column was connected through a three-way valve with two other columns: a 15 m DB-1 type column (0.32 mm i.d., 0.5 μm film thickness), leading to the MS and a 30 m x 0.32 mm i.d. GasPro column (a PLOT type column, J&W Scientific) leading to the FID. During the first few minutes after injection, the sample was eluted through the 60 m DB-1 and 30 m GasPro column and peaks were detected by the FID. After suitable time (approximately 6 – 10 min), the valve was switched and the sample was directed through the 15 m DB-1 column to the MS detector. This way, the very light hydrocarbons (C2 up to C4) are clearly separated on the Gas-Pro column and detected by the FID, and the heavier hydrocarbons (up to C12), are unequivocally identified and quantified by the ion trap MS.

The GC/FID and GC/MS response was calibrated in ppbv, using a 74 component mixture (Air Environmental, Inc., Denver, CO) in the ppbv range of concentrations, traceable to the NIST Standard Reference Materials (SRM). A three-level calibration was performed for each compound of interest and the calibration check (using median calibration standards) was analyzed every 10 samples to check for accuracy of analyses. If the relative accuracy of measurement (defined as a percent difference from the standard value) was less than 20%, the instrument was recalibrated. Blanks were performed once daily. Our analysis plan and data processing standards call for the replicate analysis of approximately 10% of the samples. The replicate analyses are flagged in our database and the programs we have for data processing extract these replicates and determine a replicate precision. These are then converted into an absolute precision for each measurement, which can be reported if required.

A.4   EC/OC Analysis Procedure

The thermal/optical reflectance (TOR) method measured organic (OC) and elemental (EC) carbon. The TOR method is based on the principle that different types of carbon-containing particles are converted to gases under different temperature and oxidation conditions. The different carbon fractions from TOR are useful for comparison with other methods, which are specific to a single definition for organic and elemental carbon. These specific carbon fractions also help distinguish among seven carbon fractions reported by TOR:

1) The carbon evolved in a helium atmosphere at temperatures between ambient and 120 °C (OC1)

2) The carbon evolved in a helium atmosphere at temperatures between 120 and 250°C (OC2)

3) The carbon evolved in a helium atmosphere at temperatures between 250 and 450 °C (OC3)

4) The carbon evolved in a helium atmosphere between 450 and 550°C (OC4)

5) The carbon evolved in an oxidizing atmosphere at 550°C (EC1)

6) The carbon evolved in an oxidizing atmosphere between 550 and 700°C (EC2)

7) The carbon evolved in an oxidizing atmosphere between 700 and 800°C (EC3)

The thermal/optical reflectance carbon analyzer consisted of a thermal system and an optical system. The thermal system consisted of a quartz tube placed inside a coiled heater. Current through the heater was controlled to attain and maintain pre-set temperatures for given time periods. A portion of a quartz filter was placed in the heating zone and heated to different temperatures under non-oxidizing and oxidizing atmospheres. The optical system consisted of a He-Ne laser, a fiber optic transmitter and receiver and a photocell. The filter deposit faces a quartz light tube so that the intensity of the reflected laser beam can be monitored throughout the analysis.

As the temperature increased from ambient (~25°C) to 550°C, organic compounds were volatilized from the filter in a non-oxidizing (He) atmosphere while elemental carbon was not oxidized. When oxygen was added to the helium at temperatures greater than 550°C, the elemental carbon burned and entered the sample stream. The evolved gases passed through an oxidizing bed of heated manganese dioxide where they were oxidized to carbon dioxide, and then across a heated nickel catalyst, which reduced the carbon dioxide to methane (CH_4). The methane was then quantified with a flame ionization detector (FID).

The reflected laser light was continuously monitored throughout the analysis cycle. The negative change in reflectance was proportional to the degree of pyrolytic conversion from organic to elemental carbon, which takes place during organic carbon analysis. After oxygen was introduced, the reflectance increased rapidly as the light-absorbing carbon was burned off the filter. The carbon measured after the reflectance attained the value it had at the beginning of the analysis cycle was classified as elemental carbon. This adjustment for pyrolysis in the analysis was significant, as high as 25% of organic or elemental carbon, and was not ignored.

The system was calibrated by analyzing samples of known amounts of methane, carbon dioxide, and potassium hydrogen phthalate (KHP). The FID response was ratioed to a reference level of methane injected at the end of each sample analysis. Performance tests of the instrument calibration were conducted at the beginning and end of each day's operation. Intervening samples were re-analyzed when calibration changes of more than ±10% were found.

Known amounts of American Chemical Society (ACS) certified reagent grade crystal sucrose and KHP were committed to TOR as a verification of the organic carbon fractions. Fifteen different standards were used for each calibration. Widely accepted primary standards for elemental and/or organic carbon are still lacking. Results of the TOR analysis of each filter were entered into the DRI database.

A.5   Metals Analysis Procedure

X-ray fluorescence (XRF) analysis was performed on Teflon-membrane filters using an energy dispersive x-ray fluorescence (EDXRF) analyzer. Table 3-2 lists the elements, together with their Minimum Detectable Limits (MDL), for three different analytical protocols. Since the required limit of detection was not specified we propose to use the protocol B (which was less expensive). However, if necessary the more expensive protocols C or D could be used.

Table A.2 X-Ray Fluorescence method minimum detectable limits using DRI standard analysis protocols

Element	Protocol A ng/cm^2	Protocol B ng/cm^2	Protocol C ng/cm^2	Protocol D ng/cm^2
Al	10	7.2	3.6	2.5
Si	6.3	4.4	2.2	1.4
P	5.6	4.0	2.0	1.4
S	5.0	3.5	1.8	1.2
Cl	10	7.4	3.7	2.6
K	6.1	4.3	2.2	1.5
Ca	4.5	3.2	1.6	1.1
Ti	2.9	2.1	1.0	0.73
V	2.5	1.7	0.87	0.62
Cr	1.9	1.4	0.67	0.48
Mn	1.6	1.1	0.56	0.40
Fe	1.5	1.1	0.54	0.38
Co	0.88	0.62	0.31	0.22
Ni	0.89	0.63	0.31	0.22

Element	Protocol A ng/cm^2	Protocol B ng/cm^2	Protocol C ng/cm^2	Protocol D ng/cm^2
Cu	1.1	0.76	0.38	0.27
Zn	1.1	0.76	0.38	0.27
Ga	1.9	1.4	0.68	0.48
As	1.6	1.1	0.56	0.39
Se	1.2	0.86	0.43	0.31
Br	1.0	0.72	0.36	0.25
Rb	1.0	0.68	0.34	0.24
Sr	1.1	0.78	0.39	0.28
Y	1.3	0.92	0.46	0.33
Zr	1.7	1.2	0.59	0.42
Mo	2.7	1.9	0.95	0.67
Pd	11	7.6	3.8	2.7
Ag	12	8.6	4.3	3.0
Cd	12	8.6	4.3	3.0
In	13	9.5	4.8	3.4
Sn	17	12	6.2	4.4
Sb	18	13	6.4	4.5
Ba	52	37	18	13
La	62	44	22	16
Au	3.1	2.2	1.1	0.77
Hg	2.6	1.8	0.91	0.65
Tl	2.5	1.8	0.88	0.62
Pb	3.0	2.2	1.1	0.76
U	2.3	1.7	0.83	0.59

XRF analyses were performed on a Kevex Corporation Model 700/8000 energy dispersive x-ray fluorescence (EDXRF) analyzer using a side-window, liquid-cooled, 60 keV, 3.3 milliamp rhodium anode x-ray tube and secondary fluorescers. The x-ray output stability was within 0.25% for any 8-hour period within a 24-hour duration. The silicon detector has an active area of 30 mm^2, with a system resolution better than 165 eV. The analysis was controlled, spectra were acquired, and elemental concentrations were calculated by software implemented on an LSI 11/23 microcomputer, which was interfaced to the analyzer. Five separate XRF analyses were conducted on each sample to optimize the detection limits for the specified elements.

Three types of XRF standards were used for calibration, performance testing, and auditing: 1) vacuum-deposited thin-film elements and compounds (Micromatter, Deer Harbor, WA); 2) polymer films; and 3) NIST thin-glass films. The vacuum deposit standards cover the

largest number of elements and were used as calibration standards. The polymer film and NIST standards were used as quality control standards. NIST standards were the definitive standard reference material, but these are only available for the species Al, Ca, Co, Cu, Mn, and Si (SRM 1832) and Fe, Pb, K, Si, Ti, and Zn (SRM 1833). A separate Micromatter (Deer Harbor, WA) thin-film standard was used to calibrate the system for each element.

During XRF analysis, filters were removed from their Petri slides and placed with their deposit sides down into polycarbonate filter cassettes. A polycarbonate retainer ring kept the filter flat against the bottom of the cassette. These cassettes were loaded into a carousel in the x-ray chamber which contains 16 openings. The filter identifications were recorded on a data sheet to correspond to the numbered positions in the carousel. The sample chamber was evacuated to 10^{-3} torr and a computer program controlled the positioning of the samples and the excitation conditions. Complete analysis of 16 samples under five excitation conditions required approximately 6 hours. The vacuum in the x-ray chamber and the heat induced by the absorption of x-rays can cause certain materials to volatilize. For this reason, labile species such as nitrate and organic carbon were measured on a quartz-fiber filter rather than on the Teflon-membrane filter, which was subjected to XRF analysis.

A quality control standard and a replicate from a previous batch were analyzed with each set of 14 samples. When a quality control value differed from specifications by more than ±5% or when a replicate concentration differed from the original value (when values exceeded 10 times the detection limits) by more than ±10%, the samples were re-analyzed. If further tests of standards showed that the system calibration had changed by more than ±2%, the instrument was re-calibrated as described above. All XRF results were directly entered into the DRI databases.

A.6 Uncertainty Calculation

All analytical results were evaluated in terms of their associated measurement errors according to the following equation:

$$Uncerata\operatorname{int} y = \sqrt{\left((AnalyteConcentration * \operatorname{Re}plicate \operatorname{Pr}ecision)^2 + (AnalyteDetectionLimit)^2\right)}$$

Replicate precision for each analyte is determined by multiple injections (replicates) of at least ten per cent of all of the analyzed samples. Precision is then determined by:

$$Re\,plicate\,Pr\,ecision = \frac{(C1 - C2)}{\left(\dfrac{C1 + C2}{2}\right)} * 100$$

By this equation the analytical minimum detection limit (MDL) will determine the analyte uncertainty when sample concentrations approach zero. Similarly, the MDL will have little impact on the uncertainty of a higher concentration sample, where the concentration is many times the detection limit. In addition to this, the uncertainty in the volume flow is incorporated into the final uncertainty by a similar root-mean-square method. In this way the uncertainty most accurately represents the true uncertainty of the sample. Also, all samples are corrected for lot-specific sampling media blank values prior to the final concentration calculations. Software programs have been developed by DRI to automate the data processing and reporting functions.

APPENDIX B - TEST VEHICLE AND ENGINE SPECIFICATIONS

Two Transit buses were used for this study. The buses were part of the Riverside Transit Authority (RTA) and Los Angeles County Metro Transit Authority (LACMTA). The vehicle and engine specification of the two buses are given below

Table B.1 Test Vehicle Specifications

	LACMTA	RTA
Vehicle Type	Transit Bus	Transit Bus
Vehicle ID Number (VIN)	1N9TA1BA7XL013312	1N90401562A140498
Vehicle Manufacturer	Neoplan	NABI, Inc.
Vehicle Model Year	1999	2002
Gross Vehicle Weight (GVW) (lb.)	40600	40600
Vehicle Total Curb Weight (lb.)	32660	33040
Vehicle Tested Weight (lb.)	37840	37840
Odometer Reading (mile)	161113	229981
Transmission Type	Auto	Auto
Transmission Configuration	4 speed	4 speed
Number of Axles	2	2

Table B.2 Test Vehicle's Engine Specifications

	LACMTA	RTA
Engine Type	Detroit Diesel S-50	Detroit Diesel S-50
Engine ID Number	04R027372	04R0040516
Engine Model Year	1999	2005
Engine Displacement (Liter)	8.5	8.5
Number of Cylinders	4	4
Engine Rated Power (hp)	275	275
Primary Fuel	CNG	CNG
Catalytic Converter Manufacturer	ECS oxidation catalyst	ECS oxidation catalyst

Table C.1 Distance specific emissions data of carbonyl compounds

g/mile	5126 With ATD	5127 Bkgd With ATD	5133 W/O ATD	5134 Bkgd W/O ATD
Formaldehyde	1.1594E-02	2.6272E-03	4.8714E-01	5.2299E-03
acetaldehyde	3.8875E-03	2.9725E-03	0.0000E+00	1.6314E-03
acetone	1.1561E-03	2.4657E-03	0.0000E+00	2.7710E-03
Acrolein	4.0089E-04	4.2196E-04	0.0000E+00	1.4150E-04
Propionaldehyde	4.8735E-04	4.1679E-04	0.0000E+00	1.7740E-04
Crotonaldehyde	0.0000E+00	0.0000E+00	0.0000E+00	0.0000E+00
methyl ethyl ketone	0.0000E+00	0.0000E+00	0.0000E+00	0.0000E+00
Methacrolein	0.0000E+00	0.0000E+00	0.0000E+00	0.0000E+00
n-butyraldehyde	6.4121E-04	3.9375E-04	1.6116E-04	4.5270E-04
benzaldehyde	0.0000E+00	2.9355E-04	0.0000E+00	0.0000E+00
Glyoxal	5.1803E-05	5.4513E-05	7.8074E-05	2.7410E-05
Valeraldehyde	3.0270E-04	1.9119E-04	1.2173E-04	0.0000E+00
m-Tolualdehyde	0.0000E+00	0.0000E+00	0.0000E+00	0.0000E+00
Hexaldehyde	0.0000E+00	0.0000E+00	0.0000E+00	0.0000E+00

Table C.2 Distance specific measurement uncertainty data of carbonyl compounds

g/mile	5126-2 With ATD uncertainty	5127-1 BG With ATD uncertainty	5133-2 W/O ATD uncertainty	5134-1 BG W/O ATD uncertainty
Formaldehyde	5.9247E-04	1.8336E-04	2.4412E-02	2.8956E-04
acetaldehyde	4.5605E-04	4.5921E-04	4.0970E-04	4.4450E-04
acetone	6.2029E-04	8.6215E-04	4.3180E-04	9.1105E-04
Acrolein	2.0922E-04	2.2021E-04	0.0000E+00	1.6524E-04
Propionaldehyde	2.3116E-04	2.2200E-04	1.4018E-04	1.8264E-04
Crotonaldehyde	1.8391E-04	1.9358E-04	1.8463E-04	1.9453E-04
methyl ethyl ketone	1.8735E-04	1.9709E-04	1.8809E-04	1.9806E-04
Methacrolein	1.8391E-04	1.9358E-04	1.8463E-04	1.9453E-04
n-butyraldehyde	2.7838E-04	1.8799E-04	1.3320E-04	2.1450E-04
benzaldehyde	2.4439E-04	2.5755E-04	2.4535E-04	2.5840E-04
Glyoxal	9.0769E-05	9.5560E-05	9.1194E-05	9.5978E-05
Valeraldehyde	2.1273E-04	2.2355E-04	2.1310E-04	2.2438E-04
m-Tolualdehyde	2.6392E-04	2.7765E-04	2.6497E-04	2.7901E-04
Hexaldehyde	2.3597E-04	2.4842E-04	2.3690E-04	2.4965E-04

Table C.3 Distance specific emissions data of nitro-polyaromatic hydrocarbons

g/mile	5126 with ATD	5127 Bkgd With ATD	5133 W/O ATD	5134 Bkgd W/O ATD
1-nitronaphthalene	2.6542E-07	1.2795E-07	1.0267E-06	1.6111E-07
2-nitronaphthalene	2.8630E-08	1.1342E-08	1.7275E-07	9.6236E-09
1-methyl-5-nitronaphthalene	0.0000E+00	0.0000E+00	6.4356E-09	0.0000E+00
1-methyl-4-nitronaphthalene	1.6841E-08	0.0000E+00	2.1000E-08	5.3465E-09
2-methyl-4-nitronaphthalene	0.0000E+00	0.0000E+00	0.0000E+00	0.0000E+00
1-methyl-6-nitronaphthalene	5.2207E-08	0.0000E+00	1.8968E-08	3.8138E-08
2-nitrobiphenyl	5.7260E-09	2.4811E-09	4.0646E-09	2.1386E-09
3-nitrobiphenyl	7.0733E-09	2.8355E-09	9.4841E-09	2.8514E-09
4-nitrobiphenyl	6.0628E-09	0.0000E+00	4.4033E-09	1.0693E-09
5-nitroacenaphthene	0.0000E+00	3.5444E-10	0.0000E+00	0.0000E+00
2-nitrofluorene	0.0000E+00	0.0000E+00	0.0000E+00	0.0000E+00
1,3-dinitronaphthalene	4.1092E-08	0.0000E+00	2.0662E-08	3.1366E-08
1,5-dinitronaphthalene	0.0000E+00	0.0000E+00	0.0000E+00	0.0000E+00
1,8-dinitronaphthalene	0.0000E+00	2.1267E-09	0.0000E+00	2.4950E-09
2-nitroanthracene	0.0000E+00	0.0000E+00	0.0000E+00	0.0000E+00
2-nitrophenanthrene	0.0000E+00	3.8989E-09	2.0323E-09	5.7029E-09
3-nitrophenanthrene	0.0000E+00	0.0000E+00	0.0000E+00	0.0000E+00
4-nitrophenanthrene	0.0000E+00	0.0000E+00	0.0000E+00	0.0000E+00
9-nitroanthracene	0.0000E+00	0.0000E+00	0.0000E+00	0.0000E+00
9-nitrophenanthrene	0.0000E+00	0.0000E+00	0.0000E+00	0.0000E+00
1-nitropyrene	0.0000E+00	0.0000E+00	5.0808E-09	0.0000E+00
2-nitrofluoranthene	2.8293E-08	1.9849E-08	1.4226E-08	4.3485E-08
2-nitropyrene	0.0000E+00	0.0000E+00	1.7613E-08	0.0000E+00
3-nitrofluoranthene	0.0000E+00	0.0000E+00	0.0000E+00	3.5643E-10
4-nitropyrene	0.0000E+00	0.0000E+00	0.0000E+00	0.0000E+00
2,7-dinitrofluorene	7.6795E-08	1.4532E-08	4.4033E-09	2.3881E-08
2,7-dinitrofluoren-9-one	0.0000E+00	0.0000E+00	0.0000E+00	0.0000E+00
6-nitrochrysene	0.0000E+00	0.0000E+00	0.0000E+00	0.0000E+00
6-nitrobenz[a]pyrene	0.0000E+00	0.0000E+00	0.0000E+00	0.0000E+00

Table C.4 Distance specific measurement uncertainty data of nitro-polyaromatic hydrocarbons

g/mile	5126 with ATD Uncertainty	5127 Bkgd (With ATD) Uncertainty	5133 W/O ATD Uncertainty	5134 Bkgd (W/O ATD) Uncertainty
1-nitronaphthalene	1.5107E-08	6.7055E-09	5.7516E-08	8.0149E-09
2-nitronaphthalene	1.4053E-09	6.7055E-10	9.1744E-09	3.3395E-10
1-methyl-5-nitronaphthalene	0.0000E+00	0.0000E+00	3.5286E-10	0.0000E+00
1-methyl-4-nitronaphthalene	1.4053E-09	0.0000E+00	1.4114E-09	3.3395E-10
2-methyl-4-nitronaphthalene	0.0000E+00	0.0000E+00	0.0000E+00	0.0000E+00
1-methyl-6-nitronaphthalene	1.0188E-08	0.0000E+00	3.8815E-09	6.6791E-09
2-nitrobiphenyl	7.0264E-10	3.3527E-10	3.5286E-10	3.3395E-10
3-nitrobiphenyl	2.1079E-09	6.7055E-10	2.8229E-09	6.6791E-10
4-nitrobiphenyl	3.5132E-10	0.0000E+00	3.5286E-10	0.0000E+00
5-nitroacenaphthene	0.0000E+00	0.0000E+00	0.0000E+00	0.0000E+00
2-nitrofluorene	0.0000E+00	0.0000E+00	0.0000E+00	0.0000E+00
1,3-dinitronaphthalene	7.7291E-09	0.0000E+00	3.8815E-09	5.3433E-09
1,5-dinitronaphthalene	0.0000E+00	0.0000E+00	0.0000E+00	0.0000E+00
1,8-dinitronaphthalene	0.0000E+00	0.0000E+00	0.0000E+00	3.3395E-10
2-nitroanthracene	0.0000E+00	0.0000E+00	0.0000E+00	0.0000E+00
2-nitrophenanthrene	0.0000E+00	3.3527E-10	0.0000E+00	3.3395E-10
3-nitrophenanthrene	7.0264E-10	0.0000E+00	0.0000E+00	0.0000E+00
4-nitrophenanthrene	0.0000E+00	0.0000E+00	0.0000E+00	0.0000E+00
9-nitroanthracene	0.0000E+00	0.0000E+00	0.0000E+00	0.0000E+00
9-nitrophenanthrene	0.0000E+00	0.0000E+00	0.0000E+00	0.0000E+00
1-nitropyrene	0.0000E+00	0.0000E+00	3.5286E-10	0.0000E+00
2-nitrofluoranthene	8.0804E-09	5.0291E-09	3.8815E-09	1.1020E-08
2-nitropyrene	0.0000E+00	0.0000E+00	1.4114E-09	0.0000E+00
3-nitrofluoranthene	0.0000E+00	0.0000E+00	0.0000E+00	0.0000E+00
4-nitropyrene	0.0000E+00	0.0000E+00	0.0000E+00	0.0000E+00
2,7-dinitrofluorene	2.5647E-08	4.3586E-09	1.4114E-09	7.0130E-09
2,7-dinitrofluoren-9-one	0.0000E+00	0.0000E+00	0.0000E+00	0.0000E+00
6-nitrochrysene	0.0000E+00	0.0000E+00	0.0000E+00	0.0000E+00
6-nitrobenz[a]pyrene	0.0000E+00	0.0000E+00	0.0000E+00	0.0000E+00

Table C.5 Distance specific emissions data of gas phase polyaromatic hydrocarbons

g/mile	5126 with ATD	5127 Bkgd With ATD	5133 W/O ATD	5134 Bkgd W/O ATD
Naphthalene	2.9559E-04	3.5929E-04	3.9768E-04	3.6972E-04
2-methylnaphthalene	5.0358E-06	2.7955E-06	1.9399E-05	4.9145E-06
1-methylnaphthalene	7.1272E-07	6.8585E-07	8.9811E-06	1.4582E-06
Biphenyl	1.2826E-06	0.0000E+00	2.4635E-06	4.3199E-07
1+2ethylnaphthalene	3.7529E-06	4.2179E-07	2.2582E-06	6.4799E-07
2,6+2,7-dimethylnaphthalene	2.4228E-06	1.7407E-06	7.2875E-06	9.7199E-07
1,3+1,6+1,7dimethylnaphth	5.8432E-06	2.0044E-06	8.3138E-06	1.9982E-06
1,4+1,5+2,3-dimethylnaphth	9.9767E-07	3.1652E-07	2.3609E-06	0.0000E+00
1,2-dimethylnaphthalene	2.8495E-07	2.1089E-07	3.0789E-07	1.6218E-07
2-Methylbiphenyl	9.5821E-05	6.0867E-05	2.5609E-04	6.1511E-05
3-Methylbiphenyl	3.5678E-05	1.9199E-05	1.0639E-04	2.1278E-05
4-Methylbiphenyl	9.5964E-06	5.5910E-06	3.7669E-05	5.8865E-06
Dibenzofuran	6.6522E-07	1.5808E-07	1.5395E-06	1.0800E-07
A-trimethylnaphthalene	6.6522E-07	1.0562E-07	1.1804E-06	5.4177E-08
1-ethyl-2-methylnaphthalene	9.5017E-07	1.0562E-07	3.7466E-06	3.2400E-07
B-trimethylnaphthalene	1.2826E-06	5.2812E-08	1.8477E-06	4.3199E-07
C-trimethylnaphthalene	1.9953E-06	2.6371E-07	0.0000E+00	2.1600E-07
2-ethyl-1-methylnaphthalene	1.1876E-06	9.4955E-07	5.1485E-08	5.3999E-07
E-trimethylnaphthalene	1.4248E-07	2.6371E-07	1.0263E-06	3.2400E-07
F-trimethylnaphthalene	1.6151E-06	5.2812E-08	0.0000E+00	0.0000E+00
2,3,5+I-trimethylnaphthalene	0.0000E+00	0.0000E+00	0.0000E+00	0.0000E+00
2,4,5-trimethylnaphthalene	0.0000E+00	1.5808E-07	3.5938E-07	0.0000E+00
J-trimethylnaphthalene	0.0000E+00	0.0000E+00	8.2105E-07	0.0000E+00
1,4,5-trimethylnaphthalene	0.0000E+00	0.0000E+00	0.0000E+00	0.0000E+00
Acenaphthylene	2.3746E-07	5.2812E-08	3.0789E-07	1.6218E-07
Acenaphthene	0.0000E+00	0.0000E+00	1.5412E-07	0.0000E+00
Fluorene	1.2351E-06	3.1652E-07	2.7714E-06	3.7817E-07
Dibenzothiophene	0.0000E+00	0.0000E+00	2.0526E-07	0.0000E+00
Phenanthrene	5.2258E-06	1.4770E-06	5.5428E-06	1.7822E-06
Anthracene	0.0000E+00	0.0000E+00	1.0263E-07	0.0000E+00
A-methylfluorene	0.0000E+00	0.0000E+00	0.0000E+00	0.0000E+00
1-methylfluorene	1.8997E-07	1.0562E-07	1.5412E-07	5.4177E-08
B-methylfluorene	9.4984E-08	0.0000E+00	1.0263E-07	0.0000E+00

Table C.6 Distance specific measurement uncertainty data of gas phase polyaromatic hydrocarbons

g/mile	5126 with ATD Uncertainty	5127 Bkgd (With ATD) Uncertainty	5133 W/O ATD Uncertainty	5134 Bkgd (W/O ATD) Uncertainty
Naphthalene	1.5768E-05	1.7323E-05	2.0866E-05	1.7450E-05
2-methylnaphthalene	6.0673E-07	3.7383E-07	2.1740E-06	5.5603E-07
1-methylnaphthalene	2.0166E-07	1.5322E-07	1.6196E-06	3.1125E-07
Biphenyl	2.0939E-07	4.9956E-08	3.4545E-07	1.0319E-07
1+2ethylnaphthalene	8.1753E-07	1.0192E-07	4.9542E-07	1.5495E-07
2,6+2,7-dimethylnaphthalene	5.1188E-07	3.5908E-07	1.4926E-06	2.0739E-07
1,3+1,6+1,7dimethylnaphth	1.0856E-06	3.6210E-07	1.5582E-06	3.6635E-07
1,4+1,5+2,3-dimethylnaphth	7.2372E-08	5.2303E-08	2.0219E-07	5.0761E-08
1,2-dimethylnaphthalene	5.1644E-08	5.0962E-08	5.5752E-08	5.1095E-08
2-Methylbiphenyl	5.9581E-06	3.5884E-06	1.5141E-05	3.5807E-06
3-Methylbiphenyl	6.2391E-06	4.0471E-06	1.5064E-05	4.2673E-06
4-Methylbiphenyl	1.4313E-06	9.8503E-07	4.2732E-06	1.0489E-06
Dibenzofuran	6.0779E-08	5.0626E-08	1.3373E-07	5.0761E-08
A-trimethylnaphthalene	1.0505E-07	5.0291E-08	1.7184E-07	5.0761E-08
1-ethyl-2-methylnaphthalene	1.5704E-07	5.0291E-08	5.1941E-07	5.2765E-08
B-trimethylnaphthalene	1.2015E-07	4.9956E-08	1.4397E-07	5.4435E-08
C-trimethylnaphthalene	1.4474E-07	5.1297E-08	5.3635E-08	5.1763E-08
2-ethyl-1-methylnaphthalene	2.5576E-07	2.0452E-07	5.3635E-08	1.0419E-07
E-trimethylnaphthalene	5.0239E-08	5.1297E-08	7.5512E-08	5.2765E-08
F-trimethylnaphthalene	1.3104E-07	4.9956E-08	5.3635E-08	5.0761E-08
2,3,5+I-trimethylnaphthalene	4.9536E-08	4.9956E-08	5.3635E-08	5.0761E-08
2,4,5-trimethylnaphthalene	4.9536E-08	9.9911E-08	1.0868E-07	5.0761E-08
J-trimethylnaphthalene	4.9536E-08	4.9956E-08	2.1807E-07	5.0761E-08
1,4,5-trimethylnaphthalene	4.9536E-08	4.9956E-08	5.3635E-08	5.0761E-08
Acenaphthylene	5.1293E-08	4.9956E-08	1.0798E-07	5.1095E-08
Acenaphthene	4.9536E-08	4.9956E-08	5.3988E-08	5.0761E-08
Fluorene	2.0869E-07	5.2303E-08	4.0120E-07	5.3767E-08
Dibenzothiophene	4.9536E-08	4.9956E-08	5.4694E-08	5.0761E-08
Phenanthrene	7.9329E-07	2.5917E-07	8.5251E-07	2.6650E-07
Anthracene	4.9536E-08	4.9956E-08	5.3635E-08	5.0761E-08
A-methylfluorene	9.9073E-08	4.9956E-08	1.0692E-07	5.0761E-08
1-methylfluorene	5.0590E-08	5.0291E-08	5.3988E-08	5.0761E-08
B-methylfluorene	4.9888E-08	4.9956E-08	5.3635E-08	5.0761E-08

Table C.7 Distance specific emissions data of particle phase polyaromatic hydrocarbons

g/mile	5126 with ATD	5127 Bkgd With ATD	5133 W/O ATD	5134 Bkgd W/O ATD
4-methylpyrene	9.4984E-08	0.0000E+00	0.0000E+00	0.0000E+00
1-methylpyrene	1.4248E-07	0.0000E+00	5.1485E-08	0.0000E+00
Benzo(c)phenanthrene	0.0000E+00	0.0000E+00	0.0000E+00	0.0000E+00
Benzo(ghi)fluoranthene	1.4248E-07	0.0000E+00	0.0000E+00	0.0000E+00
Cyclopenta(c,d)pyrene	0.0000E+00	1.0562E-07	5.1485E-08	5.4177E-08
Benz(a)anthracene	0.0000E+00	0.0000E+00	0.0000E+00	0.0000E+00
Chrysene-Triphenylene	4.7492E-08	1.0562E-07	5.1485E-08	5.4177E-08
Benzanthrone	0.0000E+00	0.0000E+00	1.5412E-07	0.0000E+00
7-methylbenz(a)anthracene	0.0000E+00	0.0000E+00	0.0000E+00	0.0000E+00
3-methylchrysene	0.0000E+00	0.0000E+00	0.0000E+00	0.0000E+00
Benz(a)anthracene-7,12-dione	1.8997E-07	0.0000E+00	1.5412E-07	0.0000E+00
5+6-methylchrysene	0.0000E+00	0.0000E+00	0.0000E+00	0.0000E+00
Benzo(b+j+k)fluoranthene	0.0000E+00	0.0000E+00	0.0000E+00	0.0000E+00
Benzo(a)fluoranthene	5.2241E-07	0.0000E+00	0.0000E+00	0.0000E+00
BeP	0.0000E+00	0.0000E+00	0.0000E+00	0.0000E+00
BaP	6.6522E-07	1.1076E-06	1.1804E-06	1.0262E-06
Perylene	4.7492E-08	0.0000E+00	0.0000E+00	0.0000E+00
7-methylbenzo(a)pyrene	0.0000E+00	0.0000E+00	0.0000E+00	0.0000E+00
9,10-dihydrobenzo(a)pyrene-7(8H)-one	0.0000E+00	0.0000E+00	0.0000E+00	0.0000E+00
Dibenzo(a,j)anthracene	0.0000E+00	0.0000E+00	0.0000E+00	0.0000E+00
Indeno[123-cd]pyrene	0.0000E+00	0.0000E+00	0.0000E+00	0.0000E+00
Dibenzo(ah+ac)anthracene	0.0000E+00	3.6933E-07	0.0000E+00	0.0000E+00
Benzo(b)chrysene	3.7994E-07	2.1089E-07	2.5675E-07	1.0800E-07
Picene	0.0000E+00	0.0000E+00	0.0000E+00	0.0000E+00
Benzo(ghi)perylene	0.0000E+00	0.0000E+00	0.0000E+00	0.0000E+00
Anthanthrene	0.0000E+00	0.0000E+00	0.0000E+00	0.0000E+00
Dibenzo(b,k)fluoranthene	0.0000E+00	0.0000E+00	0.0000E+00	0.0000E+00
Dibenzo(a,e)pyrene	0.0000E+00	0.0000E+00	0.0000E+00	0.0000E+00
Coronene	0.0000E+00	0.0000E+00	0.0000E+00	0.0000E+00
Dibenzo(a,h)pyrene	0.0000E+00	0.0000E+00	0.0000E+00	0.0000E+00

Table C.8 Distance specific measurement uncertainty data of particle phase polyaromatic hydrocarbons

g/mile	5126 with ATD Uncertainty	5127 Bkgd (With ATD) Uncertainty	5133 W/O ATD Uncertainty	5134 Bkgd (W/O ATD) Uncertainty
4-methylpyrene	4.9888E-08	4.9956E-08	5.3635E-08	5.0761E-08
1-methylpyrene	5.0239E-08	4.9956E-08	5.3635E-08	5.0761E-08
Benzo(c)phenanthrene	4.9536E-08	4.9956E-08	5.3635E-08	5.0761E-08
Benzo(ghi)fluoranthene	5.0239E-08	4.9956E-08	5.3635E-08	5.0761E-08
Cyclopenta(c,d)pyrene	4.9536E-08	5.0291E-08	5.3635E-08	5.0761E-08
Benz(a)anthracene	4.9536E-08	4.9956E-08	5.3635E-08	5.0761E-08
Chrysene-Triphenylene	4.9536E-08	5.0291E-08	5.3635E-08	5.0761E-08
Benzanthrone	4.9536E-08	4.9956E-08	5.3988E-08	5.0761E-08
7-methylbenz(a)anthracene	4.9536E-08	4.9956E-08	5.3635E-08	5.0761E-08
3-methylchrysene	4.9536E-08	4.9956E-08	5.3635E-08	5.0761E-08
Benz(a)anthracene-7,12-dione	9.9776E-08	4.9956E-08	5.3988E-08	5.0761E-08
5+6-methylchrysene	4.9536E-08	4.9956E-08	5.3635E-08	5.0761E-08
Benzo(b+j+k)fluoranthene	4.9536E-08	4.9956E-08	5.3635E-08	5.0761E-08
Benzo(a)fluoranthene	5.6914E-08	4.9956E-08	5.3635E-08	5.0761E-08
BeP	4.9536E-08	4.9956E-08	5.3635E-08	5.0761E-08
BaP	1.5283E-07	2.0653E-07	2.2266E-07	1.5930E-07
Perylene	4.9536E-08	4.9956E-08	5.3635E-08	5.0761E-08
7-methylbenzo(a)pyrene	4.9536E-08	4.9956E-08	5.3635E-08	5.0761E-08
9,10-dihydrobenzo(a)pyrene-7(8H)-one	4.9536E-08	4.9956E-08	5.3635E-08	5.0761E-08
Dibenzo(a,j)anthracene	4.9536E-08	4.9956E-08	5.3635E-08	5.0761E-08
Indeno[123-cd]pyrene	4.9536E-08	4.9956E-08	5.3635E-08	5.0761E-08
Dibenzo(ah+ac)anthracene	4.9536E-08	5.2973E-08	5.3635E-08	5.0761E-08
Benzo(b)chrysene	1.5001E-07	1.0025E-07	1.0762E-07	5.0761E-08
Picene	4.9536E-08	4.9956E-08	5.3635E-08	5.0761E-08
Benzo(ghi)perylene	4.9536E-08	4.9956E-08	5.3635E-08	5.0761E-08
Anthanthrene	4.9536E-08	4.9956E-08	5.3635E-08	5.0761E-08
Dibenzo(b,k)fluoranthene	4.9536E-08	4.9956E-08	5.3635E-08	5.0761E-08
Dibenzo(a,e)pyrene	4.9536E-08	4.9956E-08	5.3635E-08	5.0761E-08
Coronene	4.9536E-08	4.9956E-08	5.3635E-08	5.0761E-08
Dibenzo(a,h)pyrene	4.9536E-08	4.9956E-08	5.3635E-08	5.0761E-08

Table C.9 Distance specific emissions data of semi-volatile phase polyaromatic hydrocarbons

g/mile	5126 with ATD	5127 Bkgd (With ATD)	5133 W/O ATD	5134 Bkgd (W/O ATD)
9-fluorenone	2.9930E-06	1.0020E-06	1.9348E-05	1.5662E-06
Xanthone	1.8997E-07	1.5808E-07	2.5675E-07	0.0000E+00
Acenaphthenequinone	5.4158E-06	0.0000E+00	5.9533E-06	0.0000E+00
Perinaphthenone	2.6602E-06	3.1652E-07	1.1289E-06	0.0000E+00
2-methylanthracene	1.4248E-07	7.9112E-07	2.0526E-07	2.1600E-07
3-methylphenanthrene	0.0000E+00	0.0000E+00	1.0263E-06	0.0000E+00
2-methylphenanthrene	0.0000E+00	0.0000E+00	4.6201E-07	0.0000E+00
9-methylphenanthrene	9.4984E-08	1.4770E-06	5.6464E-07	5.4177E-08
4,5-methylenephenanthrene	1.8997E-07	1.5808E-07	3.5938E-07	1.6218E-07
1-methylphenanthrene	4.7492E-08	1.5822E-06	0.0000E+00	5.4177E-08
Anthrone	7.6021E-07	0.0000E+00	5.1316E-07	0.0000E+00
Anthraquinone	5.7024E-07	1.0562E-07	5.1316E-07	0.0000E+00
3,6-dimethylphenanthrene	0.0000E+00	2.2153E-06	0.0000E+00	0.0000E+00
A-dimethylphenanthrene	0.0000E+00	0.0000E+00	1.4883E-06	0.0000E+00
B-dimethylphenanthrene	1.4248E-07	0.0000E+00	1.4368E-06	0.0000E+00
C-dimethylphenanthrene	3.7994E-07	3.1652E-07	2.0526E-07	0.0000E+00
D-dimethylphenanthrene	0.0000E+00	2.1089E-07	1.5412E-07	5.4177E-08
1,7-dimethylphenanthrene	8.5519E-07	2.6371E-07	4.6201E-07	0.0000E+00
E-dimethylphenanthrene	8.5519E-07	1.5808E-07	1.0263E-07	0.0000E+00
9-methylanthracene	9.4984E-08	5.2812E-08	0.0000E+00	5.4177E-08
Fluoranthene	5.7024E-07	0.0000E+00	4.6201E-07	0.0000E+00
Pyrene	6.1773E-07	2.5318E-06	3.7977E-06	2.9163E-06
9-Anthraaldehyde	0.0000E+00	0.0000E+00	5.1485E-08	0.0000E+00
Retene	4.7492E-08	0.0000E+00	0.0000E+00	0.0000E+00
Benzonaphthothiophene	4.7492E-08	0.0000E+00	5.1485E-08	0.0000E+00
1+3-methylfluoranthene	9.4984E-08	2.1089E-07	5.1485E-08	0.0000E+00
1-MeFl+C-MeFl/Py	9.4984E-08	2.1089E-07	5.1485E-08	0.0000E+00
B-MePy/MeFl	4.7492E-08	1.5808E-07	5.1485E-08	0.0000E+00
C-MePy/MeFl	0.0000E+00	5.2812E-08	1.5412E-07	0.0000E+00
D-MePy/MeFl	9.4984E-08	5.2812E-08	5.1485E-08	0.0000E+00

Table C.10 Distance specific measurement uncertainty data of semi-volatile phase polyaromatic hydrocarbons

g/mile	5126 with ATD Uncertainty	5127 Bkgd (With ATD) Uncertainty	5133 W/O ATD Uncertainty	5134 Bkgd (W/O ATD) Uncertainty
9-fluorenone	1.6618E-07	6.9066E-08	1.0205E-06	8.9166E-08
Xanthone	5.0590E-08	5.0626E-08	5.5046E-08	5.0761E-08
Acenaphthenequinone	7.5078E-07	4.9956E-08	8.1017E-07	5.0761E-08
Perinaphthenone	2.0482E-07	5.2303E-08	1.2209E-07	5.0761E-08
2-methylanthracene	5.0239E-08	1.0662E-07	5.4694E-08	5.1763E-08
3-methylphenanthrene	4.9536E-08	4.9956E-08	1.1962E-07	5.0761E-08
2-methylphenanthrene	9.9073E-08	9.9911E-08	2.1525E-07	5.0761E-08
9-methylphenanthrene	4.9888E-08	3.0745E-07	1.6302E-07	5.0761E-08
4,5-methylenephenanthrene	5.0590E-08	5.0626E-08	5.6811E-08	5.1095E-08
1-methylphenanthrene	4.9536E-08	9.0524E-08	5.3635E-08	5.0761E-08
Anthrone	3.0003E-07	4.9956E-08	2.1560E-07	1.0119E-07
Anthraquinone	1.5177E-07	5.0291E-08	1.1009E-07	5.0761E-08
3,6-dimethylphenanthrene	4.9536E-08	1.8339E-07	5.3635E-08	5.0761E-08
A-dimethylphenanthrene	4.9536E-08	4.9956E-08	1.3197E-07	5.0761E-08
B-dimethylphenanthrene	5.0239E-08	4.9956E-08	1.3056E-07	5.0761E-08
C-dimethylphenanthrene	1.0118E-07	1.0092E-07	5.4694E-08	5.0761E-08
D-dimethylphenanthrene	4.9536E-08	5.0962E-08	5.3988E-08	5.0761E-08
1,7-dimethylphenanthrene	6.7103E-08	5.1297E-08	5.8575E-08	5.0761E-08
E-dimethylphenanthrene	6.7103E-08	5.0626E-08	5.3635E-08	5.0761E-08
9-methylanthracene	4.9888E-08	4.9956E-08	5.3635E-08	5.0761E-08
Fluoranthene	2.0061E-07	4.9956E-08	2.1525E-07	5.0761E-08
Pyrene	1.0434E-07	2.3335E-07	3.7686E-07	2.4412E-07
9-Anthraaldehyde	4.9536E-08	4.9956E-08	5.3635E-08	5.0761E-08
Retene	4.9536E-08	4.9956E-08	5.3635E-08	5.0761E-08
Benzonaphthothiophene	4.9536E-08	4.9956E-08	5.3635E-08	5.0761E-08
1+3-methylfluoranthene	4.9888E-08	5.0962E-08	5.3635E-08	5.0761E-08
1-MeFl+C-MeFl/Py	4.9888E-08	5.0962E-08	5.3635E-08	5.0761E-08
B-MePy/MeFl	4.9536E-08	5.0626E-08	5.3635E-08	5.0761E-08
C-MePy/MeFl	4.9536E-08	4.9956E-08	5.3988E-08	5.0761E-08
D-MePy/MeFl	4.9888E-08	4.9956E-08	5.3635E-08	5.0761E-08

Table C.11 Distance specific emissions data of C6+ alkanes

g/mile	5126 with ATD	5127 Bkgd With ATD	5133 W/O ATD	5134 Bkgd W/O ATD
cyclohexane	7.0720E-05	5.2094E-05	9.6365E-04	1.8709E-05
methylcyclopentane	1.1079E-04	9.1784E-05	1.0288E-03	9.4794E-05
2,2-dimethylbutane	5.0686E-05	1.8922E-04	7.6093E-04	9.3226E-05
2,3-dimethylbutane	6.6375E-05	7.1117E-05	5.4976E-04	5.2360E-05
n-hexane	1.0741E-04	1.5493E-04	2.3386E-03	1.1238E-04
2-methylpentane	2.1723E-04	2.0573E-04	2.2743E-03	1.5453E-04
3-methylpentane	1.2430E-04	1.3842E-04	1.2719E-03	9.9612E-05
2-methylhexane	2.3790E-04	1.2156E-04	7.1081E-04	1.3534E-04
methylcyclohexane	5.2256E-05	6.5119E-05	1.0842E-03	6.8395E-05
1,3-dimethylcyclopentane (cis)	3.8508E-05	4.3417E-05	2.3927E-04	5.6759E-05
3-methylhexane	1.2630E-04	1.4767E-04	5.9129E-04	9.9495E-05
n-heptane	2.0348E-04	1.7425E-04	1.3011E-03	1.2623E-04
2,3-dimethylpentane	6.0342E-05	5.7592E-05	2.5684E-04	7.1280E-05
2,4-dimethylpentane	5.4729E-05	4.4302E-05	1.7922E-04	4.3065E-05
2-methylheptane	4.7981E-06	2.6929E-05	5.6293E-05	1.8617E-05
3-methylheptane	3.5186E-05	3.3661E-05	1.8818E-04	3.2157E-05
4-methylheptane	1.7593E-05	8.4152E-06	9.3286E-05	1.5232E-05
n-octane	5.5978E-05	1.8514E-05	1.9944E-04	3.7235E-05
2,2,4-trimethylpentane	6.3975E-05	5.8907E-05	2.1070E-04	5.0775E-05
2,3,4-trimethylpentane	7.5171E-05	6.3956E-05	3.8601E-05	4.9082E-05
n-nonane	1.2039E-04	6.4289E-05	1.6805E-04	6.0847E-05
n-decane	1.1958E-04	7.5498E-05	7.6157E-05	8.0140E-05
n-undecane	8.5371E-05	6.2195E-05	5.9435E-05	3.0114E-05

Table C.12 Distance specific emissions data of C2-C5 alkanes

g/mile	5126 with ATD	5127 Bkgd With AT)	5133 W/O ATD	5134 Bkgd W/O ATD
ethane	7.4787E-02	2.7523E-03	5.3385E-01	2.1675E-03
propane	8.3935E-03	1.5995E-03	9.3774E-02	1.3640E-03
iso-butane	1.2788E-03	3.1264E-04	2.4039E-02	2.9545E-04
n-butane	1.1689E-03	4.5654E-04	2.3114E-02	4.1690E-04
cyclopentane	3.9287E-05	2.9973E-05	3.4175E-04	2.5984E-05
iso-pentane	6.7095E-04	5.3379E-04	9.9410E-03	4.3627E-04
n-pentane	3.7084E-04	2.1054E-04	6.5511E-03	2.0210E-04

Table C.13 Distance specific emissions data of C6+ olefins

g/mile	5126 with ATD	5127 Bkgd With ATD	5133 W/O ATD	5134 Bkgd W/O ATD
1,3-hexadiene (trans)	0.0000E+00	1.2106E-06	2.3137E-06	1.2173E-06
cyclohexene	1.0355E-05	1.2107E-06	2.2677E-04	3.6525E-06
c-2-hexene	2.3573E-06	2.4807E-06	2.9632E-05	1.2473E-06
2-methyl-1-pentene	4.2432E-05	4.9613E-06	3.4492E-04	4.9891E-06
t-2-hexene	5.8933E-06	1.2403E-06	5.0968E-05	1.2473E-06
1-heptene	3.8508E-05	2.4603E-05	2.2267E-04	1.8920E-05
2,3-dimethyl-2-pentene	1.3753E-06	1.4472E-06	8.2982E-06	1.4554E-06
alpha-pinene	4.7687E-05	8.0291E-06	1.1509E-05	8.0742E-06

Table C.14 Distance specific emissions data of C2-C5 olefins

g/mile	5126 with ATD	5127 Bkgd With ATD	5133 W/O ATD	5134 Bkgd W/O ATD
ethene	6.1625E-03	4.0234E-04	5.7043E-01	3.5273E-04
propene	3.4122E-04	1.0109E-04	2.8022E-02	1.7213E-04
1,2-butadiene	7.5753E-07	1.5943E-06	2.7425E-05	8.0164E-07
1,3-butadiene	1.5151E-06	8.7688E-06	1.5236E-05	1.3628E-05
1-butene + isobutene	2.2239E-04	1.3892E-04	8.8737E-03	7.9831E-05
c-2-butene	2.7504E-05	4.9616E-06	1.1862E-03	8.3157E-06
t-2-butene	1.4145E-05	4.1347E-06	1.4027E-03	1.0810E-05
isoprene	9.5389E-07	3.4129E-05	4.7963E-06	4.9461E-05
2-methyl-1-butene	2.0626E-05	1.2403E-05	4.5138E-04	1.9748E-05
2-methyl-2-butene	6.8752E-06	7.2349E-06	1.6297E-04	8.3148E-06
c-2-pentene	3.9287E-06	2.0671E-06	1.4322E-04	6.2361E-06
1-pentene	4.5180E-05	2.8940E-05	4.3261E-04	1.2472E-05
t-2-pentene	1.3750E-05	6.2013E-06	2.6273E-04	5.1968E-06
cyclopentene	6.9031E-06	2.4214E-06	2.2446E-04	1.2175E-06

Table C.15 Distance specific emissions data of C2-C5 alkynes

g/mile	5126 with ATD	5127 Bkgd With ATD	5133 W/O ATD	5134 Bkgd W/O ATD
acetylene	8.066E-04	7.664E-06	2.380E-02	3.410E-04
propyne	2.132E-05	2.362E-06	8.773E-04	4.750E-06

Table C.16 Distance specific emissions data of aromatics

g/mile	5126 with ATD	5127 Bkgd With ATD	5133 W/O ATD	5134 Bkgd W/O ATD
benzene	2.8333E-04	2.6477E-04	1.8460E-03	1.9332E-04
toluene	6.0134E-04	4.9836E-04	1.1536E-03	3.5231E-04
styrene	1.6037E-05	2.1479E-05	2.1992E-05	1.5428E-05
ethylbenzene	1.0411E-04	7.1997E-05	1.0320E-04	5.3514E-05
m&p-xylene	2.0971E-04	1.5182E-04	2.4380E-04	1.6998E-04
o-xylene	1.1601E-04	7.9822E-05	9.1238E-05	7.2401E-05
indan	1.1588E-05	6.9680E-06	1.8312E-05	7.0071E-06
1,2,3-trimethylbenzene	2.6935E-05	1.4172E-05	2.3700E-05	1.4251E-05
1,2,4-trimethylbenzene+t-butylbenzene	3.5352E-05	1.4172E-05	2.8779E-05	1.2470E-05
1,3,5-trimethylbenzene	1.8518E-05	8.8574E-06	1.3543E-05	1.7814E-05
isopropylbenzene	1.0100E-04	1.9486E-05	1.5236E-05	5.3442E-06
3-ethyltoluene	6.0603E-05	3.0115E-05	3.3858E-05	3.5628E-05
n-propylbenzene	4.7135E-05	1.9486E-05	1.8622E-05	1.2470E-05
o-ethyltoluene	2.6935E-05	1.5943E-05	1.8622E-05	1.4251E-05
4-ethyltoluene	3.0301E-05	1.9486E-05	2.0315E-05	1.7814E-05
n-butylbenzene	1.6915E-05	7.9112E-06	1.3230E-05	3.9778E-06
1,3-diethylbenzene	9.3988E-05	5.1431E-05	1.9470E-04	4.1773E-05
1,4-diethylbenzene	3.7595E-06	0.0000E+00	1.7013E-05	1.9892E-06

Table C.17 Distance specific emissions data of metals

g/mile	5126 with ATD	5127 Bkgd (With ATD)	5133 W/O ATD	5134 Bkgd (W/O ATD)
Sodium	0.0000E+00	2.4878E-04	0.0000E+00	3.7868E-04
Magnesium	0.0000E+00	0.0000E+00	0.0000E+00	0.0000E+00
Aluminum	7.8413E-05	0.0000E+00	4.6910E-05	0.0000E+00
Silicon	1.1792E-04	1.2869E-04	7.7828E-05	0.0000E+00
Phosphorous	0.0000E+00	0.0000E+00	0.0000E+00	0.0000E+00
Sulfur	3.4187E-04	2.0684E-04	2.8592E-04	0.0000E+00
Chlorine	1.1951E-06	4.4401E-06	0.0000E+00	0.0000E+00
Potassium	2.6957E-05	4.5630E-05	1.5992E-06	0.0000E+00
Calcium	1.1241E-04	7.4935E-05	6.5167E-05	0.0000E+00
Scandium	0.0000E+00	0.0000E+00	0.0000E+00	0.0000E+00
Titanium	0.0000E+00	0.0000E+00	1.8258E-05	3.2411E-05
Vanadium	0.0000E+00	0.0000E+00	0.0000E+00	0.0000E+00
Chromium	7.0446E-05	1.0260E-04	8.6557E-05	0.0000E+00
Manganese	1.2283E-05	3.8731E-05	8.3958E-06	0.0000E+00
Iron	2.9646E-04	5.3704E-04	1.4739E-04	1.5017E-05
Cobalt	1.1712E-04	0.0000E+00	1.4060E-04	2.4461E-06
Nickel	4.7805E-06	5.7858E-05	1.0328E-05	0.0000E+00
Copper	1.7462E-05	0.0000E+00	0.0000E+00	0.0000E+00
Zinc	1.5802E-05	0.0000E+00	1.9857E-05	0.0000E+00
Gallium	0.0000E+00	0.0000E+00	1.1927E-05	9.7846E-06
Arsenic	0.0000E+00	0.0000E+00	0.0000E+00	0.0000E+00
Selenium	0.0000E+00	6.8992E-06	7.5296E-06	2.9558E-05
Bromine	0.0000E+00	1.4208E-05	0.0000E+00	0.0000E+00
Rubidium	1.5470E-05	0.0000E+00	0.0000E+00	0.0000E+00
Strontium	0.0000E+00	2.2815E-05	1.8258E-05	1.6172E-05
Yttrium	8.6978E-06	8.9484E-06	7.9294E-06	7.2705E-06
Zirconium	1.5935E-06	0.0000E+00	0.0000E+00	0.0000E+00
Niobium	0.0000E+00	6.9675E-06	1.0795E-05	3.6692E-06
Molybdenum	3.0874E-05	1.3867E-05	2.1456E-05	0.0000E+00
Palladium	0.0000E+00	0.0000E+00	3.2584E-05	1.0287E-04
Silver	3.5654E-05	4.2351E-05	4.2112E-05	8.0859E-06
Cadmium	3.8377E-05	0.0000E+00	0.0000E+00	0.0000E+00
Indium	7.0844E-05	0.0000E+00	0.0000E+00	0.0000E+00
Tin	1.6267E-05	0.0000E+00	2.7386E-05	2.9558E-05
Antimony	0.0000E+00	0.0000E+00	6.9898E-05	0.0000E+00
Cesium	0.0000E+00	0.0000E+00	0.0000E+00	6.4551E-06
Barium	0.0000E+00	0.0000E+00	0.0000E+00	0.0000E+00
Lanthanum	0.0000E+00	0.0000E+00	0.0000E+00	0.0000E+00
Cerium	0.0000E+00	0.0000E+00	0.0000E+00	0.0000E+00
Samarium	0.0000E+00	4.8499E-06	0.0000E+00	0.0000E+00
Europium	0.0000E+00	0.0000E+00	0.0000E+00	0.0000E+00
Terbium	1.7462E-05	0.0000E+00	0.0000E+00	0.0000E+00
Hafnium	0.0000E+00	0.0000E+00	0.0000E+00	0.0000E+00

Tantalum	9.5012E-05	0.0000E+00	0.0000E+00	8.8333E-07
Wolfram	0.0000E+00	0.0000E+00	3.6182E-05	9.4380E-05
Iridium	0.0000E+00	1.8307E-05	1.5459E-05	0.0000E+00
Gold	0.0000E+00	0.0000E+00	0.0000E+00	0.0000E+00
Mercury	0.0000E+00	0.0000E+00	0.0000E+00	0.0000E+00
Thallium	0.0000E+00	2.4591E-06	4.7976E-06	0.0000E+00
Lead	0.0000E+00	0.0000E+00	0.0000E+00	0.0000E+00
Uranium	0.0000E+00	0.0000E+00	0.0000E+00	2.8538E-06

Table C.18 Distance specific emissions data of EC/OC

g/mile	5126-2 With ATD	5127-1 BG With ATD	5133-2 W/O ATD	5134-1 BG W/O ATD
Organic Carbon Fraction 1 concentration	0.01009	0.00513	0.01101	0.00440
Organic Carbon Fraction 2 concentration	0.00563	0.00321	0.00505	0.00243
Organic Carbon Fraction 3 concentration	0.00241	0.00066	0.00223	0.00012
Organic Carbon Fraction 4 concentration	0.00244	0.00000	0.00226	0.00000
Organic Carbon Fraction 5 concentration	0.00000	0.00000	0.00000	0.00000
Pyrolyzed organic carbon, thermal method, transmittance concentration	0.00000	0.00000	-0.00226	0.00000
Pyrolyzed organic carbon, thermal method,reflectance concentration	0.00000	0.00000	-0.00226	0.00000
Organic carbon,thermal method, transmittance concentration	0.01813	0.00900	0.01829	0.00696
Organic carbon,thermal method, reflectance concentration	0.01813	0.00900	0.01829	0.00696
Elemental Carbon Fraction 1 concentration	0.00000	0.00000	0.00000	0.00000
Elemental Carbon Fraction 2 concentration	0.00000	0.00000	0.00000	0.00000
Elemental Carbon Fraction 3 concentration	0.00000	0.00000	0.00000	0.00000
Elemental Carbon Fraction 4 concentration	0.00000	0.00000	0.00000	0.00000
Elemental Carbon Fraction 5 concentration	0.00000	0.00000	0.00000	0.00000
Elemental carbon,thermal method, transmittance concentration	0.00244	0.00000	0.00226	0.00000
Elemental carbon,thermal method, reflectance concentration	0.00244	0.00000	0.00226	0.00000
Total Carbon concentration	0.02057	0.00900	0.02055	0.00696